FEDERAL UNIVERSITY OF RIO GRANDE DO NORTE
GRADUATE PROGRAM IN NEUROSCIENCE
BRAIN INSTITUTE

MARGARETH DE BRITO NOGUEIRA LIMA

On the anxiolytic effects of 5-MeO-DMT in the mouse brain and behavior

Thesis presented to the degree of Doctor of Philosophy to the graduate program in Neuroscience of Brain Institute - Federal University of Rio Grande do Norte.
Advisor: Dr. Richardson Naves Leão
Co-Advisor: Dr. Emelie Katarina Svahn Leão

Natal, 2022

UNIVERSIDADE FEDERAL DO RIO GRANDE DO NORTE
PROGRAMA DE PÓS-GRADUAÇÃO EM NEUROCIÊNCIAS
INSTITUTO DO CÉREBRO

MARGARETH DE BRITO NOGUEIRA LIMA

Dos efeitos ansiolíticos da 5-MeO-DMT no cérebro e comportamento do camundongo

Natal, 2022

Universidade Federal do Rio Grande do Norte - UFRN
Sistema de Bibliotecas - SISBI
Catalogação de Publicação na Fonte. UFRN - Biblioteca Setorial Árvore do Conhecimento - Instituto do Cérebro - ICe

Lima, Margareth de Brito Nogueira.
Dos efeitos ansiolíticos da 5-MeO-DMT no cérebro e comportamento do camundongo / Margareth de Brito Nogueira Lima. - Natal, 2022.
110f.: il.

Tese (doutorado em Neurociências) - Universidade Federal do Rio Grande do Norte, Instituto do Cérebro, 2022.
Orientador: Richardson Naves Leão.
Coorientador: Emelie Katarina Svahn Leão.

1. 5-MeO-DMT. 2. Psicodélicos serotonérgicos. 3. Ansiedade. 4. Plasticidade neuronal. 5. Atividade neuronal. I. Leão, Richardson Naves. II. Leão, Emelie Katarina Svahn. III. Título.

RN/UF/BS-ICe CDU 616.89-008.441

"'It's just love. Everything. All of it. That is all that exists. Love is it.'

'transformed on a cellular level into infinite energy and pure love,'
'all of stress and difficulties throughout life felt like they occurred for a meaningful purpose, and the traumas of past were washed over by an infinitely loving energy.'
Upon debriefing from his session several hours afterwards, he believed this experience was the single most peak transformational experience of his life."

(Barsuglia et al., 2018)

Abstract

Anxiety is a worldwide prevalent circuitopathy, in other words, a circuit disorder that substantially affects people's quality of life. To treat it properly, it is necessary to reverse the processes that lead to the malfunctioning of neuronal circuits mainly implicated in anxiety behavior. There is still no completely effective treatment for such a disorder. Several studies have presented promising and safe results with serotonergic psychedelics, evidencing the therapeutic potential of these compounds. However, their mechanisms of action have not yet been fully elucidated. Many clinical studies have managed to durably mitigate the symptoms of depression and anxiety with just a single dose, which makes these compounds very interesting alternatives to the classical treatments available in psychiatry. These lasting effects can be explained by a possible induction of neuroplasticity, neuroprotection, and modulation of inflammation-related agents. Some studies have shown an increase in neuritogenesis, synaptogenesis, and neurogenesis from treatment with psychedelic compounds. In this study, we sought to identify how the serotonergic psychedelic 5-methoxy-N,N-dimethyltryptamine (5-MeO-DMT) durably affects neuronal activity and the expression of plasticity-related genes (BDNF, CREB, ARC, ZIF268, mTORC1, NF-kB e TRIP8b) in brain structures classically related to anxiety, such as the basolateral amygdala, the ventral hippocampus, and the anterior cingulate cortex of adult mice one hour, five hours, and five days after treatment. Assessing the electrophysiological properties of mice after 5 days of 5-MeO-DMT treatment, we found differences in passive membrane properties, as well as changes in amplitude and frequency of neuronal firing in the hippocampal dentate gyrus. Evaluating gene expression one hour after treatment, we showed increased expression of ARC and ZIF268 immediate early genes in the anterior cingulate cortex and basolateral amygdala. After 5 hours of treatment, the NR2A gene was significantly decreased in ventral CA1. Finally, 5 days after the treatment with 5-MeO-DMT we found a significant increase of the TRIP8b gene in ventral CA1. We investigated if 5-MeO-DMT produces changes in the behavior of mice after 24hours and 5 days of treatment, with and without stress conditions. We also assessed mice basal corticosterone serum levels under and after acute restraint stress. We found that 5-MeO-DMT treated mice presented significantly less basal corticosterone levels after 5 days. They also presented less anxious behavior. These molecular, cellular, and behavioral findings suggest that 5-MeO-DMT produces

immediate and long-lasting effects in mice, although further studies are necessary to consider the therapeutic possibility and to unravel which signaling pathways underlie the 5-MeO-DMT role on synaptic plasticity.

Keywords: 5-MeO-DMT, serotonergic psychedelics, anxiety, plasticity, neuronal activity, basolateral amygdala, anterior cingulate cortex, ventral CA1, ventral dentate gyrus

Resumo

Ansiedade é uma desordem de circuitos, ou seja, uma circuitopatia mundialmente prevalente que afeta substancialmente a qualidade de vida das pessoas. Para tratá-la adequadamente, é necessário que sejam revertidos os processos que levam ao mau-funcionamento dos circuitos neuronais. Ainda não há um tratamento completamente eficaz para tratar tal transtorno. Inúmeras pesquisas vêm apresentando resultados promissores e seguros com psicodélicos serotonérgicos, evidenciando um potencial terapêutico desses compostos. No entanto, os seus mecanismos de ação ainda não foram completamente elucidados. Muitos estudos clínicos têm conseguido mitigar duradouramente os sintomas da depressão e da ansiedade com apenas uma dose, o que faz desses compostos alternativas bastante interessantes aos tratamentos clássicos disponíveis na psiquiatria. Esses efeitos duradouros podem ser explicados por uma possível indução à neuroplasticidade, à neuroproteção e a uma modulação de agentes ligados à inflamação. Alguns estudos comprovaram um aumento na neuritogênese, sinaptogênese e neurogênese proveniente do tratamento com esses compostos. Neste estudo, procuramos identificar como o psicodélico serotonérgico 5- metoxi-N,N-dimetiltriptamina (5-MeO-DMT) afeta prolongadamente a atividade neuronal e a expressão de genes relacionados à plasticidade (BDNF, CREB, ARC, ZIF268, mTORC1, NF-kB e TRIP8b) em estruturas cerebrais classicamente relacionadas à ansiedade, como a amígdala basolateral, a região CA1 do hipocampo ventral e o córtex cingulado anterior, localizado no córtex medial pré-frontal de camundongos adultos uma hora, cinco horas e cinco dias após o tratamento. Após avaliarmos as propriedades eletrofisiológicas de camundongos 5 dias depois do tratamento com 5-MeO-DMT, verificamos diferenças nas propriedades passivas da membrana, além de alterações na amplitude e frequência dos disparos neuronais na região do giro denteado hipocampal. A avaliação da expressão gênica uma hora após o tratamento revelou um aumento na expressão dos genes iniciais imediatos ARC e ZIF268 no córtex cingulado anterior e na amígdala basolateral. Outra avaliação feita 5 horas após o tratamento mostrou uma diminuição do gene NR2A em CA1 ventral. Verificamos também um aumento significativo do gene TRIP8b em CA1 ventral 5 dias após o tratamento. Investigamos se o 5-MeO-DMT produz mudanças no comportamento de camundongos após 24 horas e 5 dias de tratamento, com e sem condições de estresse. Também avaliamos os níveis séricos basais de corticosterona em

camundongos e após estresse de contenção aguda. Verificamos que camundongos tratados com 5-MeO-DMT apresentaram níveis significativamente menores de corticosterona basal após 5 dias, além de apresentar um comportamento menos ansioso. Estes achados moleculares, celulares e comportamentais sugerem que a 5-MeO-DMT produz efeitos imediatos e duradouros em camundongos, embora sejam necessários mais estudos para considerar a sua possibilidade terapêutica e também para desvendar quais vias de sinalização são subjacentes ao papel da 5-MeO-DMT na plasticidade sináptica.

Palavras-chave: 5-MeO-DMT, psicodélicos serotonérgicos, ansiedade, plasticidade, atividade neuronal, amígdala basolateral, cortex cingulado anterior, CA1 ventral, giro denteado ventral.

Dedication

This thesis is dedicated with all my love to my parents

Maria José de Brito Lyra Nogueira and **Valdir de Mello Nogueira**

my masters in life

This thesis is also dedicated to

Roti Nielba Turin – *my master in Semiotics and in the Art of teaching*

Jorge Oswaldo Caron – *my master in Architecture*

Bento Prado de Almeida Ferraz Júnior – *my master in Philosophy*

Henrique Schützer del Nero – *my master in Science*

In memory of all

Dedicatória

Esta tese é dedicada com todo o meu amor aos meus pais

Maria José de Brito Lyra Nogueira e **Valdir de Mello Nogueira**

Meus mestres na vida

Esta tese também é dedicada a:

Roti Nielba Turin – *minha mestra na Semiótica e na Arte de ensinar*

Jorge Oswaldo Caron – *meu mestre na Arquitetura*

Bento Prado de Almeida Ferraz Júnior – *meu mestre na Filosofia*

Henrique Schützer del Nero – *meu mestre nas Ciências*

A todos, in memoriam

Acknowledgments

Three people were fundamental for this doctorate. The first one opened the doors to neuroscience and to his laboratory for me, where I could have access to meet incredible and intelligent people, besides getting to know fantastic techniques. I love neuroscience and by his hands, I could enter this new world. Eternal gratitude, **Richardson Leão**. I thank you for all the doors you have opened for me, also for the ones you have closed, all of which have made me a better scientist and a stronger person. The progress of a doctorate is not always easy and I have encountered difficulties along the way, which I might not have been able to overcome if I had not had **Daiane Golbert**'s accompaniment and help. I am grateful for every minute we spent together in the doctorate, and her presence was invaluable. I learned much more than a technique, but the rigor of well-conducted science, the commitment to the experiments, and the lightness of doing one's duty with love. I cannot fail to register that this accompaniment was only possible due to her voluntary initiative, leaving her work several times to spend the day with me in the laboratory, in a demonstration of rare friendship and love for science. Every smile we gave in the lab will be forever marked in my memory and my heart. I gained much more than a teacher, I gained a friend for life. All my gratitude and recognition. Finally, difficulties also crossed my path during the period of completion of my doctorate, but I was graced with one more gift from life. To have had the privilege of being mentored by and working in partnership with **Kia Leão** was one of the most pleasant surprises in the last three months. I thank her for recognizing my work, for encouraging and motivating me every day, but mainly for sharing her scientific expertise with me. An example of competence, commitment, and responsibility. The writing days were a daily shower of learning at each comma corrected, each comment made. I am grateful for the partnership and synergy that we generated throughout the days. Gratitude, admiration, and respect.

Everyday life in science is done inside the laboratory. Human relationships and coexistence determine the outcome of the work and the quality of our own lives. To my colleagues, I thank you for all the light moments, the companionship, the good and collaborative environment, without disagreements or competition. My heart beats strong and my eyes are filled with gratitude and affection, my dear journey companions **Jessica**

Winne (Jess), **Elis Brisa dos Santos** (Brizoca), **Rafael Lima** (Rafaelzinho), **Ingrid Nogueira** (Bicha linda), **Aelton Araújo** (Aeltinho), **Rodolfo Diógenes** (Rodolfinho), **Thawann Malfatti**, **Barbara Ciralli**, **Marcos Gonzaga**, **George Nascimento**, **Markus Hilscher** (Markito), **Annara Soares** (Annarinha), **Rafael Franzon**, **Cibele Leônidas** (Cibas), and **Hanna Arruda**.

2017 was a special year. I thank **Klas Kullander** for being so welcome in his lab. **Sanja Mikulovic**, **Samer Siwani**, **Jennifer Vieillard**, **Angelica Thulin**, and **Robin** were excellent colleagues. Gratitude to everyone from my time at the BMC at Uppsala University. Thanks also to Professor **Adriano Tort** for providing me with such a great learning experience.

Few people change professions in maturity, with an established career, as was my case. It takes courage and detachment. If I had not found in ICe an environment of total identification, perhaps I would not have persevered. I thank all the people who make up the Brain Institute, which I now proudly call my *alma mater*. I start by thanking my Advisory Committee, formed by professors **Diego Laplagne** and **Maria Bernardete Cordeiro de Sousa**, for their support and orientation. To professor **Draulio Araujo** for my first opportunity in a laboratory, to professor **Kerstin Schmidt** for leading the ship and making it all happen, and to professor **Sidarta Ribeiro**, who so often is our voice crying out against the outrages to science. To the professors **Marcos**, **Rodrigo**, **Martin**, **Sérgio**, **Dudu**, **Claudio**, **Tarciso**, **Lia**, and **Takahashi**, my gratitude. There is no way to name everyone who contributed, so I thank the animal house staff, represented by **Mariana Medeiros**. To the laboratory technicians, represented by **Juliana Brandão**. To the collaborators in the maintenance, cleaning, and security areas, represented by **Eronildo**, and to the technical-administrative staff, represented by **Akaline Dantas**. I would also like to thank my fellow students at ICe, represented by **Annie** and **Bryan**. To the articles' collaborators, scientists **Raíssa Nóbrega**, **Nicole Galvão Coelho**, and **Richardson Santiago**, my gratitude.

I thank the loves of my life, **Floriano**, **Melissa**, **Gabriel**, and **Ana Júlia**, for all the cheer, understanding, support, and love. Also to **Rosinha** (Rosalind Franklin), our little cat who accompanied the writing of this thesis beside the computer. I also thank all my family and friends who love me and cheer for me.

Finally, to all the animals that were part of this study, my thanks and respect.

Agradecimentos

Três pessoas foram fundamentais para que esse doutorado pudesse acontecer. A primeira abriu-me as portas para a neurociência e para o seu laboratório, onde eu pude ter acesso a conviver com pessoas incríveis e inteligentes, além de conhecer técnicas fantásticas. Eu amo a neurociência e por suas mãos pude entrar nesse mundo novo. Gratidão eterna, **Richardson Leão**. Agradeço por todas as portas que me abriu e também pelas que fechou, todas tornaram-me uma cientista melhor e uma pessoa mais forte. O andamento de um doutorado nem sempre é fácil e eu encontrei dificuldades pelo caminho, que talvez não conseguisse transpor se não tivesse tido o acompanhamento e a ajuda de **Daiane Golbert**. Agradeço cada minuto que passamos juntas nesse doutorado, a sua presença foi inestimável. Aprendi muito além de uma técnica, mas o rigor da ciência bem conduzida, o comprometimento com os experimentos e a leveza de cumprir o dever com amor. Não posso deixar de registrar que este acompanhamento como um todo só foi possível devido à sua iniciativa voluntária, deixando em vários momentos o seu trabalho para passar o dia comigo no laboratório, numa demonstração de rara amizade e amor pela ciência. Cada sorriso que demos no laboratório vai ficar marcado para sempre na minha memória e no meu coração. Ganhei muito mais do que uma professora, eu ganhei uma amiga para a vida toda. Todo o meu reconhecimento e gratidão. Por fim, dificuldades também atravessaram o meu caminho no período de conclusão do meu doutorado, mas fui agraciada com mais um presente da vida. Ter tido o privilégio de receber o acompanhamento e trabalhar em parceria com **Kia Leão** foi uma das surpresas mais agradáveis e inesperadas nestes últimos três meses. Agradeço por reconhecer o meu trabalho, por me incentivar e motivar a cada dia, mas principalmente por dividir comigo a sua experiência científica. Exemplo de competência, compromisso e responsabilidade. Os dias de escrita foram uma chuva diária de aprendizado a cada vírgula corrigida, a cada comentário feito. Agradeço a parceria e sinergia que geramos ao longo dos dias. Gratidão, admiração e respeito.

O dia-a-dia na ciência se faz dentro do laboratório. As relações humanas e de convivência determinam o resultado dos trabalhos e a qualidade da nossa própria vida. Aos meus colegas agradeço por todos os momentos leves, o companheirismo, o ambiente bom e colaborativo, sem desavenças ou competição. O coração bate forte e os olhos marejam de gratidão e carinho, meus queridos companheiros de jornada **Jessica Winne** (Jess), **Elis**

Brisa dos Santos (Brizoca), **Rafael Lima** (Rafaelzinho), **Ingrid Nogueira** (Bicha linda), **Aelton Araújo** (Aeltinho)**, Rodolfo Diógenes** (Rodolfinho), **Thawann Malfatti**, **Barbara Ciralli**, **Marcos Gonzaga, George Nascimento**, **Markus Hilscher** (Markito), **Annara Soares** (Annarinha), **Rafael Franzon**, **Cibele Leônidas** (Cibas) e **Hanna Arruda**.

2017 foi um ano especial. Agradeço a **Klas Kullander** por ter sido tão bem recebida em seu laboratório. **Sanja Mikulovic**, **Samer Siwani**, **Jennifer Vieillard, Angelica Thulin** e **Robin** foram excelentes colegas. Gratidão a todos da minha convivência no BMC, na Universidade de Uppsala. Agradeço também ao professor **Adriano Tort** por ter me proporcionado essa experiência de enorme aprendizado.

Poucas pessoas mudam de profissão na maturidade, com uma carreira estabelecida, como foi o meu caso. É preciso coragem e desprendimento. Se eu não tivesse encontrado no ICe um ambiente de total identificação, talvez não tivesse perseverado. Por isso agradeço a todas as pessoas que fazem o Instituto do Cérebro, que com todo orgulho agora chamo também de minha *alma mater*. Começo agradecendo ao meu Comitê de Assessoramento, formado pelos professores **Diego Laplagne** e **Maria Bernardete Cordeiro de Sousa,** pelo apoio e orientação. Ao professor **Draulio Araújo** pela minha primeira oportunidade em um laboratório, à professora **Kerstin Schmidt** por comandar a nave e fazer tudo acontecer e ao professor **Sidarta Ribeiro,** que por tantas vezes é a nossa voz a clamar contra os ultrajes à ciência. Aos professores **Marcos, Rodrigo**, **Martin, Sérgio**, **Dudu**, **Claudio**, **Tarciso**, **Lia** e **Takahashi,** a minha gratidão. Não há como nomear a todos que contribuíram, desta forma agradeço aos técnicos do biotério, representados por **Mariana Medeiros**. Aos técnicos de laboratório, representados por **Juliana Brandão**. Aos colaboradores das áreas de manutenção, limpeza e segurança, representados por **Eronildo**, e ao corpo técnico-administrativo, representados por **Akaline Dantas**. Agradeço também aos meus colegas estudantes do ICe, a quem represento pelos irmãos **Annie** e **Bryan**. Aos colaboradores dos artigos, os cientistas **Raíssa Nóbrega, Nicole Galvão Coelho** e **Richardson Santiago**, a minha gratidão.

Agradeço aos amores da minha vida, **Floriano**, **Melissa**, **Gabriel** e **Ana Júlia**, toda torcida, compreensão, apoio e amor. Também à **Rosinha** (Rosalind Franklin), a nossa gatinha que acompanhou toda a escrita desta tese ao lado do computador. Agradeço também à toda minha família e amigos que me amam e torcem por mim. Por fim, a todos os animais que fizeram parte deste estudo, meu agradecimento e respeito.

List of Abbreviations

5-HT	Serotonin
5-HT1A	Serotonin receptor 1A
5-HT2A	Serotonin receptor 2A
5-HT7	Serotonin receptor 7
5-MeO-DMT	5-methoxy-N,N-dimethyltryptamine
ACC	Anterior cingulate cortex
aCSF	Artificial cerebrospinal fluid
ACTH	Adrenocorticotropic hormone
AD	Alzheimer disease
AHP	Afterhyperpolarization
Akt	Serine-threonine protein kinase
AMPA	a-amino-3-hydroxy-5-methyl-4-isoxazolepropionic acid
ARC	Activity regulated cytoskeleton associated protein
AP	Action potential
BAC	Bacteriophage
BDNF	Brain-derived neurotrophic factor
BLA	Basolateral amygdala
BNST	Bed nucleus of the stria terminalis
CAMK2	Calcium/calmodulin-dependent protein kinase 2
CamKIV	Calcium/calmodulin-dependent protein kinase 4
cDNA	complementary DNA
CeA	Central amygdala
CEUA	Ethics committee on animal use (*Comissão de ética no uso de animais*)
cFOS	Proto-oncogene c-Fos
CONCEA	National council for the control of animal experimentation (*Conselho nacional de controle de experimentação animal*)
CORT	Corticosterone
CRE	Cyclic recombinase
CREB	cAMP response element-binding protein

CRF	Corticotropin-releasing factor
CRH	Corticotropin-releasing hormone
Chrna2	Cholinergic receptor nicotinic alpha 2 subunit
CRISPR	Clustered regularly interspaced short palindromic repeats
Ct	Cycle threshold
DEPC	Diethyl pyrocarbonate
DG	Dentate gyrus
dHipp	Dorsal hippocampus
DMN	Default mode network
DMT	Dimethyltryptamine
DOI	2,5-dimethoxy-4-iodoamphetamine
DSM	Diagnostic and Statistical Manual of Mental Disorders
EGR-1	Early growth response 1
EPM	Elevated plus maze
EPSP	Excitatory postsynaptic potential
ER	Endoplasmic reticulum
FFPE	Formalin-fixed, paraffin-embedded
GAD	Generalized anxiety disorder
GAPDH	Glyceraldehyde-3-phosphate dehydrogenase
GC	Granule cell
GOI	Gene of interest
GPCR	G protein–coupled receptor
GRIN2A	Glutamate Ionotropic Receptor NMDA Type Subunit 2A
HCN	Hyperpolarization-activated cyclic nucleotide-gated
Hif-1	Hypoxia-inducible factor-1
HPA	Hypothalamic-pituitary-adrenal
ICV	Intracerebroventricular
IEG	Immediate early gene
$\boldsymbol{I_h}$	Hyperpolarization-activated current
iHipp	Intermediate hippocampus
ilPFC	Infralimbic prefrontal cortex
IL	Infralimbic
IP	Intraperitonial

IP3R	Inositol 1,4,5-trisphosphate receptor
ISI	Interspike interval
LCM	Laser capture microdissection
LFP	Local field potential
LMD	Laser microdissection
lncRNA	Long noncoding RNA
LPC	Laser pressure catapulting
LSD	lysergic acid diethylamide
LTP	Long-term potentiation
MAOI	Monoamine oxidase inhibitor
MC	Martinotti cell
MDD	Major depressive disorder
MDMA	3,4-methylenedioxymethamphetamine
MIQE	Minimum information for publication of quantitative Real-Time PCR experiments
miRNA	Micro RNA
mPFC	Medial prefrontal cortex
mRNA	Messenger RNA
mTOR	Mammalian target of rapamycin
mTORC1	Mammalian target of rapamycin complex 1
nACHr	Nicotinic acetylcholine receptor
NF-κB	Nuclear factor kappa-light-chain-enhancer of activated B cells
NMDA	N-methyl-D-aspartate
NMDG	N-methyl-D-glucamine
***N*,*N*-DMT**	N,N-dimethyltryptamine
NPTX	Neuronal pentraxin
NR2A	N-methyl D-aspartate receptor 2A
OCT	Optimal cutting temperature
OF	Open field
OLM	Oriens-lacunosum moleculare
PBS	Phosphate buffered saline
pDips	Protected head dippings
PEN	Polyethylene naphthalate

PEX5l	Peroxisomal biogenesis factor 5 like
PFC	Prefrontal cortex
PI3K	Phosphatidylinositol 3-kinase
PL	Prelimbic
PLA_2	Phospholipase A_2
PLC	Phospholipase C
plPFC	Prelimbic prefrontal cortex
PPARγ	Peroxisome Proliferator-activated Receptor Gamma
PTSD	Posttraumatic stress disorder
RIN	RNA integrity number
R_{inp}	Input resistance
RMP	Resting membrane potential
ROI	Region of interest
RT-qPCR	Reverse transcription-quantitative polymerase chain reaction
scRNA-seq	Single-cell RNA sequencing
SEM	Standard error of the mean
SNRI	Serotonin-norepinephrine reuptake inhibitor
S1R	Sigma-1 receptor
SSRI	Selective serotonin reuptake inhibitor
TAAR	Trace amine-associated receptor
TrkB	Tyrosine receptor kinase B
TRIP8b	Tetratricopeptide repeat–containing Rab8b-interacting protein
uDips	Unprotected head dippings
UV	Ultra violet
vCA1	Ventral CA1
vhipp	Ventral hippocampus
WHO	World Health Organization
ZIF268	Zinc finger-containing transcription factor 268

List of Figures

Manuscript 3

Appendices

Appendix 1

Appendix 2

Appendix 3

Index

Rationale

Serotonergic psychedelics have been reported to mitigate anxiety and mood disorders symptoms (Nutt et al., 2020). Anxiety is an adaptive body and *mental* response to potential danger, different from the definition of fear that is a fight-or-flight response to a *real* immediate threat. Still, both of them are important evolutionary traits that help survival (Liberzon et al., 2015). Instead, an anxiety disorder is a maladaptive response to a potential threat in the future that may or may not be real. Any biological system that is engaged in uncontrolled and excessive responses, high arousal, and negative valence in such a way may lead to a decreased quality of life (Schmidt, 2018; Calhoon and Tye, 2015). According to the World Health Organization (WHO), in 2017, 13% of people around the world have developed some kind of anxiety disorder, and 31% of the total world population will have it in some moment of their lives, which is expected to make it the first leading cause of disability by 2030 (WHO, 2017; Benko and Vranková, 2020). Brazil is the leading country in anxiety prevalence, with 9.3% of the population affected. The prevalence of anxiety disorders varies by gender. Women are almost twofold more susceptible than men, something particularly seen in American women (Figure 1; WHO, 2017).

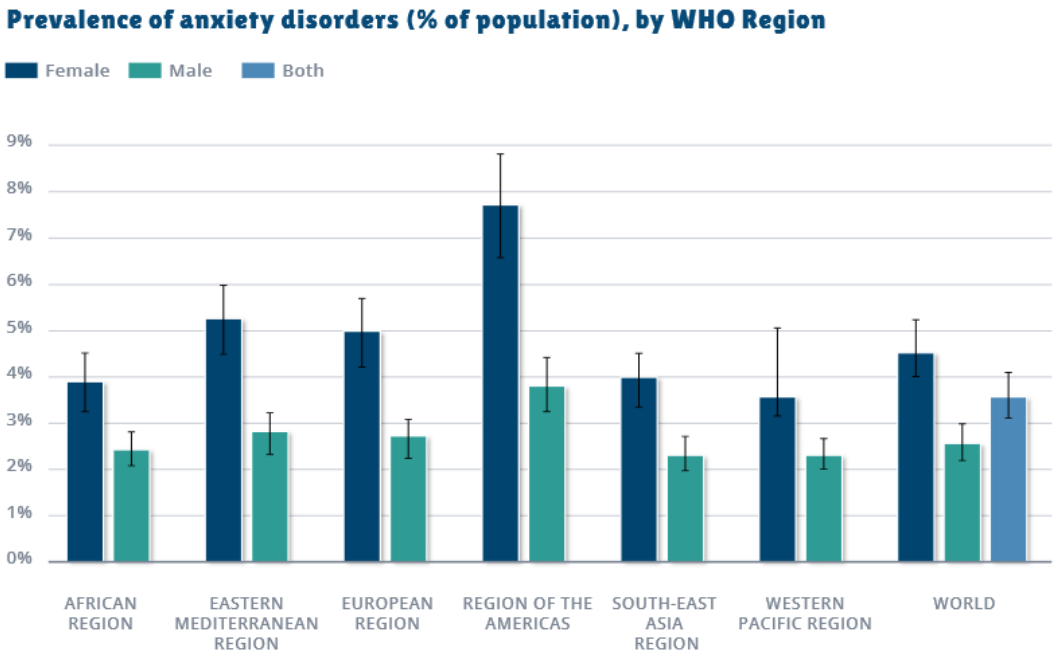

Figure 1: Prevalence of anxiety disorders by WHO region (adapted from WHO, 2017).

According to “Diagnostic and statistical manual of mental disorders” (DSM-V), several pathologies are part of the spectrum of anxiety disorders with the most common one being generalized anxiety disorder (GAD) (Terluin et al., 2014). Tachycardia, feeling short of breath, fatigue, nausea, lack of focusing, sweating, trembling, tingling or numbness in the hands or feet, with or without a feeling of cold in them, pain or pressure in the chest, muscle tension, lack or excess of sleep, lack or excess appetite and feeling on-edge or in imminent death in more acute cases are classical symptoms of GAD (Terluin et al., 2014). Considering the whole spectrum, anxiety disorder is a worldwide prevalent disabling circuitopathie among the leading causes that significantly impair people's welfare and quality of life (Liberzon et al., 2015; McGregor, 2014). However, to date, there are still no fully efficient medications to treat GAD. The selective serotonin reuptake inhibitors (SSRIs) and serotonin-norepinephrine reuptake inhibitors (SNRIs) allow mood improvement by increasing serotonin, norepinephrine, or both levels in the brain. Nonetheless, it takes about 2-4 weeks to take effect, and about 30% of patients remain refractory to the treatment, while others respond only partially (Benko and Vranková, 2020). Tricyclic antidepressants also help to get a better mood and treat physical anxiety symptoms, but with severe possible side effects. Benzodiazepines promote relaxation and reduce tension but in many countries have become a public health issue due to benzodiazepine addiction (Chang et al., 2018). Although the above-mentioned drugs have some success in treating anxiety disorders, the lack of completely adequate treatments leads to an urgent need for researchers to find alternative new potential compounds, capable of offering better treatment with fewer side effects. Here, we will focus on the potential therapeutic role of the classical serotonergic psychedelic 5-methoxy-*N*,*N*-dimethyltryptamine (5-MeO-DMT) in modulating anxiety-related brain structures.

Overview

This thesis consists of a general introduction followed by three manuscripts and a general discussion (format accepted by the Neuroscience Graduate Program). Appendices present other studies and collaborations developed along with this thesis project. The introduction is a guide-chapter on the topics of the thesis. First, focusing on the brain structures underlying the experiments developed throughout the presented manuscripts and the circuits related to anxiety. The introduction then turns to the topics of psychedelics and in particular to 5-MeO-DMT. References are related to introduction and general discussion. Each manuscript presents own references.

The first manuscript describes a new approach for the standard laser capture microdissection (LCM) protocol and RNA molecular analysis. In summary, anxiety-related structures were dissected using the LCM technique, due to the capability of precisely dissecting defined structures and avoiding interfering signals from unwanted tissue. We initially performed several tests, set protocol parameters, and then validated the experiment. Our studies revealed that by optimizing the standard protocol with a new workflow that diminishes handling and tightly controls time, we could reach a large percentage of high-quality RNA yield, 94% from a total of 70 samples, and 100% in the third experiment. These results were unexpected, as it is not that easy to find RNA with this level of purity. On the contrary, this is a challenge in the LCM technique when using mouse brain tissue, because neuronal cells and brain tissue are rich in lipids, difficulting the action of the lysis buffer (Sharma et al., 2018). An optimal protocol for laser dissection and RNA extraction is essential for the validity of these results as the quality of RNA samples can differentially alter RNA quantification, biasing the results.

The second manuscript focuses on the effects of 5-MeO-DMT, specifically regarding gene expression modulation in anxiety-related structures, and mice anxiety-related behavior. This study observes the expression of immediate early genes and late-response genes as an instantaneous response to the treatment in three anxiety-related structures (collected by the LCM optimized protocol described in manuscript 1): the anterior cingulate cortex (ACC), the basolateral amygdala (BLA) and the ventral hippocampus (vHipp). In addition, this study analyses long-term gene modulation in hippocampal structures. The genes of interest (GOI) were chosen by their broad presence in several

pathways, notably involved in synaptic plasticity. To identify emergent behavior after 5-MeO-DMT, this study presents anxiety and locomotor tests, besides evaluation of serum corticosterone levels.

A large body of evidence suggests a protagonist role of serotonergic psychedelics in anxiety and mood disorders therapy. Several reports show that patients with antidepressant-resistant depression/anxiety benefit from a single dose os these compounds (Davis et al., 2019). This long-lasting effect is possibly due to neuroprotective properties and structural plasticity (Duman and Li, 2012). Therefore, the third manuscript investigates any longer-lasting effect of 5-MeO-DMT in the electrophysiological profile of dentate gyrus neurons, i.e, persistent passive and active neuronal membrane changes 5 days after treatment. The findings reveal that 5-MeO-DMT leads to a decrease in the ventral dentate gyrus firing frequency.

Introduction

Anxiety-related structures

Several brain circuits and regions are related to anxiety and their pattern of activation differs among the subtypes of anxiety disorder. Despite the difficulties in unraveling this profusion of different circuits, some are widely known. The prefrontal cortex and limbic system are brain regions directly involved in stress and anxiety. Emotional processing stands in more evolutionary ancient parts of the cortex (Schmidt et al., 2018). The ventral hippocampus (vHipp), basolateral amygdala (BLA), and medial prefrontal cortex (mPFC) are structures required for anxiety-like behavior, but their individual role in the circuit remains unclear. Yet, understanding the neural circuits underlying anxiety is crucial for developing better treatments (Padilla-Coreano et al., 2016).

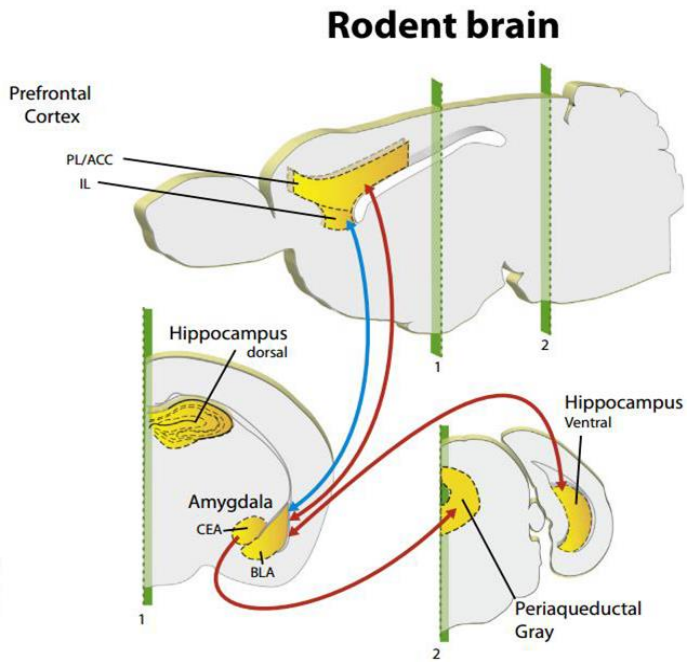

Figure 2: Schematic representation of the tripartite circuit involved in fear behaviour in humans and rodents. The first key neuronal structure is the amygdala (composed of the basolateral amygdala (BLA) and the central amygdala (CEA)); the second is the medial prefrontal cortex (mPFC) (composed in rodents of the anterior cingulate cortex (ACC), the prelimbic cortex (PL) and the infralimbic cortex (IL)). Finally, the last brain structure is the hippocampus. Red line represents schematic connectivity during expression of fear behavior whereas the blue line represents the one involved during fear inhibition (Adapted from Chaudun, 2016, apud C. Dejean et al., 2015).

Amygdala

The amygdala is a complex of several subnuclei and is considered a central structure in the regulation of emotions, fear, and anxiety-related memories. It modulates autonomic, endocrine (Hypothalamic-Pituitary-Adrenal (HPA) axis), and behavioral responses to environmental emotional inputs (Knapska et al., 2007). The literature regarding the involvement of the amygdala in anxiety is consistent, and the most studied subnuclei are the basolateral amygdala (BLA) and the central nucleus of the amygdala (CeA) (LeDoux, 2000). Several inputs trigger responses through the amygdala, which modulates behavioral arousal and implicit emotion-related memories (Janak and Tye, 2015). The basolateral and central amygdala have been implicated in aversively motivated learning, while the medial and cortical amygdala has been studied in sexual and social behaviors. Some studies have shown that activity in the basolateral and medial amygdala is correlated with anticipatory anxiety (Knapska et al., 2007).

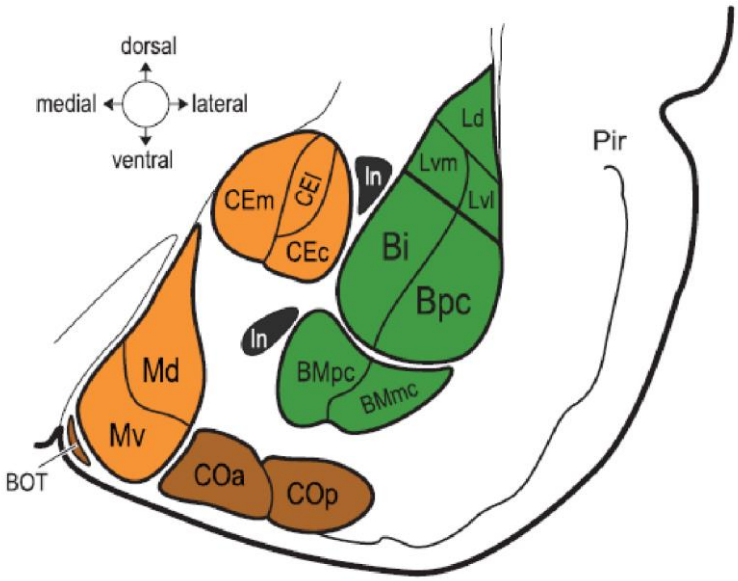

Figure 3: Nuclear divisions and subdivisions of rat amygdala. In green is the basolateral group, in brown is the cortical amygdala and in orange is the centro-medial amygdala. The intercalating nuclei are in black. The medial amygdala is divided into ventral and dorsal. The cortical amygdala has an anterior and posterior part. The central amygdala has three subdivisions, lateral, central, and medial. Finally, the basolateral group is divided into three main parts, the basomedial (magnocellular and parvocellular divisions), basal (intermediate and parvocellular subdivisions), and lateral (dorsal, ventromedial, and ventrolateral subsets) nuclei (adapted from Knapska et al., 2007).

Studies have identified increased amygdala activation and higher volume in anxious patients (Tye et al., 2011) and the hyperactivation of the amygdala is related to PTSD, social anxiety disorder, and specific phobias, besides general anxiety disorder (Schmidt, 2018).

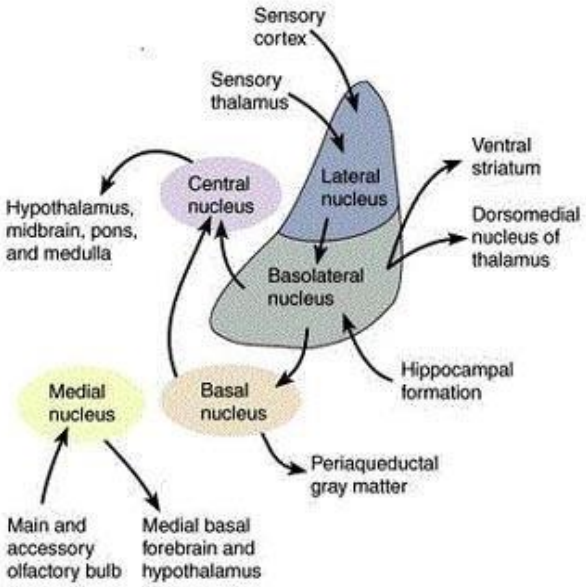

Figure 4: Diagram of the major divisions and connections of the Amygdala (adapted from Janak and Tye, 2015). The connections of the amygdala to outer brain structures are well studied (Figure 4), where the lateral nucleus of the amygdala receives information of sensory cortex and sensory thalamus while projecting to the basolateral nucleus. The basolateral nucleus, in turn, receives inputs from the hippocampus and sends innervation to the ventral striatum, the dorsomedial nucleus of the thalamus, and the central nucleus of the amygdala. The central nucleus of the amygdala is the principal amygdalar output, connecting to the hypothalamus, midbrain, pons, and medulla, (LeDoux, 2000). In short, the BLA nucleus strongly excites CeA that inhibits its central medial region (Tye et al., 2011).

The activation of BLA may enhance anxiety, corroborating studies that show increased anxiety under optogenetic activation of the whole BLA. On the other hand, the BLA projections activation to the CeA decreased anxiety, probably due to the increased inhibition of the medial central nucleus and impairing its outputs (Calhoon and Tye, 2015; Tye, 2011). In this study, we have opted to investigate the effect of 5-MeO-DMT in amygdala gene expression specifically in the BLA due to the robust data regarding the participation of BLA in anxiety-related circuits. Furthermore, the almond-shaped anatomy facilitates the identification of microdissection.

Ventral hippocampus

The hippocampus is strongly involved in memory, spatial recognition, and emotions, but it is a heterogeneous structure. There is a gradient in the dorsal /ventral longitudinal axis from cognition (dorsal) to emotion (ventral) relevant innervation. It is divided into three anatomically, physiologically, and biochemically distinct regions: dorsal (dHipp), intermediate (iHipp), and ventral (vhipp) hippocampus (Fanselow and Dong, 2010). The dorsal part is associated with learning, memory, and spatial navigation. The ventral part of the hippocampus is related to learning and memory but engaged with emotions, not spatial navigation, and connects to the prefrontal cortex and amygdala (Dougherty et al., 2012).

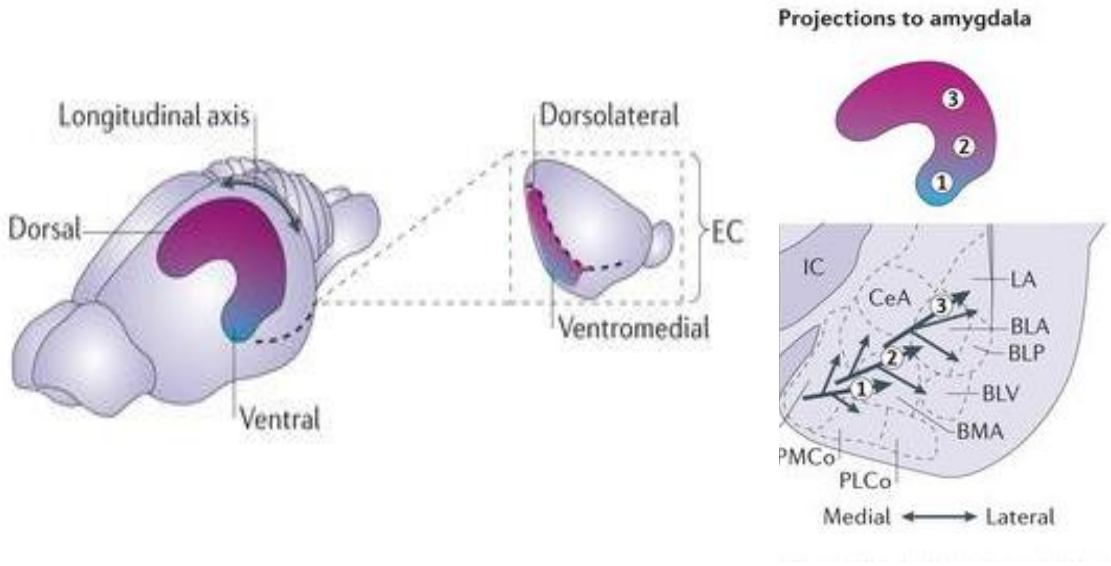

Figure 5: Extrinsic connectivity gradients in mouse hippocampus (adapted from Strange et al., 2014). Dorsal and intermediate hippocampus project to basolateral amygdala, ventral hippocampus projects to medial, cortical, and basomedial amygdala.

Ventral hippocampus connections to the amygdala facilitate the link between fear and anxiety behaviors (Felix-Ortiz et al., 2013). The vhipp projections to the hypothalamus control the hypothalamic-pituitary-adrenal axis (HPA axis) (Tye et al., 2015). Internally, studies point to CA1 and CA3 as important areas for fear conditioning (Hunsaker and Kesner, 2008) and the ventral dentate gyrus is related to the expression of anxiety-like behaviors (Tye et al., 2011; Tye et al., 2015). The third manuscript analyzes long-lasting changes in the ventral dentate gyrus electrophysiological profile.

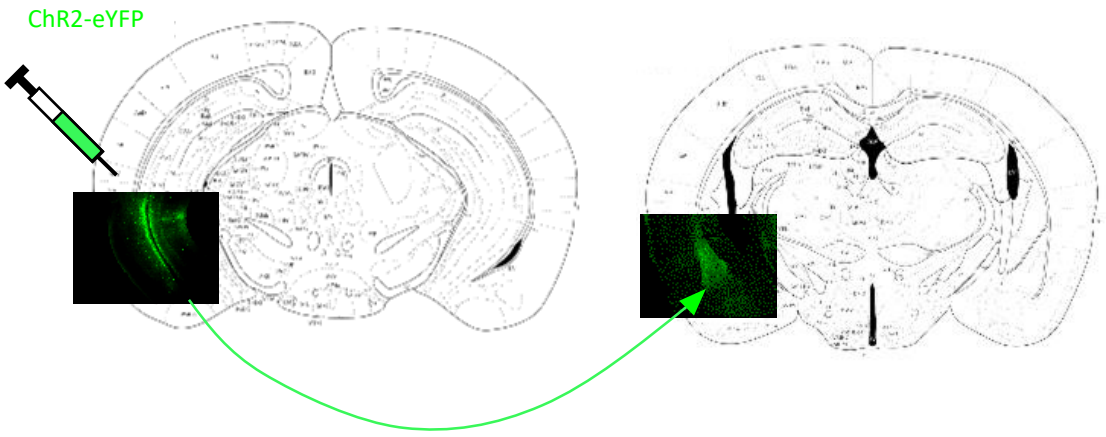

Figure 6: Anterograde tracing injection from vHipp to BLA (Nogueira, 2018; unpublished data). Intermediate and ventral hippocampal projects to basolateral and basomedial amygdala.

Anterior cingulate cortex

Initially, it is important to highlight the anatomy analogous to humans and mice, specifically for the mPFC. Inconsistencies in the determination of anatomical limits and the nomenclature may complicate interpretations of results across species, and hinder comparison of data. The mouse mPFC has three main subregions: the anterior cingulate cortex (ACC), prelimbic (plPFC), and infralimbic (ilPFC). Their human analogous are Broadmann areas 24b, 32, and 25, respectively (McKlveen et al., 2015; Laubach et al., 2018).

The prefrontal cortex contains higher cognitive regions related to thinking, planning, and socializing. The ACC is involved in associative and fear memory formation and expression, as well as pain sensation. It is implicated in anxiety disorders, together with other structures, such as the BLA and the vHipp (Ressler, 2020). While the amygdala increases the volume, anxiety-suffering patients presented a reduction in ACC volume (Ortiz et al., 2019).

Anxiety-related circuits

Connections among mPFC, BLA, and vHipp are related to innate anxiety and learned fear (Padilla-Coreano et al., 2016), although the connectivity of the vHipp-mPFC-BLA circuit is complex. The ventral hippocampus and mPFC project to the CeA, that is related to defensive behaviors (Adhikari, 2014; Adhikari et al., 2011). They are also engaged in the evaluation of threats. The amygdala receives projections from mPFC, vHipp, and the Bed Nucleus of Stria Terminalis (BNST). Altogether, the vHipp-mPFC-BLA circuit works synergistically to evaluate threats and generate defensive responses (Adhikari et al., 2011).

The output of hippocampal network activity can often be recorded as local field potentials (LFP), where neural electrical activity is defined by oscillations in LFP. Theta and gamma oscillations are the most studied frequencies and it has been shown that in rodents, vHipp-BLA and BLA-mPFC synchronize in the theta frequency (4-12 Hz) during fear and anxiogenic events (Padilla-Coreano et al., 2016; Adhikari, 2014; Mikulovic et al., 2018) corroborating to clinical findings showing disruption of theta oscillations under anxiolytics treatment (McNaughton and Gray, 2000; Adhikari, 2014). Our group has previously shown that the specific theta 2 frequency (4-6 Hz) correlates to anxiety-like behavior in mice (Mikulovic et al., 2018; Winne et al., 2020). Also, the inhibition of inputs from vHipp to the mPFC disrupts theta-frequency but conserves other frequencies (Padilla-Coreano et al., 2016). BLA-vHipp projections under optogenetic stimulation increase anxiety. On the contrary, the inhibition of this pathway is anxiolytic (Adhikari, 2014; Felix-Ortiz, 2013). Long-term experience of anxiety leads to changes in specific brain structures. Locally, anxiety triggers the hyperactivation of the amygdala, increasing its volume in chronic states. On the other hand, individuals presented a decrease in ACC and hippocampal volume under anxiety conditions (Ortiz et al., 2019). Hippocampus is most likely involved in multiple processes, such as the modulation of fear responses, so its complete role in anxiety remains unclear (Liberzon et al., 2015). Besides, anxiety disorder has a hormonal component, which complicates the whole picture (Adhikari, 2014).

Since anxiety-related structures are widely interconnected and disruption in any region can affect the whole system, effective therapeutics for anxiety disorders must consider the circuit level. Therefore, plasticity mechanisms must be taken into account, as they can lead to relief and posterior mitigation of undesirable symptoms of anxiety disorders. Studying new drugs that have a neuroplasticity potential could be a promising future strategy towards the treatment of anxiety and other mental illnesses (Tye et al., 2011; Tye, 2015).

Hyphotalamic-Pituitary-Adrenal axis (HPA axis)

The hypothalamic-pituitary-adrenal axis, or HPA axis, is a set of three main structures involved in stress control. The hypothalamus and the pituitary gland are localized in the brain, while the adrenal glands are found on top of the kidneys. After an initial response mediated by the sympathetic nervous system secreting epinephrine and norepinephrine, the hypothalamus secretes the corticotropin-releasing hormone (CRH), increasing the activity of the sympathetic nervous system. The corticotropin-releasing hormone then signals to the pituitary gland to secrete the adrenocorticotropic hormone (ACTH), which reaches the adrenal gland, which in turn releases glucocorticoids, like cortisol, who helps the body to deal with many changes produced by stress. When cortisol levels are high, brain sensors in the hypothalamus and hippocampus detect and shut off the stress response, a mechanism known as negative feedback (Chrousos, 2009). However, together with neurotransmitter dysregulation, decreased neuroplasticity and chronic subclinical inflammation (which can also be triggered by HPA axis malfunction), when the HPA axis is overstimulated, it can lead to several disorders, such as anxiety and depression (Benko and Vranková, 2020).

In order to maintain the homeostatic balance, the glucocorticoids hormones produced by the HPA axis acting in the brain are beneficial for a while, but prolonged exposure can lead to deleterious effects in the emotional, metabolic, and immune systems. Therefore, glucocorticoid secretion is strongly regulated by feedback inhibition mechanisms. When stressful overloads occur in terms of intensity, predictability, and duration, allostatic regulatory systems are activated, which start to regulate homeostasis at higher levels of demand. The activation of this system generates an allostatic charge, which in excess can trigger physical and mental pathologies (Sousa et al., 2015). The neurocircuitry involved

in chronic stress has not been clearly defined. However, the literature focus on the hippocampus, the amygdala, and the prefrontal cortex as key central structures related to pathologies caused by chronic stress (Herman et al., 2016). However, regarding acute stress, an imbalance in the circuitry involved this three regions due to the deleterious effets of cortisol on hippocampal neurons would deregulate the inhibitory feedback of the HPA axis and could contribuite to the hyperactivation of the HPA axis. We have measured serum corticosterone levels in mice under acute stress after 5 days of 5-MeO-DMT treatment.

Animal models of anxiety

The concept of anxiety in non-human animals is often defined as a behavioral state induced by threatening stimuli, while in humans is a state of high arousal and the overestimation of a potential threat. Humans can report their symptoms of anxiety, different from rodents. On the other hand, one can precisely measure specific avoidance behavior in open spaces in rodents, for instance, as they are vulnerable to predators. Despite these differences, the affected circuits are similar (Sylvers et al., 2011) where humans and rodents share brain structures underlying anxiety. For example, anxiolytic drugs in humans such as benzodiazepines can also decrease the anxiety-like behavior in rodents (Adhikari, 2014). Therefore, researchers have developed many strategies for evaluating observable anxiety-related phenotypes in animals. The elevated plus maze and the open field are two historically used paradigms for studying anxiety behavior. They have shown pharmacological validity, as anxiolytic drugs, such as benzodiazepines can decrease anxiety in humans and the aversion behavior to open spaces in rodents (Adhikari, 2014).

To understand the neural circuits underlying anxiety more in-depth it is necessary to study effects on several levels, such as *in vivo*, *ex vivo*, pharmacological perturbation, and behavioral models (Tye, 2015; Adhikari, 2014). We have measured anxiety-like behavior, locomotor activity, and ethological profile in the elevated plus maze and open field experiments under 5-MeO-DMT treatment in two different time points and stress conditions (cf. Manuscript 2, figures 2-5). From a translational point of view, extrapolating animal results to humans is difficult in psychedelic research, due to natural behavioral and pharmacokinetic differences (Kelmendi et al., 2022). However, animal data indeed presents clues to unravel mechanisms of action that may become applicable to future human therapy.

Preclinical psychedelic studies

Psychedelic research is having an intense growth of studies due to the promising clinical findings of the treatment of several psychiatric disorders and effects to specific brain networks (Palhano-Fontes et al., 2015; Palhano-Fontes et al., 2015; dos Santos et al., 2018; Nutt et al., 2020; Carhart-Harris et al., 2016) . Basic and translational research are required to complement and push forward this field. In the very last years, we have seen a profusion of new centers for psychedelic research in the US and Europe, due to the large financial incentives generated by public and private sectors. However, basic research on psychedelic substances is lacking and mechanisms of action of drugs, the signaling cascades, relevant pathways, pharmacology, biomarkers, and the reflexes on physiology and behavior need to be elucidated through tighter control of experimental parameters (Murnane, 2018; Vollenweider and Kometer, 2010). For example, molecular and cellular studies are crucial to unraveling drug binding and signaling pathways downstream, besides the neuronal pattern of activity. Studies *in vitro* and *ex vivo,* like neural tracing, single-cell electrophysiology, and calcium imaging, especially when coupled to protein and RNA evaluation, can improve the understanding of the neurobiology of psychedelics. In addition, animal models are important elements in the drug discovery process and the effect on neuropathologies. Studies *in vivo* add to the understanding of neurophysiology and brain activity where electrophysiology, optogenetics, chemogenetics, brain microdialysis, calcium imaging, assessment of biomarkers, and behavioral patterns allow for a more detailed assessment of neural circuits.

It is important to highlight that the preclinical animal approach has limits in psychedelic research, as animals cannot tell us or even have experiences like “ego dissolution”, “absence of perception of time”, sense distortions, feelings of “completeness”, and it is impossible to assess the entheogenic characteristics of these drugs. The absence of the expected sequence of research, from preclinical to clinical trials is probably due to the traditional use of these substances, for religious, therapeutics, or recreational purposes, which makes them old acquaintances of mankind. Nonetheless, the difficulties in the study with animals can contribute to this mismatch in science. However, it seems that preclinical studies in psychedelic science will see a major boost in the upcoming years, considering their notable potential to expand our knowledge and contribute to translational research and consequently, to clinical therapeutics.

Serotonergic psychedelics

Psychedelic compounds have been used for thousands of years in the context of healing, religiosity, and recreational purposes (Aday et al., 2020). These substances act directly in the brain, shifting consciousness, cognition, and emotions. Perceptiveness, the concept of self, connection with the whole, besides greater feelings of gratitude, pure love, detachment and acceptance, among others, emerge under drastic changes in brain circuits, alleviating symptoms of anxiety and mood disorders and increasing spirituality (Aday et al., 2020). Serotonergic psychedelics have a similar mechanism of action based on affinities by several types of neurotransmitter serotonin (5-HT) receptors (dos Santos et al., 2021), which is tied to positive mood. In 1938, Albert Hoffmann synthesized the molecule of LSD for the first time, but in 1943, he discovered its effects (Nichols et al., 2017). From then on, the recreational use has spread across much of the US, driven in part by the neuroscientist Timothy Leary, an enthusiast, in the mid-1960 (Pollan, 2018). The North American counterculture movement caught the attention of politicians at the time who linked it to defections during the Vietnam War. Than, a real war against psychedelics began, demonizing them and creating the image of highly dangerous substances. In 1968, LSD was banned and in 1971 they became part of schedule 1, a list of prohibited substances for use and sale in the US that also contains psilocybin, DMT, mescaline, 5-MeO-DMT, MDMA among others. With the ban, psychedelic research was practically extinct (Pollan, 2018). However, the nineties have seen a renaissance of psychedelic science.

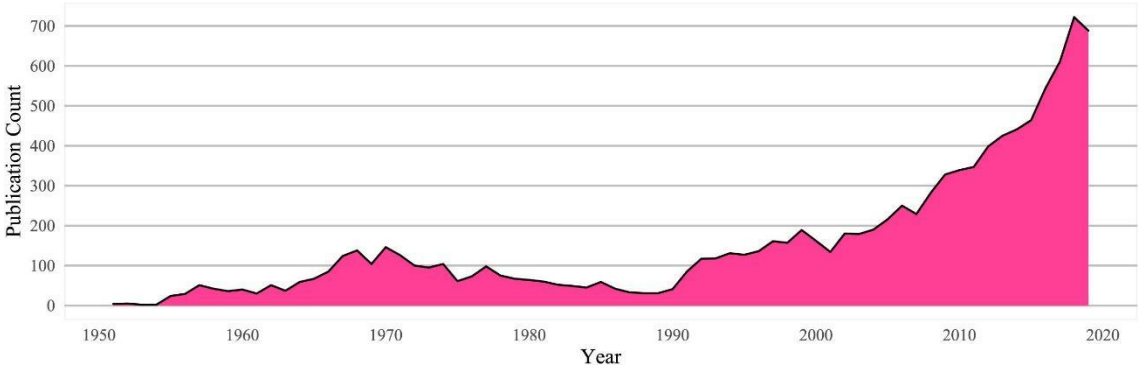

Figure 7: Web of science psychedelic publication count by year (Adapted from Petranker, 2020).

Nowadays, psychedelic research is growing and moving towards a consensus that they bring numerous benefits to the brain and mental health. (Benko and Vranková, 2020; Cameron et al., 2020). In this way, serotonergic psychedelics are getting attention due to growing evidence pointing to their therapeutic capabilities against anxiety and mood disorders, often with a single dose.

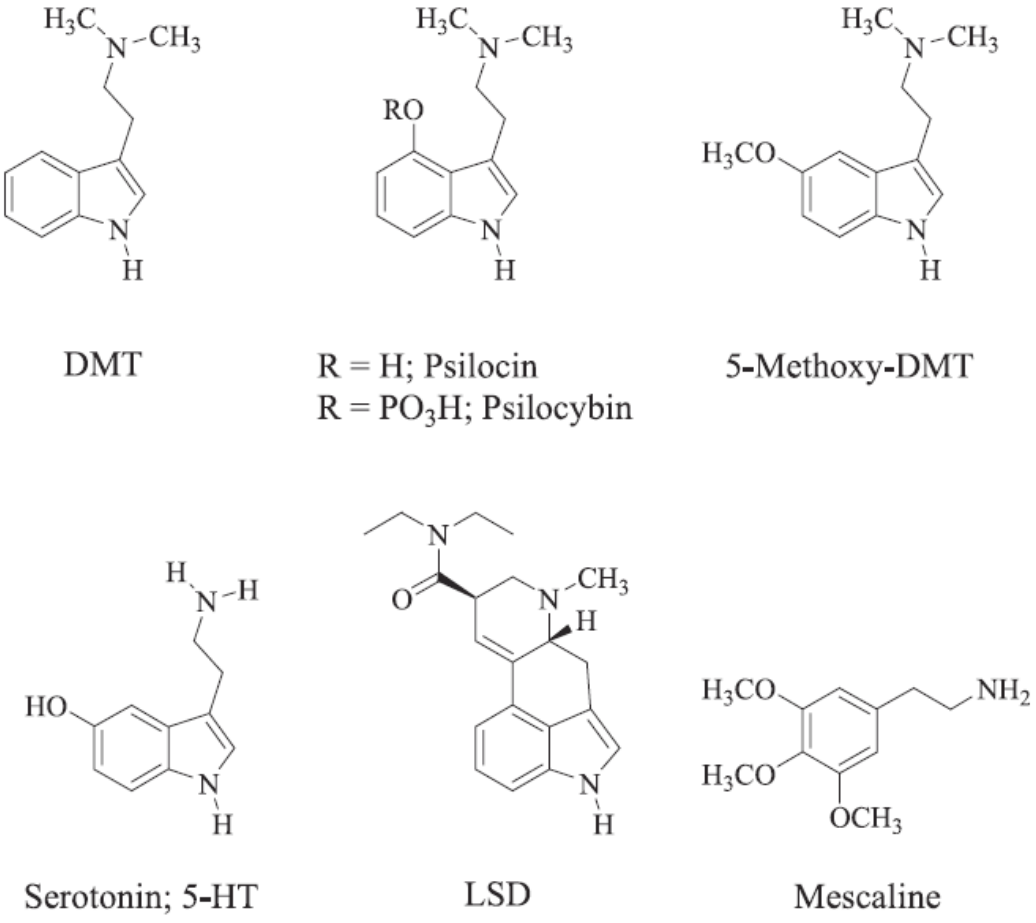

Figure 8: Molecular structure of different psychedelics (adapted from Nichols, 2004).

5-MeO-DMT

The target of this thesis, 5-methoxy-*N*,*N*-dimethyltryptamine (5-MeO-DMT) is a classic serotonergic psychedelic found in numerous plants, such as the *Dictyoloma incanescens*, and mostly in the venom produced in the skin and the parotid glands of the Bufo Alvarious, the Colorado River toad. It has been reported that this potent compound can be produced synthetically and endogenously in mammalians, and is about 5-10 times stronger than *N*,*N*-DMT (Uthaug et al., 2019; Barsuglia et al., 2018). Studies have shown that with just a single dose, 5-MeO-DMT is capable of triggering sensations of ego dissolution, increasing satisfaction, creativity, non-judgement and awareness in life at the same time that decreases symptoms of depression, PTSD, anxiety and stress sustainably after a single dose (Aday et al., 2020; Uthaug et al., 2019).

Pharmacology

The 5-MeO-DMT chemical structure is analogous to *N*,*N*-DMT, melatonin, and serotonin (5-HT) (Nichols et al., 2017). It acts as a 5-HT receptor agonist (Davis et al., 2018; Shen et al., 2010), activating 5-HT1A and 5-HT2A receptors, with higher affinity for the 1A receptor subtype (Davis et al., 2018). Regarding the effects on neuronal excitability, 5-HT2A receptors are mainly excitatory while 5-HT1A activation mainly promotes inhibition and reduces firing (Rojas et al., 2016; Polter et al., 2010; Carhart-harris and Nutt, 2017). 5-MeO-DMT has also been suggested to inhibit reuptake of serotonin (Davis et al., 2018). Metabotropic 5-HT2A receptors are mostly expressed at dendrites of layer V pyramidal cells in the PFC, and the stimulation increases the excitatory postsynaptic potentials (EPSPs) (Benko et al., 2020). On the other hand, the activation of metabotropic 5-HT1A receptors, mostly expressed at the proximal dendrites, generates local inhibition (Savalia et al., 2021). Previous study revealed that 5-MeO-DMT disrupts oscillatory activity in the PFC, likely through 5-HT1A receptors (Riga et al., 2018; Lukasiewicz et al., 2021). The integration of 5-HT1A and 5-HT2A receptors has been hypothesized to modulate PFC activity (Savalia et al., 2020; Benko et al., 2020). The stimulation of 5-HT1A and 5-HT2A receptors by 5-MeO-DMT also modulates the glutamatergic and dopaminergic systems associated with anxiety, depression and addiction (Barsuglia et al.,

2018). Furthermore, the activation of another serotonin receptor, the 5HT7, suggests to induce addiction remission, specifically in alcohol abuse (Barsuglia et al., 2018).

In summary, 5HT-2A receptors are suggested to modulate cross-cortical information by affecting pyramidal cells, mainly in layer 5 (Nutt et al., 2020). Pyramidal cells integrate functions and have a high expression of 5HT-2A receptors (Savalia et al., 2021; Olson, 2018). Psychedelic stimulation of pyramidal cells is suggested to disrupt cross cortical communication, which breaks down the ongoing patterns of neuronal activity, allowing different patterns of thoughts, emotions and behavior (Alamia et al., 2020). Psychedelics can thereby disrupt undesirable thoughts. Mental conditions and disorders related to rumination of thoughts are particularly affected by cross-cortical information (Nutt et al., 2020).

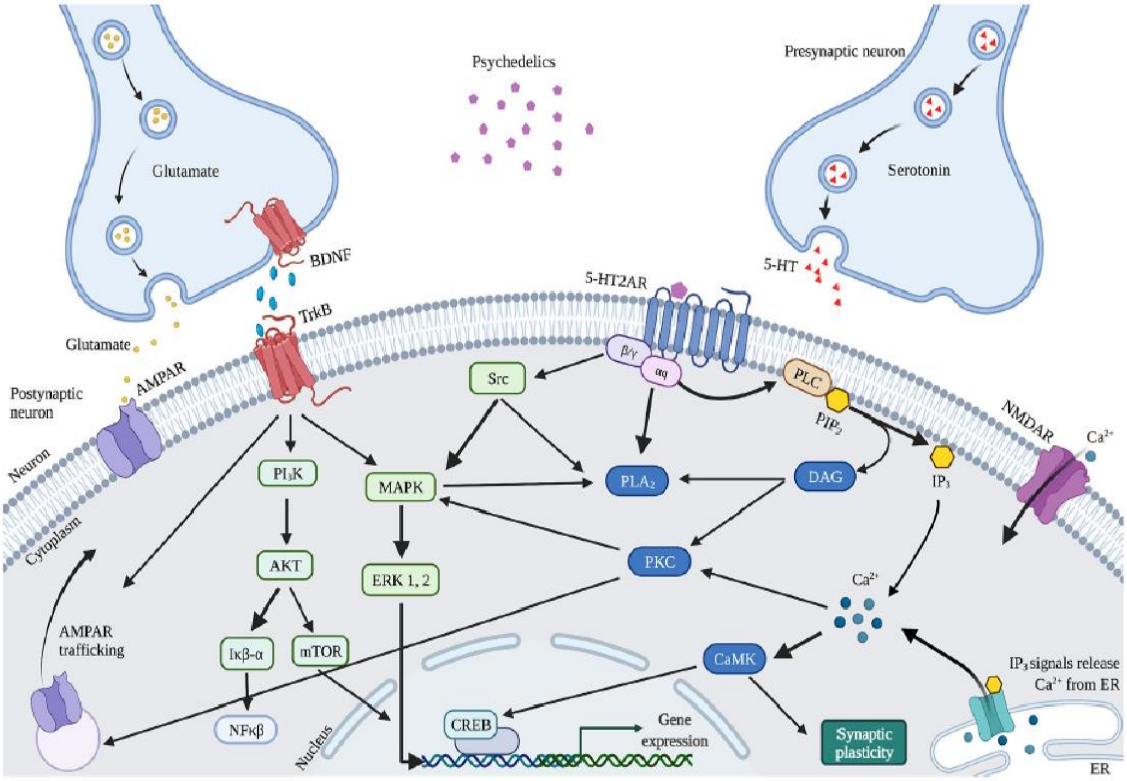

Figure 9: Scheme showing 5-HT2A activation by psychedelics and proposed mechanism of action of cellular and molecular effects of serotonergic psychedelics. 5-HT2A coupling to g-proteins leads to activation of PLC or PLA_2 signaling, further reaching synaptic plasticity.TrkB receptor, when activated by BDNF, also activates mTOR leading to stimulation of synaptic plasticity. Glutamate activation through NMDA and TrkB receptors also triggers AMPA receptor membrane availability (adapted from de Vos et al., 2021).

The psychedelic mechanisms of action are not believed to be based on 5HT-receptors overstimulation, as this could trigger a serotonergic syndrome (mild or life-threatening alterations in the mental status, neuromuscular abnormalities and autonomic hyperactivity), but possibly through their neuroplasticity stimulation. 5HT-2A controls pyramidal cell activity and their activity is closely related to the number of synaptic spines (inputs) they have (Nutt et al., 2020).

Regarding signaling cascades, the canonical 5-HT2 receptor pathway is through Gαq signaling, activating phospholipase C (PLC) and stimulating inositol phosphate production and activation of protein Kinase C (PKC) (Canal, 2018a). In addition, 5-HT2 increases channels responsible for Ca^{2+} releasing on cell membranes or the inositol phosphates (IP3) receptors on endoplasmic reticulum (ER) (figure 9, 10).

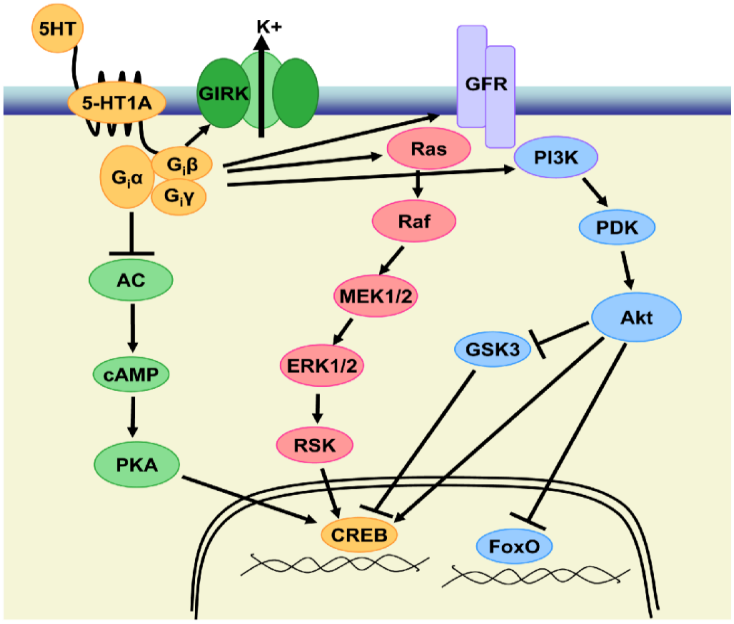

Figure 10: 5-HT1A Receptor signaling pathways (adapted from (Polter and Li, 2010).

With lower affinity, DMT and 5-MeO-DMT are agonists for the sigma-1 receptor (Fontanilla et al., 2009; Szabo et al., 2016; Inserra et al., 2021; De Gregorio et al., 2018), a chaperone found in the endoplasmic reticulum membrane that migrates to the cell membrane and binds to voltage-gated ion channels, modulating their activity (Inserra, 2018). These properties control homeostasis, because sigma-1 helps other proteins in the folding and if there is no correct transcription, in destroying the protein, causing apoptosis. It has a protective function and modulates the activity of noradrenergic, serotonergic, dopaminergic and glutamatergic (through NMDA-receptors) systems. The

activation of sigma-1 leads to a regulation of synaptic transmission through the L-type Ca^{2+} channel modulation, Na^{+} channel downregulation diminishing firing rate and K^{+} channel inhibition increasing the neuron excitability. Sigma-1 is related to several functions and disorders, such as memory, learning, stress, anxiety and depression (Kourrich et al., 2012; Inserra, 2018). Thereby, sigma-1 receptor may have a role in neuroplasticity activated by the 5-MeO-DMT agonism (Lukasiewicz et al., 2021). Also, BDNF though TrkB receptor and mTOR signaling pathways have been reported to trigger neuroplasticity under psychedelics activation (Ly et al., 2018; De Gregorio et al., 2021; Inserra et al., 2021; Lukasiewicz et al., 2021)) and modulates 5-HT system leading to antidepressant and anxiolytic effects (JiaWen et al., 2018). Also, the activation of sigma-1 increases the expression of brain-derived neurotrophic factor (BDNF) possibly through NR2A (subunit 2A of NMDA) pathway, that regulates synaptic plasticity (Xu et al., 2017) (figure 11). In other words, 5-MeO-DMT has affinity for 5HT1A, 5HT2A, and sigma-1 receptors, where the Sigma-1 receptor also regulates the BDNF pathway, which in its turn also can regulate the 5-HT system, in a positive-feedback loop. Moreover, a Sigma-1 agonist, PRE084, has previously been shown to prevent decline of BDNF, NR2A, CamKIV and mTORC1 (transducer of regulated CREB activity) and to improve the expression of BDNF, an important factor in controlling anxiety behavior (Xu et al., 2017). Considering the whole picture, it is possible to hypothesize that 5-MeO-DMT acts on receptors in a synergistic way to modulate neurotransmission and neuroplasticity.

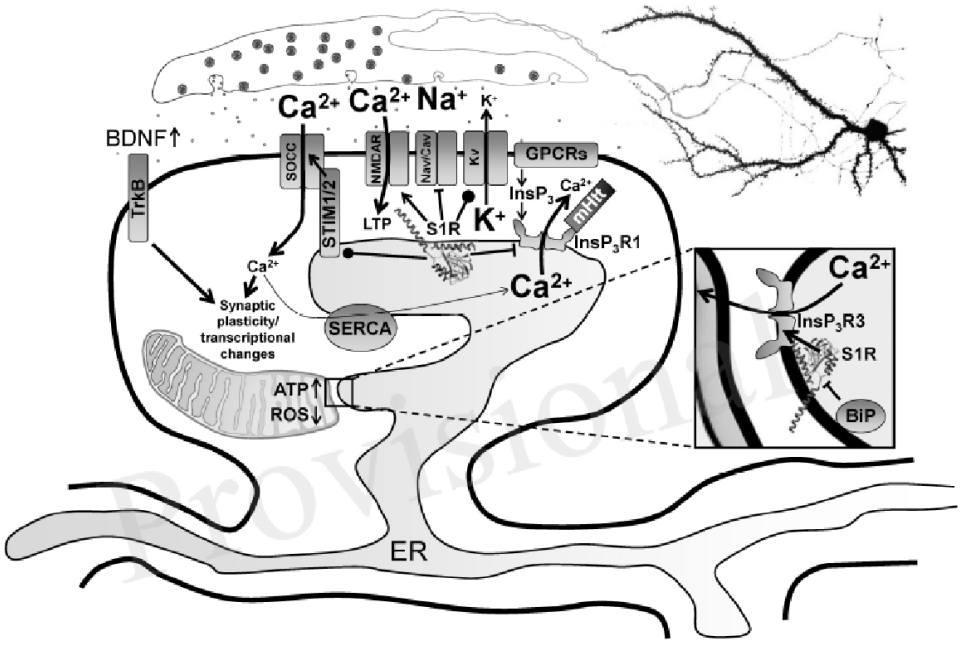

Figure 11: Sigma-1 Receptor signaling pathways (adapted from (Ryskamp et al., 2019).

Psychedelic plasticity-induction

Drugs capable of plasticity-induction have therapeutic potential by leading to a rearrangement in brain circuits (Olson, 2018) and recent studies have pointed to a role of serotonergic psychedelics in synaptic plasticity (Ly et al., 2018; Olson, 2018; Shao et al., 2021; de Vos et al., 2021; Lukasiewicz et al., 2021). Psychedelic compounds have shown promising results compared to conventional treatments, mainly because they are mostly single-dose treatments with long-lasting effects (Palhano-Fontes, 2019). In humans, chronic anxiety and major depressive disorder (MDD) present retraction and loss of dendritic spines in regions such as PFC and hippocampus and such changes in circuitry may lead to maladaptive behavior (Olson, 2018; Duman and Li, 2012). Brain-derived neurotrophic factor (BDNF) is anxiolytic when applied as an infusion into the PFC or hippocampus directly, however with no systemic efficacy *in vivo* (Olson, 2018). The relative expression of BDNF is increased under traditional antidepressant treatment and leads to increased plasticity. Psychedelics are small molecule compounds able to easily cross the blood-brain barrier and promote sustained changes in behavior most likely due to rapidly trigger circuit-induced plasticity (Olson, 2018; Inserra et al., 2021). A previous study reported that serotonergic psychedelics could promote neuritogenesis and/or spinogenesis both *in vitro* and *in vivo*, apparently induced by the stimulation of TrkB, mTOR and 5-HT2A signaling pathways (Ly et al., 2018). Another study has shown through two-photon microscopy imaging *in vivo* that a single dose of psilocybin increases approximately 10% spine size and spine density in the mouse ACC, results that were persistent up to one month later (Shao et al., 2021). A recent systematic review revealed biological underpinnings of serotonergic psychedelics and neuroplasticity (de Vos et al., 2021). Specifically regarding 5-MeO-DMT, an *in vitro* study has shown acute effects where 5-MeO-DMT (13µM applied to brain organoids, cultured brain tissue, for 24 hours) stimulated synthesis of proteins related to NMDA and AMPA receptors pathways (Dakic et al., 2017). Another *in vitro* study reported plasticity-related changes under 5-MeO-DMT treatment, where a single intracerebroventricular dose (100µg/µl) of 5-MeO-DMT stimulated neurogenesis and spinogenesis in mice hippocampal granule cells (Lima da Cruz et al., 2019). However, there is a need to increase the amount of specific *in vivo* studies on the potential of 5-MeO-DMT to induce neuroplasticity. We evaluated whether 5-MeO-DMT modulates plasticity-related gene expression in the mouse brain (cf. Manuscrip 2, figure 1).

Objectives

The main objective of this thesis was to investigate molecular, cellular and behavioral effects of 5-MeO-DMT in mice.

The specific objectives of this study were as follows:

1. Optimize methods of RNA extraction to study how 5-MeO-DMT treatment alters plasticity-related genes.
2. To evaluate immediate and long-term effects of 5-MeO-DMT treatment on plasticity-related gene expression in mouse brain anxiety-related structures (anterior cingulate cortex, basolateral amygdala and ventral hippocampus).
3. To assess physiological and behavioral characteristics of 5-MeO-DMT-treated mice.

Manuscript 1

This manuscript describes the optimization for high-quality RNA in mouse brain tissue collected by Laser Capture Microdissection (LCM). It is submitted for publication in Current Protocols in Molecular Biology. LCM is a powerful technique that allows the harvesting of single cell populations from within their anatomical locus, and combined with RNA extraction can give high quality genetic information. This manuscript is submitted as a preprint in the bioRxiv under number BIORXIV/2021/458265.

Laser Capture Microdissection optimization for high-quality RNA in mouse brain tissue

Margareth Nogueira[1], Daiane CF Golbert[1], Richardson Leão[1]

1. Neurodynamics Lab, Brain Institute, Federal University of Rio Grande do Norte, Natal, Brazil

Laser Capture Microdissection (LCM) is a method that allows the selection and dissecting of well-defined structures, specific cell subpopulations, or even single cells from different types of tissue to extract DNA, RNA, or proteins. Its precision allows the dissection of specific groups of cells avoiding unwanted signals from unwanted cells. However, despite its efficiency, several steps can affect the sample RNA integrity. RNA instability represents a challenge in the LCM method and low RNA integrity can introduce biases as different transcripts often have different degradation rates. Here we describe an optimized protocol to provide good concentration and high-quality RNA in specific structures: Dentate Gyrus and CA1 in the hippocampus, basolateral amygdala and anterior cingulate cortex of mouse brain tissue.

Keywords: Laser capture microdissection, high-quality RNA, RNA integrity, mouse brain tissue.

INTRODUCTION

Quantification of gene expression based on RNA has been primarily used for neuron profiling. However, advances in sequencing techniques allowed the widespread usage of RNA quantification in assessing neuronal plasticity (Maag et al., 2015), the effect of psychotropics in specific pathways (Ly et al., 2018) and neurological diseases (Gallo et al., 2018). Nevertheless, RNA-based gene quantification is hampered by the RNA degradation (Reiman et al., 2017). To make matters worse, degradation affects transcripts differently, generating a bias in gene quantification (Reiman et al., 2017). Hence, extraction of high-quality RNA is critical in gene quantification studies, especially when changes in expression are minute (e.g. changes in gene expression after long-term potentiation induction; Maag et al., 2015). In this work, we describe an optimized Laser Capture Microdissection protocol for acquiring high-quality RNA from specific structures in the mouse brain tissue. LCM method permits precise isolation of single cells or groups of cells from heterogeneous tissues to extract DNA, RNA, or proteins for

further analysis through RT-qPCR, sequencing, or proteomics studies, among others. It is a powerful tool that leads to an experimental refinement, allowing more accurate results due to the collected material specificity (Sonntag and Woo, 2018; Erickson et al., 2009). This ability to acquire defined regions or cell types eliminates the transcriptional background noise of unwanted tissue leading to a localized analysis of gene expression. LCM allows single cell resolution but a larger quantity of RNA can be obtained by dissecting several cells based on morphology or expressing a specific genetic marker (expressing a fluorescent reporter). As LCM does not require dissociation, information on precise cell location within the brain is not lost. However, due to the specificity of LCM, isolating high-quality RNA often still represents a challenge, because RNA is an unstable molecule, susceptible to degradation by a wide variety of RNases, both endogenous and exogenous (Mahalingam, 2018). This is a common reason for failing experiments. Tissue manipulation, LCM process, and RNA extraction have a lot of critical steps that can affect RNA integrity. RNase is present in large quantities in human skin and is difficult to inactivate. Everything that contacts human skin will be contaminated, and can destroy the RNA quickly (Nichols et al., 2008; Morrison et al., 2012; Garrido-Gil et al., 2017; Meda et al., 2019). Therefore, preserving RNA integrity is crucial for the success of the research and some cautions are required (Schaeck et al., 2016). Endogenous control of RNase is mainly done by low temperatures. Exogenous control is more complex, and depends on a wider range of actions. We have optimized critical steps and adapted the workflow of the basic LCM protocol to minimize handling, transport, and temperature variation on the samples to obtain high-quality RNA for gene expression analysis in different structures, as the hippocampus, amygdala, and anterior cingulate cortex from mouse brain sections. It is important to highlight that the LCM protocol presented here allows the analysis of gene expression in several mammalian brain structures and not only in adult mice but also in embryonic stages. In order to validate this new protocol to reach a good quality of the LCM-derived RNA, we performed three independent experiments. We analyzed the BDNF gene expression in three different regions of the mouse brain with RT-qPCR ranging from one hour, five hours, and 5 days after two different treatments. The result of our quality control presented a total of 94% of high-quality RNA in 70 samples, obtained under a bioanalyzer device. 18 samples obtained RIN = 10, totalizing 26%. This optimized protocol can be useful for experiments using microdissected mouse brain tissue, resulting in RNA with a high degree of purity.

STRATEGIC PLANNING

Before starting the acquisition of samples, there are many solutions, material decontamination, brain dissections, and LCM settings to be prepared. All of this work can be done previously or a day in advance to avoid work overload, since cryosectioning, staining, and microdissection are time-consuming processes that are required to be performed carefully to prevent any contamination and RNA degradation. Our workflow starts with cleansing RNase free, then cryosectioning followed by staining/fixation, and finally the LCM collecting sample. As soon as the first slide of tissue is ready to use, it is taken to the LMC system for microdissection and only after that, the second slide will be cut. During this period, the brain stays in the cryostat, protected from RNase at -20 ^{o} C. In other words, we only prepare the subsequent slide after collecting the previous one. This new approach avoids excessive manipulation and exposure to RNase preventing consequent RNA degradation. We work continuously for at least 8 slides, where each slide contains 6 to 8 slices. Each slide sample takes between 50 minutes and one hour to be acquired (10-15 minutes for cryosectioning / staining / dehydration and 40-45 min on LCM system). After cutting and catapulting, we transfer the isolated tissue to a collection tube inserted in an icebox. After 8 – 10 repetitions, that is, 8-10 slides with 6 – 8 slices, we spin down the amount collected and store it in the -80^{o}C freezer for further RNA extraction (Fig 1).

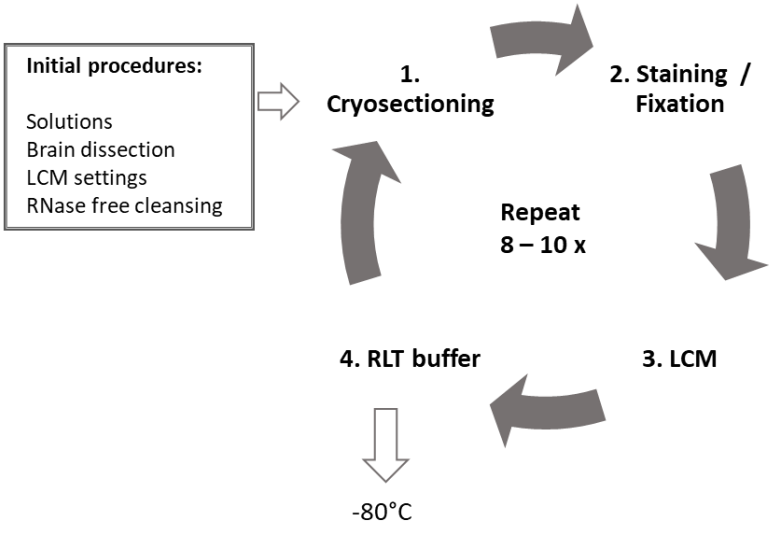

Figure 1. Schematic workflow for the experiment of isolating subpopulation regions from the mouse brain using the LCM technique. The initial procedures are listed as previous work in the box, and the following steps include 1. Cryosectioning, 2. Staining/Fixation, 3. LCM, 4. Transfer collected tissue to collection tube with RLT buffer, repeated from 8 to 10 times, to each sample. The collected samples are stored in the -80° C until posterior RNA extraction.

LASER CAPTURE MICRODISSECTION OF MOUSE BRAIN TISSUE

The following protocol for LCM employs the PALM MicroBeam laser microdissection and catapulting system (Fig 2A). Although the procedure collected dentate gyrus, CA1, amygdala, and anterior cingulate cortex tissue, this method can be used for a variety of regions in brain tissue, without modifications. It is not applicable for Formalin-Fixed Paraffin-Embedded (FFPE) sections.

Materials List

Materials

1. PEN Membrane Slides (P.A.L.M.microbeam)
2. PALM adhesive cap tubes (Carl Zeiss)
3. RNeasy Micro kit (QIAGEN)
4. Cryostat blade
5. Falcon tube RNase free 50mL
6. Pipettes
7. Filtered tips RNase free
8. RNase free tips
9. Tubes RNase free (Eppendorf)
10. Amber bottle
11. Gloves and mask
12. Needles
13. Parafilm
14. Aluminum foil
15. Pen
16. Pencil
17. Storage box
18. RNase free wipes
19. Paper towels
20. Paintbrush (fine point)
21. Scissor
22. Tweezer
23. Single edge Razor Blade

Solutions

1. Violet Cresyl Acetate Solution (1% w/v)
2. Water DEPC 0.01%
3. Water DEPC 0.1%
4. PBS DEPC
5. 50% RNase free ethanol
6. 70% RNase free ethanol
7. 100% RNase free ethanol
8. RLT buffer

Equipment

1. PALM MicroBeam System (Carl Zeiss)
2. Computer
3. PALM RoboSoftware (Zeiss)
4. Cryostat
5. Fume hood
6. Microcentrifuge MiniSpin (Eppendorf)
7. Autoclave and Lab oven
8. Thermocycler
9. ABI ViiA 7 Real-Time PCR System (Applied Biosystems, NY, USA)
10. Bioanalyzer (Agilent)
11. Bioanalyzer RNA 6000 Nano assay
12. ND8000 spectrophotometer (Thermo Scientific NanoDrop Products)
13. Freezer -80^{o} C
14. Fridge
15. Timer

Initial procedures

a. Preparing solutions: *see recipes below*

b. Cleaning PEN slides
    1. Wear gloves, lab coats and a cap.

2. Wipe the PEN slides with RNase-Zap, wash with DEPC water and then put to UV (ultra-violet) dry under the fume hood for 30 minutes, or overnight at 200^{o} C in the bath or at 180^{o} C in the oven for 4 hours.

Put the slides in the UV for 30 minutes each time they will be used, even if they are previously cleaned.

The cleansing process is crucial for the maintenance of RNA integrity. Wear gloves all the time and change them frequently. Cleaning the gloves with RNase-Zap wipes is a good practice either. Before starting any procedure involving tissue samples, wipe all the instruments and equipment with 70% ethanol RNase free (with DEPC water 0.01%) and RNase-Zap (Sigma). Use certified RNase-free materials whenever possible and be sure they are well cleaned. Avoid handling the samples when it is not necessary to diminish contamination and RNA degradation (Nichterwitz et al., 2018).

Store all materials and reagents for RNA separate from others.

RNase-Zap must be used sparingly, otherwise the excess may affect the sample purity.

c. Dissection and storage of the brain

3. Wear gloves, lab coats and a cap.
4. Clean workbenches and tools with RNase free 70% ethanol. Wipe RNase-Zap on all the surfaces and materials that contact directly the sample.
5. Deeply anesthetize the mouse.
6. Decapitate and quickly dissect the brain. The dissecting process must be done in approximately 2 minutes to maintain the integrity of RNA.
7. Remove the blood excess with PBS RNase free. This step is important due to the large amount of RNase found in blood.
8. Submerge the brain in isopentane at -40 ^{o} C for 30 seconds. Use a styrofoam box with dry ice for transportation, if necessary.
9. Wrap the brain in a clean aluminum foil and store in the -80 ^{o} C freezer until cryosectioning.

d. LCM settings

We performed the LCM calibration test using the PALM RoboSoftware, from Zeiss. For cut energy, the optimal value we found was 50 and for laser pressure catapult (LPC) energy the best value was 80. During adjustment always keep the LPC energy higher than cut energy. We used magnification (5x) to draw the region of interest (Fig 2B). Before cutting and catapulting, always set up focus and energy in a piece of tissue outside your ROI. As the cell density and the extracellular matrix can vary according to the age of the animal and the brain region, it is important to highlight that these values may vary among tissues or staining procedures, so they can be used just like a first reference, and sometimes they have to be adjusted.

Cryosectioning

10. Wear gloves, coats and a cap.
11. Clean cryostat and tools with RNase free 70% ethanol. Wipe RNase-Zap on all the surfaces and materials that contact directly the sample, like brush tips and cutting blades.
12. Stabilize the brain on -20^{o} C inside the cryostat, for 30 min.
13. Organize materials for staining to keep them cold (see in staining and fixation section).
14. Number and label the slides with a pencil, pen dye may not work at cold and in stained slides.
15. Lay down some slides inside the cryostat to maintain them cold. We put in groups of three.
16. Cut 12μm slices and at the moment of transferring the sections to the slide, heat a lower part of the slide with the finger underneath the slices to favor adhesion to the cut.
17. Wait for the slide to dry inside the cryostat for 2-3 min.

Cut between 6 and 8 slices in a slide, the optimal time is between 10-15min to prepare each slide. 30 – 45 min is the optimal time in the LCM system. Slides must

not take more than one hour at room temperature, otherwise, RNA quality may be compromised, as endogenous RNases may still be active.

We strongly suggest turning on all the LCM equipment before cryosectioning to be sure that everything is working fine.

Avoid embedding the whole brain in OCT because it can cause some damage to RNA integrity. This freezing medium interferes with laser efficiency. In this protocol, we use a few amounts of OCT just to fix the brain in the cryostat where it will be at -20^{o} C until the end of the work.

We performed thickness tests, with 10µm, 12µm and 16µm. Adult mouse brain hippocampus, and amygdala tissue presented better results with 12µm thickness. These values can vary among structures due to different patterns of extracellular matrix and cell density.

Staining and fixation

18. After drying in the cryostat, soak the slide in 70% ethanol RNase free (falcon tube inserted in an icebox) for 2 min.
19. Soak the slide in violet cresyl for 30 seconds (falcon tube inserted in icebox).
20. Remove the excess of violet cresyl with paper towels.
21. Dip the slide quickly in 70% ethanol RNase free (falcon tube inserted in icebox).
22. Dip the slide quickly in 100% ethanol RNase free (falcon tube inserted in icebox).
23. Allow it drying at room temperature for 1-2 minutes.
24. Use immediately on LCM for no more than 45 min. This precaution is important for the maintenance of RNA integrity.

We followed the manufacturer orientations for staining (PALM Protocols – RNA handling, from Carl Zeiss)

Fill a big styrofoam box with ice. Organize a 50ml falcon tube with 70% ethanol Rnase free, then a 50ml falcon tube with violet cresyl, a 50ml falcon tube with 70% ethanol Rnase free to be used after violet cresyl and a 50ml falcon tube with

100% ethanol Rnase free. Let some paper towels beside the box to clean the violet cresyl excess. Control the time with a timer.

In our experience, fixation is crucial to ensure a high-quality RNA and any failure can degrade the RNA. Be sure to have clean gloves and do not touch anything unnecessarily.

Proper dehydration of tissue slices minimizes upward adhesive force between the slide and the tissue (Datta et al., 2015).

Violet cresyl shows good visualization and absorbs the laser energy, preventing damage to the cellular components (Chabrat et al., 2015; Mahalingam, 2018). In our experience, it was a good choice (Fig 2C).

High temperature degrades RNA. When the tissue is out of cryostat, at room temperature, all the solutions must be inserted on ice, to keep them cold.
RNA is quickly degraded, so it requires stringent RNase-free sterile conditions during handling and preparation with, in some cases, additional use of commercially available RNase inhibitors.

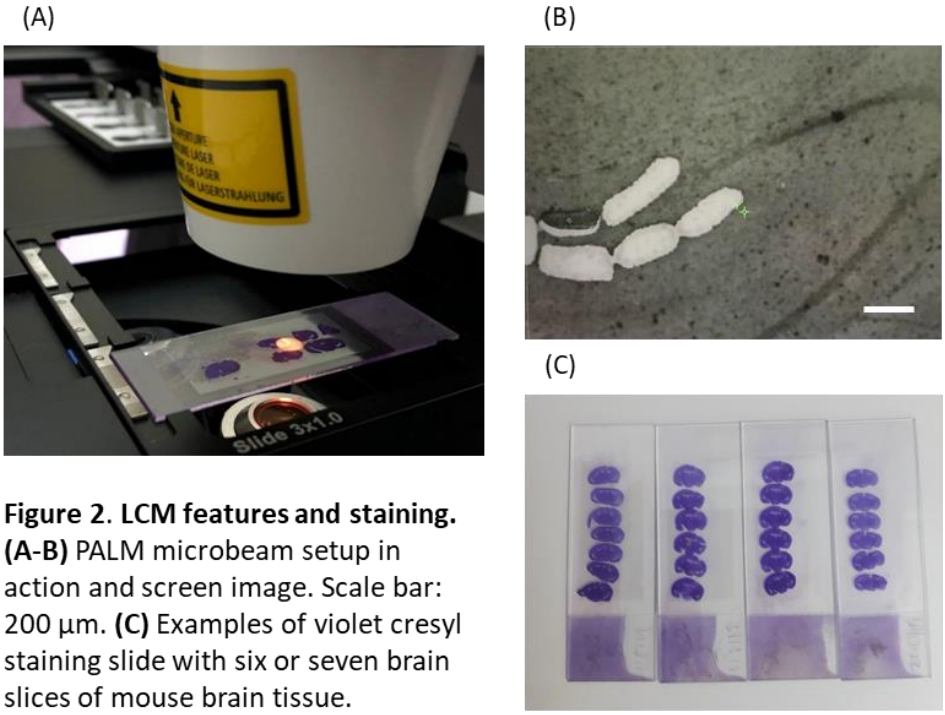

Figure 2. LCM features and staining. **(A-B)** PALM microbeam setup in action and screen image. Scale bar: 200 µm. **(C)** Examples of violet cresyl staining slide with six or seven brain slices of mouse brain tissue.

Slide storage

It is important to highlight that there is no storage before LCM in our protocol, we do not use previously frozen slides. The brain stays in the cryostat at -20^{o} C. We prepare the slide and collect the sample in sequence, one by one, as explained earlier. Time and temperature are crucial to maintaining the integrity of RNA and we consider this step fundamental to the process.

Laser Capture Microdissection (LCM)

We used a PALM MicroBeam system (Anon, n.d.). The system utilizes an inverted microscope with a focused laser beam to cut out and catapult precisely selected areas without any contact. The microdissection process was visualized with an AxioCam camera coupled to a computer and controlled by a PALM RoboSoftware, which controls a motorized stage (Garrido-Gil et al., 2017).

25. Turn on the LCM system.
26. Proceed calibration test, following manufacturer instructions. Define the best settings of cutting and catapulting energies;
27. Clean workbenches and tools with RNase-free 70% ethanol.
28. Place microtubes fixing the cap facing down at the LCM system.
29. Prepare an icebox and insert an RNase-free tube to receive collected samples. In a previous clean area, place a 10µl pipette, tip box, RLT buffer, and a needle.
30. After making the first slide, pin it on the LCM system and choose the working stage. Place slides into the slide holder with the membrane facing up.
31. Adjust the timer to 30 min.
32. Start drawing the region of interest (ROI). Search for cells of interest at 5x magnification. Draw cutting outlines not so close to the cells to avoid burning the tissue of interest. If there is a little distance from the cells, they can be preserved. Observe that we did not work with single cells where the procedure adopted could be different.

33. Cutting and catapulting (Fig 3A).
34. Transfer the isolated material into the sticky cap tube to the collection tube. Add 5 µl of RLT buffer into the sticky cap tube, pull the tissue with the pipette taking care to not pull too much, and transfer catapulted sections from the adhesive microtube cap to the RNase free collection tube. When enough ROI has been collected, inspect the collector and unload the tube holder (Fig 3B, 3C).
35. Insert the collection tube with sample and RLT buffer in the icebox.
36. Go to the cryostat and proceed to the subsequent slide.
37. Keep this process until the eighth slide.
38. After finishing the acquisition, spin down the collection tube in a microcentrifuge for 15 seconds.
39. Seal collection tube with Parafilm. Store the collection tube at -80 º C freezer until RNA extraction.

Do the entire procedure within 30 - 45min.

If the material is microdissected but not catapulted, we used a previous RNase-Zap cleaned needle to remove the tissue from the slide and transfer it to the collection tube.

Samples were stored in an RLT buffer at -80 º C for up to one month.

We made two types of collection, small pieces with a high probability of catapulting success and large extensions with a low probability of catapulting. In these cases, not catapulted laser-cut areas were removed from the slide with the slight touch of a needle to which they stuck, and then we transferred to the RLT buffer tube. In our experience, this second type of collection presented samples with higher concentrations, although it took longer. It is important to highlight that this conclusion is based on mouse hippocampus and amygdala tissue. Other types of tissues may present other patterns of RNA concentration due to differences in the extracellular matrix and cellular density, for instance. Thus, largest pieces may not configure a pattern of high-quality RNA control for all tissues.

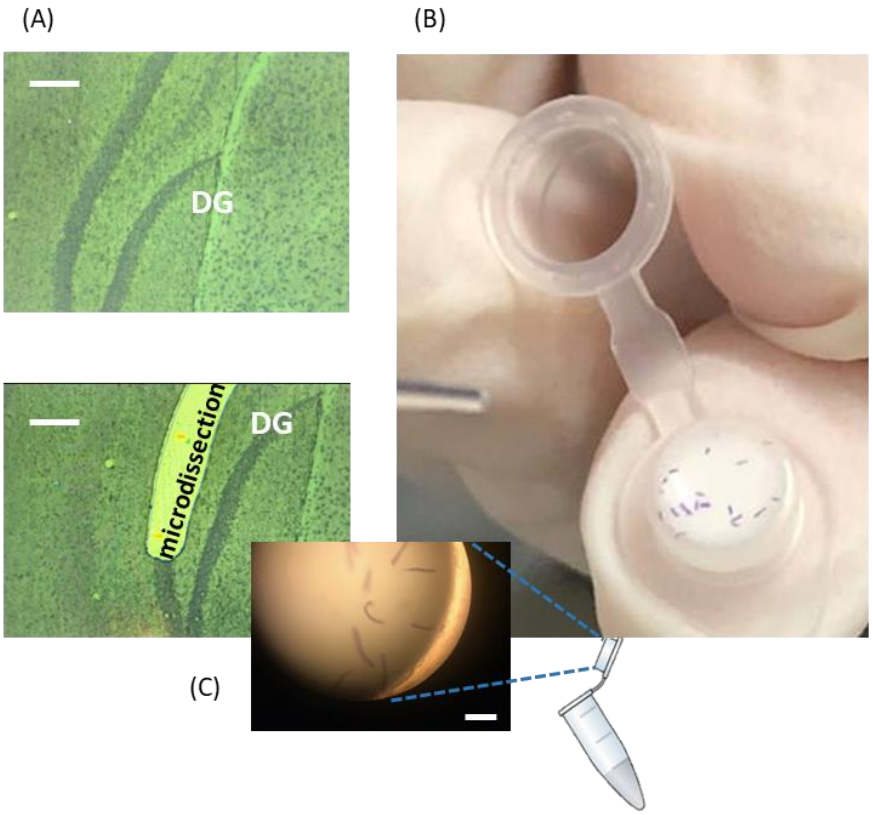

Figure 3. Laser Capture Microdissection process. (A) Dentate Gyrus before (top picture) and after (bottom picture) microdissection. Scale bar: 200 µm. **(B)** Collection of microdissected tissue from the sticky cap tube to the collection tube containg RLT buffer. **(C)** Amplified image of sticky cap tube containing Dentate Gyrus collected small pieces. Scale bar: 800 µm.

REAGENTS AND SOLUTIONS

Reagents

1. 96-100% Ethanol. Keep the container tightly closed. Keep away from heat / spark / open flame / hot surfaces.
2. RNaseZap (Ambion, #9780). Store at room temperature.
3. Tissue-Tek® O.C.T.™ (Sakura). Store at room temperature.
4. Diethyl Pyrocarbonate (DEPC) (Sigma). Keep the container tightly closed. Store at 2 - 8°C.
5. Milli-Q water.
6. Violet Cresyl Vetec V 000 178 (Aldrich). Store at 15 - 30° C.

7. β-Mercaptoethanol (Sigma). Keep container tightly closed in a dry and well-ventilated place. Containers that are opened must be carefully resealed and kept upright to prevent leakage. Store at 2 -8 °C.
8. Isopentane. Store below 50°C. Keep out of direct sunlight. May be stored under nitrogen.
9. PBS tablet (Sigma-Aldrich). Store at room temperature.
10. Ice, dry ice. Store in the freezer.
11. RNeasy Micro kit (Qiagen). Store the RNeasy MinElute spin columns and the RNase-Free DNase Set (i.e., the box containing RNase-free DNase, Buffer RDD and RNase-free water) immediately upon receipt at 2–8°C. Store the remaining components of the kit dry at room temperature (15–25°C).
12. SyBR Green/ROX PCR Mix (QIAGEN, CA, USA). SYBR Green PCR Kit should be stored immediately upon receipt at –20°C in a constant-temperature freezer and protected from light.
13. SuperScript IV Reverse Transcriptase (ThermoFisher Scientific, NY, USA). Store in the fridge.

Solutions

a. **Water DEPC 0.01%:** Store at room temperature in an amber bottle protected from light.
    1. Add 100µl DEPC to 1L Milli-Q water, shake and leave at 37° C overnight.
    2. Autoclaving the next day. Better for washing slides and for making alcohol.

b. **Water DEPC 0.1%:** Store at room temperature in an amber bottle protected from light.
    1. Add 1mL DEPC to 1L Milli-Q water, shake and leave at 37° C overnight.
    2. Autoclaving the next day. Better for direct sample contact.

Do all the procedures under the fume hood. DEPC is toxic before autoclaving.

Water nuclease-free is a DEPC water substitute but is more expensive. Water DEPC inhibits only RNase, while nuclease-free water inhibits RNase and nuclease either.

c. PBS DEPC: Store at room temperature in an amber bottle protected from light.

1. Dissolve a PBS RNase free pellet in 200 mL of **0.01%** DEPC water.

d. 70% RNase free ethanol: Store in the fridge.

1. Add 35ml of 100% ethanol and 15ml of **0.01%** DEPC water.
2. Store in a 50mL falcon tube for cleaning.

e. 70% RNase free ethanol: Store in the fridge.

1. Add 70ml of 100% ethanol and 30ml of **0.1%** DEPC water.

2. Store in two 50mL falcon tubes for the fixation process.

f. 50% RNase free ethanol: Store in the fridge.

1. Add 50ml of 100% ethanol and 50ml of **0.1**% DEPC water.
2. Store for preparing the violet cresyl solution.

g. Violet Cresyl Acetate Solution (1% w/v): Store in the fridge in an amber bottle protected from light.

1. Dissolve 1g of solid violet cresyl acetate in 100ml of 50% RNase free ethanol at room temperature with agitation overnight in the dark.

Prepare all the solutions one day in advance before the start of acquiring samples.

h. **RLT buffer:** Store at room temperature.

1. Add 10µl Beta-Mercaptoethanol in each 1mL RLT Buffer.

COMMENTARY

Background Information

The combination of a laser beam to a microscope cell microsurgery with laser was first described in the early 1960s. The laser beam of LCM has evolved for years from ultraviolet (UV) to high-energy nitrogen, infrared, and carbon dioxide lasers. In the middle of the nineties, another laser microdissection technique was developed. A carbon dioxide laser for polymerization was combined with a transparent thermoplastic membrane (ethylene vinyl acetate polymer on a glass slide). This system was successfully developed and marketed by Arcturus and later by PALM Microbeam System from Zeiss and LMD system from Leica Microsystems (Gilbrich-Wille, 2013; Chung and Shen, 2015). Although several gains have been reached, the main challenge of working with RNA analysis persists. Commonly, the results are not the most satisfactory in terms of RNA integrity, so optimization for better quality in the final product is essential.

Critical Parameters and Troubleshooting

Previous work

A frequent issue at the beginning of the work is not preparing solutions and LCM settings properly, previously. Time spent in each procedure influences the final result, so it is a common problem having to stop everything to set the energy of LCM or to make a solution when time is passing on. Regarding PEN slides, it is important to observe whether the slide membrane does not have bubbles, as the adhesion of the tissue can be compromised and the process of cutting and catapulting fails. Solution: if bubbles are found, switch slides immediately.

Laser Capture Microdissection

A common problem in LCM is the failure of cutting or catapulting phases, resulting in the material standing over the tissue. A lot of issues can be addressed to explain not removed tissue in the LCM process. The first is a lack of adherence of the tissue to the slide membrane. A solution is performing a complete and precise in-time dehydration. Another issue may be due to a low cut or LPC energy on the LCM system. LCM's

previous settings are important, but if it is not possible, a quick calibration may be necessary to adjust the energy. However, even taking these precautions, targeted tissue may not be removed. So, a needle tip or a microcapillary can be used to remove the material with a slight touch to which they stick and then can be transferred to the collection tube cap containing 5µl of RLT buffer. This procedure requires skill and practice (Fend and Raffeld, 2000; Mahalingam, 2018).

Understanding Results

RNA extraction and Quality control

The concentration and integrity of RNA are crucial for gene expression analysis. Laser Capture Microdissection generally collects a low amount of RNA. Since LCM is a complex method, several steps can affect RNA yield and quality, like cutting, staining, microdissecting, and capturing (Garrido-Gil et al., 2017, 2017; Mauney et al., 2018). We optimize these critical parameters to reach better quality control. However, the RNA extraction may affect RNA quality either. There is no point in controlling the LCM process if RNA extraction is not controlled either (Cummings et al., 2018). We extracted RNA from LCM collected tissue using RNeasy® Micro Kit (QIAGEN, #74004), which includes a genomic DNA elimination step. We followed all steps according to the manufacturer's protocol and followed indications from The MIQE guidelines (Bustin et al., 2009). Regarding the quality control, purity, and quantity of total RNA, we applied two relevant tools: ND8000 spectrophotometer (Thermo Scientific NanoDrop Products, DE, EUA) and microfluidic analysis Agilent Technologies' Bioanalyzer (Agilent, CA, USA) (supplementary data, table 1). The absorption spectroscopy provided by NanoDrop is an important indicator of nucleic acid purity, where absorbance reading at 260 nm (A260) is quantitative for relatively pure nucleic acid preparations in microgram quantities. Furthermore, contaminants that can be present during RNA extraction could be accessed through absorbance. The most common are protein and aromatic moieties, which have a peak absorption at 280 nm and 230 nm respectively. Absorbance ratios 260/230 and 260/280 are used to assess the purity of RNA samples after all steps up to RNA extraction, where ratios around 2 are generally accepted as "pure" for RNA (Thermo Fisher Scientific, 2010; Gallagher, 2011). Specifically, according to Thermo Fisher Scientific (2010), NanoDrop spectrophotometers works with a lower limit of 2

ng/μL per sample, if the sample presents a low concentration (as commonly verified in LCM samples) this may result in an inconclusive result, becoming not considered 260/280 and/or 260/230 ratios, as observed in some of our samples. Bioanalyzer RNA 6000 Nano assay was used to assess RNA quality through the tool RIN (RNA Integrity Number) from brain samples, considering the RNA possibility of being rapidly digested in the presence of ubiquitous RNase enzyme. This classification is based on a numbering system with 1 to most degraded RNA and 10 to the most intact one. We defined the threshold for high-quality as RIN higher than 8.5. The RIN software algorithm is robust and based on a combination of different features of RNA, such as the 18 and 28S ratio, provided by microcapillary electrophoresis. It was developed to classify RNA characteristics using the Bayesian approach to train and select a prediction model based on artificial neural networks (Mueller et al., 2000; Schroeder et al., 2006).

We determined the RIN of 70 mouse brain samples. Tissues were collected from the anterior cingulate cortex, BLA amygdala, dentate gyrus, and CA1 region from the hippocampus. In the first experiment, RNA analysis shows that from a total of 19 samples, 16 presented high-quality RNA (between 8.5 and 10.0), meaning that 84% of the RNA samples were highly intact and only three presented degradation (1, 7 and 18, fig 4A). However, samples 1 and 2 are from the same animal, similar to (7 and 8) and (18 and 19). 1, 7, and 18 presented bad integrity, but 2, 8, and 19 presented high-quality RNA. As the entire procedure of slides staining and LCM were done at the same time (for example, 1 refers to the dentate gyrus of the same animal than 2, which refer to the amygdala), this suggests that the observed RNA degradation is not related to the LCM protocol, but probably to posterior RNA extraction procedure, when the samples were separate in brain regions. In the second experiment, we achieved 17 from 18 samples with high-quality RNA, representing 95% of all samples (Fig 4B). Experiment 3 presented 100% of high-quality RNA from 33 samples. The RIN range was over 9.2. The RIN of 17 from 33 samples was 10, representing 51% of all samples (Fig 4C). Figure 4D shows the percentage of RIN range among all the 70 samples, as follows: 94% from 8.5 to 10, as high-quality RNA; 1% from 7 to 8.5, good-quality RNA; 0% from 5 to 7 is a regular-quality RNA, and 4% from 0 to 5, a bad-quality RNA. This classification of RIN in quality levels was considered by this group in this specific case, with mouse brain frozen tissue.

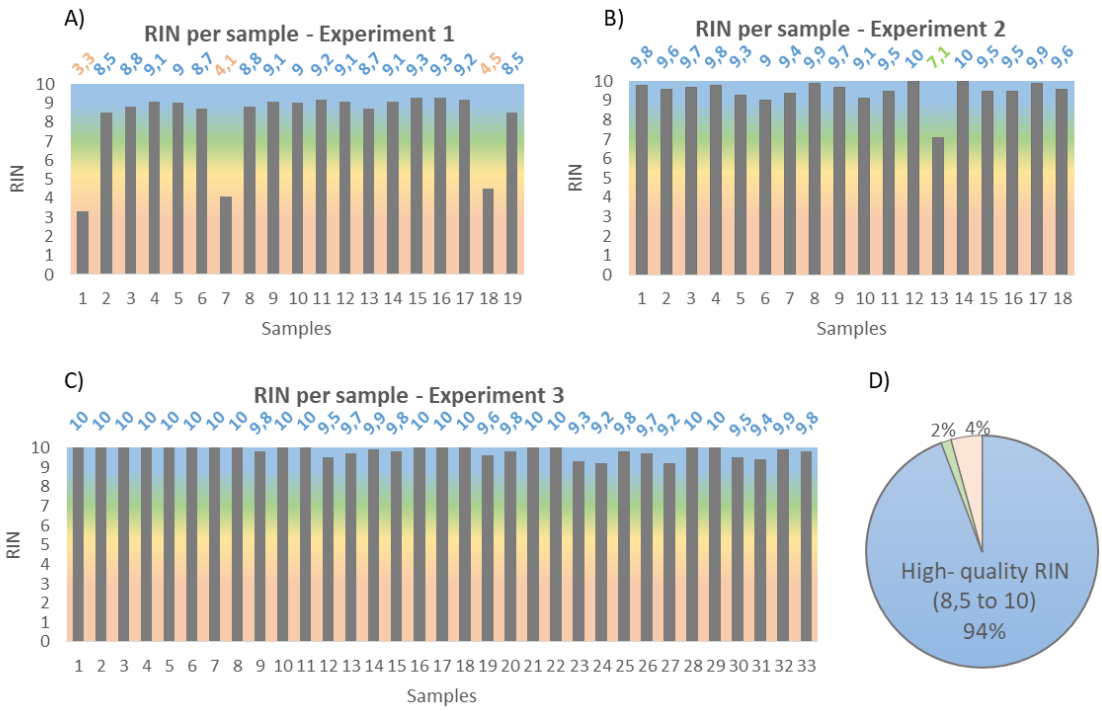

Figure 4. RNA Integrity Number per sample. (A) RIN values from experiment 1 **(B)** RIN values from experiment 2 **(C)** RIN values from experiment 3. **(D)** Pie chart showing percentage of RIN quality control from total samples. RIN below 5 is considered bad (orange), 5 - 7 regular (yellow), above 7 is good integrity (green) and between 8.5 and 10.0 is a high-quality RNA (blue).

Quantitative RT-qPCR

The first-strand cDNA was synthesized using the SuperScript IV Reverse Transcriptase (ThermoFisher Scientific, NY, USA) following the manufacturer's instructions, using 90ng of extracted RNA per sample. Notably, this low quantity of RNA (almost 10 times lower than standard RNA quantity for Real-Time PCR) is due to the limitation of the yield characteristic of LCM collection. Conditions for each cycle of amplification were as follows: heating the RNA-primer mix 5 min at 65º C; after combining the RT reaction mix incubate at 10 min at 55º C, 10 min at 80º C. The final cDNA products were amplified using SyBR Green/ROX PCR Mix (QIAGEN, CA, USA) in 10 µL of a reaction mixture, following the manufacturer's protocol, using previously designed primers for mouse glyceraldehyde-3-phosphate-dehydrogenase (GAPDH) housekeeping gene (forward, 5'-CCGCCTGGAGAAACCTGCCAAGTAT-3', reverse, 5'-

TTGCTCAGTGTCCTTGCTGGGGT-3'), BDNF (forward: 5'-CTTTGGGGCAGACGAGAAAG-3', reverse: 5'-TCTCACCTGGTGGAACTCAG-3'), and primers AB from control RNA from cDNA synthesis kit. Real-time PCR was performed using a two-step cycling program, with an initial single cycle of 95° C for 10 min, followed by 40 cycles of 95° C for 15 seconds, then 60° C for 1 min, in an ABI ViiA 7 Real-Time PCR System (Applied Biosystems, NY, USA) with Sequence Detector System software v1.2. A first derivative dissociation curve was built (95°C for 1 min, 65°C for 2 min, then ramped from 65° C to 95° C at a rate of 2° C/min). Non-template control (NTC) was included in the plate to eliminate the possibility of PCR contamination. RNA electrophoretic traces indicates the absence of RNA degradation and high quality, as shown in the two peaks (markers, 18S, and 28S ribosomal RNA; fig 5A). The amplification acquired by RT-qPCR shows a confident expression of the GAPDH gene that is inside the assurable range (cycle threshold>12), according to MIQE (Bustin, 2009; Schroeder, 2006; fig 5B). As expected, we found an opposite association of Ct values from all of 70 samples and RIN. Furthermore, to quantify these results obtained by Agilent Bioanalyser and Ct values, we analyzed the normalized expression of the Brain Derived Neurotrophic Factor (BDNF) gene by ΔCt showing PCR amplification among all samples (Fig 5C).

Accurate genetic data from LCM samples are implicated in preserving the good quality of genetic molecules. In the case of a brain microdissected sample, RNA quality depends critically on the time between freezing tissue, the temperature of manipulation, proper slides preparation and staining, and choosing an adequate method of RNA extraction and isolation. Our protocol shows a high percentage of high-quality RNA. We, therefore, conclude that our optimized protocol can be useful for experiments using microdissected mouse brain tissue, resulting in a high degree of purity of RNA.

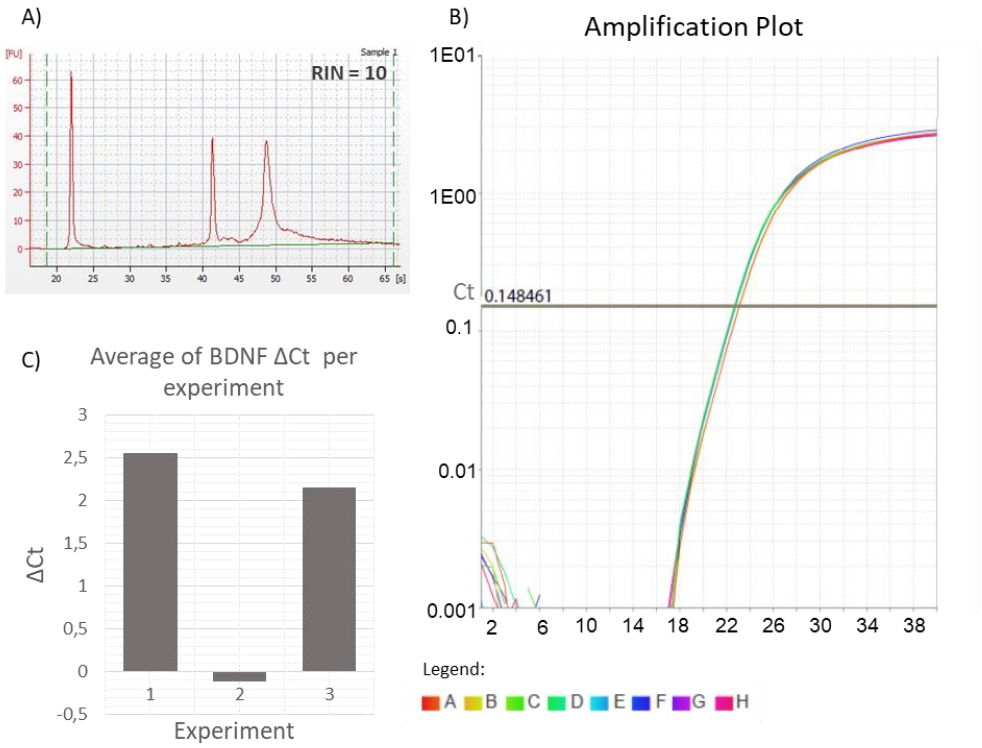

Figure 5. RNA quality verification and validation. (A) Electropherogram and electrophoresis assay from representative of anterior cingulate cortex RNA (RIN = 10). **(B)** Amplication plot of housekeeping gene using LCM sample. qPCR detecting valid expression (Ct between 18 and 19) of the housekeeping gene GAPDH in RNA isolated from LCM collected dentate gyrus from nine mice. cDNA from non-template control was used as a negative control. Delta Rn corresponds to normalized reporter SYBR by passive reference dye minus the baseline fluorescence signal. The threshold line was automatically defined as 0,148461. **(C)** Mean BDNF ΔCt values per experiment.

Time Considerations

In order to prevent degradation, time management is crucial. LCM is a powerful tool, however, a disadvantage of the method is that it is time-consuming (S et al., 2000), especially in our approach, in which we prepare slides and collect the samples on the same day. It takes one day of work to collect brain tissue from one single animal. Experiments with several animals and a control group may take several days to be concluded. However, it is worth ensuring high-quality RNA. If initial procedures are done beforehand, the basic protocol can be completed in a single day, for three different regions from one brain. The cleaning process and stabilizing the brain at -20°C takes at least 30 min. Each slide should take ~1 hr to cryosectioning, staining, and dissecting. We recommend preparing around 8 slides per day containing 6 slices. This quantity can vary depending on the expected amount. 2 minutes to dissect the brain, 30 minutes to stabilize

the brain at -20 ^{o}C, 2-3 minutes to the slide dry in the cryostat, 2 minutes in the 70% ethanol RNase free, 30 seconds in violet cresyl, a short dip in 70% ethanol RNase free, a short dip in 100% ethanol RNase free, 1-2 minutes to dry at room temperature, ~ 30 minutes to cut and catapult. Temperature is important too. To ensure high RNA quality, we strongly recommend keeping all the solutions cold. If all this time is strictly followed, there will be great chances to get optimal results.

Conflicts of Interest

The authors report no conflict of interest in this article.

Literature Cited

PALM MicroBeam. Available at: https://www.zeiss.com/microscopy/int/products/laser-microdissection/microbeam.html [Accessed February 25, 2020c].

Bustin SA, Benes V, Garson JA, Hellemans J, Huggett J, Kubista M, Mueller R, Nolan T, Pfaffl MW, Shipley GL, Vandesompele J, Wittwer CT (2009) The MIQE guidelines: minimum information for publication of quantitative real-time PCR experiments. Clin Chem 55:611–622.

Chabrat A, Doucet-Beaupré H, Lévesque M (2015) RNA Isolation from Cell Specific Subpopulations Using Laser-capture Microdissection Combined with Rapid Immunolabeling. J Vis Exp JoVE.

Chung SH, Shen W (2015) Laser capture microdissection: from its principle to applications in research on neurodegeneration. Neural Regen Res 10:897–898.

Clayton DF, Anreiter I, Aristizabal M, Frankland PW, Binder EB, Citri A (2020) The role of the genome in experience-dependent plasticity: Extending the analogy of the genomic action potential. Proc Natl Acad Sci 117:23252–23260.

Cummings M, Mappa G, Orsi NM (2018) Laser Capture Microdissection and Isolation of High-Quality RNA from Frozen Endometrial Tissue. Methods Mol Biol Clifton NJ 1723:155–166.

Datta S, Malhotra L, Dickerson R, Chaffee S, Sen CK, Roy S (2015) Laser capture microdissection: Big data from small samples. Histol Histopathol 30:1255–1269.

Erickson HS, Albert PS, Gillespie JW, Rodriguez-Canales J, Marston Linehan W, Pinto PA, Chuaqui RF, Emmert-Buck MR (2009) Quantitative RT-PCR gene expression analysis of laser microdissected tissue samples. Nat Protoc 4:902–922.

Fend F, Raffeld M (2000) Laser capture microdissection in pathology. J Clin Pathol 53:666–672.

Gallagher SR (2011) Quantitation of DNA and RNA with absorption and fluorescence spectroscopy. Curr Protoc Neurosci Appendix 1:Appendix 1K.

Garrido-Gil P, Fernandez-Rodríguez P, Rodríguez-Pallares J, Labandeira-Garcia JL (2017) Laser capture microdissection protocol for gene expression analysis in the brain. Histochem Cell Biol 148:299–311.

Gilbrich-Wille C (2013) History of Laser Microdissection. Available at: https://www.leica-microsystems.com/science-lab/history-of-laser-microdissection/ [Accessed February

Mahalingam M (2018) Laser Capture Microdissection: Insights into Methods and Applications. Methods Mol Biol Clifton NJ 1723:1–17.

Mauney SA, Woo T-UW, Sonntag KC (2018) Cell Type-Specific Laser Capture Microdissection for Gene Expression Profiling in the Human Brain. Methods Mol Biol Clifton NJ 1723:203–221.

Meda S, Freund N, Norman KJ, Thompson BS, Sonntag K-C, Andersen SL (2019) The use of laser capture microdissection to identify specific pathways and mechanisms involved in impulsive choice in rats. Heliyon 5:e02254.

Morrison JA, Bailey CM, Kulesa PM (2012) Gene profiling in the avian embryo using laser capture microdissection and RT-qPCR. Cold Spring Harb Protoc 2012.

Mueller O, Hahnenberger K, Dittmann M, Yee H, Dubrow R, Nagle R, Ilsley D (2000) A microfluidic system for high-speed reproducible DNA sizing and quantitation. Electrophoresis 21:128–134.

Nichterwitz S, Benitez JA, Hoogstraaten R, Deng Q, Hedlund E (2018) LCM-Seq: A Method for Spatial Transcriptomic Profiling Using Laser Capture Microdissection Coupled with PolyA-Based RNA Sequencing. Methods Mol Biol Clifton NJ 1649:95–110.

S C, Ja M, Hl M, Gi M (2000) Laser capture microscopy. Mol Pathol MP 53:64–68.

Schaeck M, De Spiegelaere W, De Craene J, Van den Broeck W, De Spiegeleer B, Burvenich C, Haesebrouck F, Decostere A (2016) Laser capture microdissection of intestinal tissue from sea bass larvae using an optimized RNA integrity assay and validated reference genes. Sci Rep 6:21092.

Schroeder A, Mueller O, Stocker S, Salowsky R, Leiber M, Gassmann M, Lightfoot S, Menzel W, Granzow M, Ragg T (2006) The RIN: an RNA integrity number for assigning integrity values to RNA measurements. BMC Mol Biol 7:3.

Sharma D, Golla N, Singh D, Onteru SK (2018) A highly efficient method for extracting next-generation sequencing quality RNA from adipose tissue of recalcitrant animal species. J Cell Physiol 233:1971–1974.

Sonntag K-C, Woo T-UW (2018) Laser microdissection and gene expression profiling in the human postmortem brain. Handb Clin Neurol 150:263–272.

Thermo Fisher Scientific TFSI (2010) Nucleic Acid. Thermo Scientific NanoDrop Spectrophotometers. Available at: https://assets.thermofisher.com/TFS-Assets/CAD/manuals/ts-nanodrop-nucleicacid-olv-r2.pdf.

Manuscript 2

This manuscript put together molecular and behavioral data from the administration of 5-MeO-DMT in mice, and it is in the final step of preparation to be submitted to Molecular Psychiatry.

Serotonergic psychedelic 5-MeO-DMT induces alterations in plasticity-related gene expression and anxiolytic effects in stressed mice

Margareth Nogueira[1], Daiane Golbert[1], Richardson Santiago[2], Raíssa Almeida[3], Nicole Coelho[3], Katarina E. Leão[4] & Richardson N. Leão*[1]

1. Neurodynamics Lab, Brain Institute, Federal University of Rio Grande do Norte
2. Automation and Robotics Laboratory (ARL), School of Science & Technology, Federal University of Rio Grande do Norte
3. Laboratory of Hormonal Measurements-ELISA, Center for Biosciences, Federal University of Rio Grande do Norte
4. Hearing and Neuronal Activity Lab, Brain Institute, Federal University of Rio Grande do Norte

Corresponding author: richardson.leao@neuro.ufrn.br

Funding: The Coordination for the Improvement of Higher Education Personnel (CAPES)

Author contribution: MN conceived the project; MN and DG designed the experiments; MN, DG and RA performed the experiments; MN, DG, RA, NC and RS analyzed the data; MN and KEL wrote the original-draft with input from DG and RA; MN, KEL and RNL wrote the reviewing manuscript; RNL provided resources.

Conflict of interest: The authors declare no conflict of interest.

Abstract

Serotonergic psychedelics have potential therapeutic effects in treating anxiety and mood disorders, often after a single dose. Here, we sought to investigate the effects of 5-methoxy-*N*,*N*-dimethyltryptamine (5-MeO-DMT) on gene expression in anxiety-related brain regions and also analysed the behavior of mice in the elevated plus maze and open field test. Using laser capture microdissection and RT-qPCR, we evaluated the modulation of genes involved in synaptic plasticity and neuronal activity from specific subregions, such as ventral CA1 (vCA1), dentate gyrus (DG), basolateral amygdala (BLA), and anterior cingulate cortex (ACC). We compared the gene expression of ARC, ZIF268, BDNF, CREB, NFkB, mTORC1, NR2A, and TRIP8b in mice injected with 5-MeO-DMT at different time points (1hr, 5hrs or 5 days later) to control animals injected with saline. We found that 5-MeO-DMT treated mice increased the mRNA expression of immediate early genes in ACC and BLA while decreased NR2A expression in hippocampal ventral CA1 compared to control mice. Interestingly, we also found a long-term increase in TRIP8b, a gene related to the modulation of neuronal activity, in the ventral CA1. Besides molecular changes, 5-MeO-DMT treated mice exhibited anxiolytic behavior and lower corticosterone levels when compared to control. Taken together, these findings suggest that 5-MeO-DMT may be a candidate for anxiolytic therapeutics producing responses beyond subjective effects.

Introduction

Serotonergic psychedelics have been reported to mitigate anxiety and mood disorders symptoms after just a single dose [1,2,3,4,5,6,7,8] with long-lasting effects possibly due to structural plasticity induced by these compounds [9,10,11,12,13,14,15,16,17,18]. Neuroplasticity impairment is presumed to be the core of mood psychiatric disorders, as it promotes changes in neural circuits that may lead to malfunction [19]. Some studies have shown that psychedelics such as lysergic acid diethylamide (LSD), N, N-Dimethyltryptamine (DMT), 2,5-Dimethoxy-4-iodoamphetamine (DOI), psilocybin, and 5-MeO-DMT promote dendritic spine growth, increase dendritic arbor complexity, stimulate synaptic formation and that DMT regulates adult neurogenesis both *in vitro* and *in vivo* [13]. We have previously shown *in vitro* that a single dose of 5-MeO-DMT

stimulates cell proliferation, neuronal survivability, morphological and functional changes in adult mice ventral dentate gyrus [11]. Also, 5-MeO-DMT has been reported to alter cytoskeletal organization protein expression in brain organoids after 24 hours of acute treatment, which points to a possible involvement in structural plasticity [20]. However, how these effects are regulated genetically is still not well understood, although it has been shown that psychedelics and psychotropics trigger long-term neuronal signaling, leading to changes in mRNA expression [21]. Understanding the mechanisms of action generated by possible transcriptional changes is necessary for the development of therapeutic strategies that consider both risks and benefits of psychedelics.

Classic psychedelics activate serotonergic 5-HT2A receptors and cascades of $G\alpha_q$ signaling, with downstream inositol phosphate generation and activation of protein kinase C that can modulate synaptic activity [21,22]. Specifically, the fast-acting 5-MeO-DMT has a higher affinity for 5-HT1A receptors [23]. The 5-HT1A pathway usually reduces neuronal activity and is involved in neuritogenesis, synapse formation [24], and long-lasting changes in brain circuits related to psychiatric disorders regulating mood, anxiety, and cognition [24,25,21]. 5-MeO-DMT also has affinity for the Sigma-1 receptor that has a multi-functional role in neuroprotection [26,27]. It has been reported that sigma-1 activation increases the expression of brain-derived neurotrophic factor (BDNF) possibly through NR2A-CREB-BDNF signaling pathway that regulates synaptic plasticity and is an important factor in controlling anxiety behavior [28,29]. The role of 5-MeO-DMT in modulating mRNA transcription of key plasticity-related genes is still largely unknown.

We analyzed the immediate early genes (IEG) ARC and ZIF268, as IEGs encode growth factors, cytoskeletal proteins, and transcription factors, triggering further transcription of late-response genes [21]. We also investigated BDNF and CREB genes as they are part of the 5-HT1A, 5-HT2A and sigma-1 receptor pathways [24,25,26]. Alterations in BDNF expression result in structural changes, such as modulation of neurogenesis, neuritogenesis, synaptogenesis, and dendrite length [21,30,31,32,33]. For example, the hippocampus and prefrontal cortex (PFC) have shown reduced volume and the amygdala increased volume under stress conditions [30,34]. Other candidate genes such as mTORC1, TRIP8b and NF-kB are interesting as they are involved in neuronal activity and synaptic plasticity [9,35,20]. The mammalian target of the rapamycin (mTOR) pathway is involved in long-term synaptic plasticity and protein translation through activation of BDNF in the synapse, where rapamycin inhibition of mTORC1 prevented

the translation of proteins related to long-term potentiation (LTP) [36]. Lastly, TRIP8b is an auxiliary subunit of the hyperpolarization-activated cyclic nucleotide-gated (HCN) channel, with potential antidepressive effects [35,37,38].

Along with mRNA expression fold changes, it is also important to investigate emergent effects of a single 5-MeO-DMT dose on mice behavior. We analysed anxiety-like behavior, locomotor activity, and ethological patterns in animals treated with 5-MeO-DMT 24 hours and 5 days after injection. We found 5-MeO-DMT to induce lower baseline levels of the stress hormone corticosterone and specifically produced anxiolytic effects in stressed mice.

Material and Methods

Animals

Adult male C57BL6J mice, 8-12 weeks old, were housed under a 12h light/12h dark cycle, with food and water *ad libitum* and controlled temperature at 23°C. The study was approved by the local ethics committee on animal care of the Federal University of Rio Grande do Norte (Protocol 110.035/2018) and followed the guidelines of the National Council for the Control of Animal Experimentation (CONCEA), Brazil.

Pharmacology

For 5-MeO-DMT treatment, male mice received a single intraperitoneal (i.p.) injection of 20mg/kg, prepared fresh in saline (0.9%) and control mice received a saline i.p. injection. A subgroup of mice received an intracerebroventricular (i.c.v.) injection of 5-MeO-DMT (100µg/µl) or saline [11] through stereotaxic surgery. In brief, mice were anesthetized with isoflurane (4% for induction and 1.5% for maintenance) and a rostrocaudal head incision was done followed by craniotomy using a 1.0mm drill in the right lateral ventricle (AP: 0.2mm, ML: 1.0mm, DV: 2.25mm). Next using a Nanofil syringe 1µL of 5-MeO-DMT solution was slowly injected (0.2µl/min). The skull was rehydrated with 0.9% saline during the suture procedure. After recovery from anaesthesia, the animals were returned to the animal house and monitored for the following days.

Laser Capture Microdissection (LCM)

After either 1 hour, 5 hours or 5 days of 5-Meo-DMT/saline i.p./i.c.v. injection, C57BL6J male mice (n = 35) 8 - 12 weeks old had their brains quickly dissected and stored in a -80℃ freezer until cryosectioning. Slides were at room temperature for less than an hour. Staining and fixation followed the manufacturer orientations for staining with violet cresyl (PALM Protocols – RNA handling, Carl Zeiss). Next, the slide was ready for immediate microdissection. Our group, minimizing handling and avoiding temperature changes previously optimized this procedure, which increases the integrity of RNA, reaching high-quality RNA [39]. LCM was performed in a PALM MicroBeam system. After cutting and catapulting, the sections were transferred to the RNase-free collection tube containing 5µl RLT buffer. Collected microdissections of vCA1, DG, BLA and ACC were stored in the RLT buffer at -80℃ freezer until RNA extraction.

RT-qPCR

RNA extractions were carried using the RNeasy Micro Kit (QIAGEN, CA, USA), which includes a genomic DNA elimination step. Quality control was estimated using an ND8000 spectrophotometer (Thermo Scientific NanoDrop Products, DE, EUA) for quantity and microfluidic analysis Agilent Technologies' Bioanalyzer (Agilent, CA, USA) for assessing purity and integrity of RNA. Bioanalyzer RNA 6000 Nano assay was used to measure RIN (RNA Integrity Number). We only acquired samples with RIN over 8.5, indicative of high-quality RNA. The first-strand cDNA was synthesized using the SuperScript IV Reverse Transcriptase (ThermoFisher Scientific, NY, USA) following the manufacturer's instructions, using 90ng of extracted RNA per sample. Conditions for each cycle of amplification were as follows: heating the RNA-primer mix 5 min at 65℃; after combining the RT reaction mix incubates at 10 min at 55℃, 10 min at 80℃. The final cDNA products were amplified using SyBR Green/ROX PCR Mix (QIAGEN, CA, USA) in 10 µL of a reaction mixture, following the manufacturer's protocol, using previously designed primers for mouse glyceraldehyde-3-phosphate-dehydrogenase (GAPDH) housekeeping gene (forward: 5'-CCGCCTGGAGAAACCTGCCAAGTAT-3', reverse: 5'-TTGCTCAGTGTCCTTGCTGGGGT-3'), the values used in the normalization was the mean of the mouse GAPDH gene. The genes of interest (GOI) primers used were as follows: TRIP8b (forward: 5'-TGAGCAACAAGAGAGCAGACC-3', reverse: 5'-

TTGGATGTCACTGGCTTTGC-3'), NR2A (forward: 5'-TGGGACAGTACCCAATGGAA-3', reverse: 5'-CGTCCAACTTCCCAGTTTTC-3'), BDNF (forward: 5'-CTTTGGGGCAGACGAGAAAG-3', reverse: 5'-TCTCACCTGGTGGAACTCAG-3') and CREB (forward: 5'-AAGCAGTGACTGAGGAGCTT-3', reverse: 5'-GGCATGGATACCTGGGCTAA-3', mTORC1(forward: 5'- AGAAGGGTCTCCAAGGACGACT – 3', reverse: 5'-GCAGGACACAAAGGCAGCATTG – 3') and NFkB (forward: 5'-GAAATTCCTGATCCAGACAAAAAC – 3', reverse: 5'-ATCACTTCAATGGCCTCTGTGTAG – 3'). Primers AB from control RNA were used from the cDNA synthesis kit. Real-time PCR was performed using a two-step cycling program, with an initial single cycle of 95℃ for 10 min, followed by 40 cycles of 95℃ for 15 seconds, then 60℃ for 1 min, in an ABI ViiA 7 Real-Time PCR System (Applied Biosystems, NY, USA) with Sequence Detector System software v1.2. A first derivative dissociation curve was built (95℃ for 1 min, 65℃ for 2 min, then ramped from 65℃ to 95℃ at a rate of ℃/min). Non-template control (NTC) was included in the plate to eliminate the possibility of PCR contamination. The amplification observed of the housekeeping gene is inside the reliable range (cycle threshold>12).

Open field tests and Elevated Plus Maze

For evaluating locomotor and anxiety-like behavior, mice (n=35) were screened and randomized order in an Open Field, a rectangular arena (45cm X 34cm X 16.5cm) or the Elevated Plus Maze (EPM), a cross-shaped maze with two open arms, two closed arms (33.0cm x 6.0cm), and a central region (6.0cm x 6.0cm), sustained 60cm above the ground by four columns, custom-built in white PVC. For the OF, mice were placed in the center of the arena (60% of total area) and for the EPM, animals were placed in the middle of the maze, turned to the closed arms. Next, locomotion of mice was video recorded (Logitech C920 HD Pro, 30 frames/s) for 10 min/arena, respectively. Both arenas were routinely cleaned with ethanol 70% and next with water to remove residual smell in between individual animal trials.

Blood collection and corticosterone quantification

Tail-collected blood samples were centrifuged (10 min, 4°C at 3,000 rpm) and serum was distributed in aliquots of 20µL and stored in freezers at −80°C. We used the DRG® ELISA (EIA-4164) for corticosterone dosage, which used a direct competitive technique for measurement [40]. The absorbance was read using a spectrophotometer microplate reader (Epoch, Biotek Industries, Highland park, United States) with a Gen5 Data Analysis software interface.

Acute Restraint Stress

Male mice (n=11) were randomized [41] and cloistered in a 50ml conical propylene Falcon® tube, 3cm diameter × 11.5cm length, customized with 0.5cm diameter holes along the sidewall of the tube, spaced at 2cm to enable air circulation. The duration of the procedure was 20min. Immediately after, mice were submitted to anxiety and locomotor activity tests, and finally tail blood samples were collected for stress hormone quantification. Procedure was concentrated at noon and finalized at least until two hours before the end of the light cycle (between 13:00 and 16:00h).

Analysis and statistics

All statistical analyses are presented as the mean ± standard error of the mean (SEM). Statistically significant differences were assessed by comparisons between the cycle threshold (ΔCt) from treated group and control using unpaired *t*-test (GraphPad Prism). For fold change of relative expression, the $2^{(-\Delta\Delta Ct)}$ method was performed using normalized cycle threshold (Ct) values [42]. A positive value indicates gene up-regulation and a negative value indicates gene down-regulation.

The locomotor activity and anxiety tests performed in the open field and in the elevated plus maze were analysed by a custom-made software (available on GitHub, *github.com/vanluwin/proj-pca*, R. Menezes and H. Maia). Statistically significant differences were assessed by comparisons between 5-MeO-DMT treated group and saline control group using unpaired two-tailed Student's t-test (GraphPad Prism). Confidence interval is 95%, p value ≤ 0.05.

Results and Discussion

5-MeO-DMT modulates gene expression in brain anxiety-related structures.

To study altered immediate early gene (IEG) expression 1 hour after i.p. injection, 5-MeO-DMT (20 mg/kg, n=4 adult male mice) or saline 0.9% i.p. injection as control (n=4), we microdissected brain sections containing the vCA1, the BLA and the ACC, visualised by RNase free violet cresyl staining (Figure 1A, C) and genes ARC, ZIF268, BDNF, and CREB were analysed for relative expression. We found no statistically significant changes in the vCA1 (Figure 1B) while the BLA presented upregulation in ARC (2.1 fold, p=0.008) and ZIF268 (1.8 fold, p=0.02, Figure 1B) and the ACC presented upregulation of ARC (1.2 fold, p=0.03, Figure 1B). ARC and ZIF268 (also known as EGR-1) are two important immediate early genes, with peak RNA expression levels between 30 and 60 minutes after induction, involved in synaptic plasticity and induction of late-response gene transcription [43,44,45,46]. The expression of ZIF268 depends on synaptic activity and NMDA activation, where induction of long-term potentiation (LTP) increases ZIF268 expression [43]. In turn, the activity-regulated, cytoskeletal protein ARC, is rapidly expressed when synapses are active and mostly expressed in excitatory neurons, depressing glutamatergic transmission [43]. These results points to a potential inductive role of 5-MeO-DMT in synaptic plasticity. Next, we compared the late response genes BDNF, mTORC1, NFkB, CREB, TRIP8b, and NR2A five hours after an i.p. injection in male mice treated with 5-MeO-DMT (20mg/kg, n=6) or control saline (0,9%, n=6). Here, the only gene showing significant alteration was NR2A, (or GRIN2A), the gene that encodes the subunit 2A of the NMDA receptor, which showed downregulation (-6.8 fold, p=0.01) in the vCA1 of the hippocampus (Figure 1B, bottom left). We studied the ventral CA1 area, due to its connectivity with the basolateral amygdala, associated with the activity of the hypothalamic–pituitary–adrenal axis, and has an expressive role in anxiety disorder [47]. According to several studies, ventral, but not dorsal hippocampus, has a strong link to emotional maladaptive behavior such as anxiety [48,49,50,51,52,53,54,55]. It has been reported that NR2A promotes LTP while NR2B promotes long-term depression in the CA1 region of the hippocampus [56] and that the NR2A subunit regulates electrophysiological properties of the NMDA receptor [22,57,58,28]. It has been previously shown that genetic inactivation of NR2A has anxiolytic effects in mice [59], corroborating our results. The BLA and ACC presented no changes in the mRNA

expression of the late response genes of interest (Figure 1B). This shows that despite immediate early gene activation in the BLA and ACC areas, none of the examined late response genes showed altered expression in these regions. As only the vCA1 showed changes in gene expression following 5-MeO-DMT treatment, we wanted to see if gene expression alteration in this area was longer-lasting after 5-MeO-DMT treatment. Therefore, we next examined the alterations in mRNA expression 5 days after 5-MeO-DMT treatment (n=6), or control saline (n=5). Here, we included the dentate gyrus of the hippocampus as a control structure and examined expression of NR2A, BDNF, CREB and TRIP8b. Analysis of relative gene expression showed a significant upregulation of the TRIP8b in the vCA1 (0.49 fold change, p=0.0004; Figure 1D, top). TRIP8b (or PEX5l) is a gene that encodes an auxiliary subunit of hyperpolarization-activated cyclic nucleotide-gated (HCN) channels that can regulate activation kinetics and voltage dependency of HCN channels [35]. Interestingly, knock-out of HCN channel expression in subregions of the hippocampus has been associated with alterations in anxiolytic and antidepressant behavior [60] and HCN channels are also involved in pathologies such as anxiety, depression and epilepsy [37,61,62]. This shows that a single 5-MeO-DMT dose can cause long-lasting alteration in gene expression in the vCA1 while the dentate gyrus showed no significant changes in mRNA expression of the examined genes (Figure 1D, bottom). Altered gene expression of the vCA1 could potentially modulate the amygdala, an interconnectivity related to anxiety behaviour [49,53,47].

5-MeO-DMT alters mice anxiety-like behavior 24 hours and 5 days after treatment

It is crucial to assess behavioral effects of 5-MeO-DMT to infer emergent behavior from molecular changes. Therefore, we studied anxiety-like behavior and locomotor activity from 10-minutes videos of 5-MeO-DMT (20mg/kg) and control saline (0.9%) treated adult male mice (2-3 months old, n=24). Mice were studied in behavioral tests either 24 hours or 5 days after a 5-MeO-DMT injection or control saline injection (four experimental groups, n=6 per group). Data was first evaluated from the Elevated plus maze test (Figure 2A) by comparing trajectory traces and position heatmaps of 5-MeO-DMT and saline-treated mice 24 hours and 5 days after injection (Figure 2B). We found that 5-MeO-DMT treated mice spent significantly higher percentage of time in the open arms 5 days after the i.p. injection compared to the saline treated group (p=0.017) and made more percentage of entries into the open arms 24 hours and 5 days after treatment

(p=0.001 and p=0.009, respectively). Traveling distances and speed analysis showed no significant changes for either group (Figure 2C). This indicates that 5-MeO-DMT can have a long-term anxiolytic effect, already seen 24 hrs after treatment as mice entered more often into the open, unprotected arms of the maze.

To further assess anxiety and locomotor activity, we next analyzed 10 minutes videos of the 5-MeO-DMT and saline treated mice (n=24) in the Open Field test (Figure 3A) by generating trajectory traces (Figure 3B, *top*) and heatmaps of total group spatial position over time (Figure 3B, *bottom*) 24 hours or 5 days after injection of 5-MeO-DMT or saline. When comparing the four experimental groups we found the two groups of 5-MeO-DMT treated mice made fewer entries into the center of the open field 24 hours and 5 days after treatment (p=0.016 and p=0.003, respectively). Still, the percentage of time spent in the center of the arena, total travelled distances and locomotion speed presented no significant changes (Figure 3C). This showed that 5-MeO-DMT treated mice explored less the center of the open field, which could indicate increased anxiety, thereby opposing the results from the EPM.

5-MeO-DMT alters mice anxiety-like behavior and serum corticosterone levels 5 days after treatment under stress conditions

To clarify the contradictory data seen from the elevated plus maze and open field test, we refined the experiments to better study anxiety parameters by generating an anxiogenic or stressing pre-conditions. To also optimize delivery of 5-MeO-DMT, and avoid any possible metabolic effects, the drug administration was done under anesthesia as stereotaxic intracerebroventricular injections (1µl, 100 µg/µl of 5-MeO-DMT; n=6 or control i.c.v saline 0.9%; n=5; Figure 4A). Tail blood samples were collected to measure corticosterone levels before the acute restraint condition (20min duration), as has been done for acute administration of psychedelics like ayahuasca [33], and after the behavior tests (Figure 4A). Five days following the 5-MeO-DMT i.c.v. administration, serum analysis showed mice previously injected with 5-MeO-DMT to have lower basal corticosterone levels compared to control saline injected mice (p=0.0327, Figure 4B). Following the stress-inducing acute restraint condition, mice were placed in the open field and elevated plus maze arena and ten minute videos of behavior were recorded per arena. Tail blood samples showed a similar increase in serum corticosterone for 5-MeO-DMT or saline i.c.v injected mice (basal vs. stressed for both groups; p<0.0001, Figure 4B)

validating that the stress condition raised hormonal stress levels to similar values for both groups.

Next, we again analyzed trajectory traces and heatmaps of group data of animal location within the elevated plus maze and open field arena from the mice that 5 days prior had been treated with 5-MeO-DMT or saline (Figure 4A, C). We found that 5-MeO-DMT treated mice immediately after a stress condition spent a significantly higher percentage of time in the open arms of the elevated plus maze compared to saline treated mice ($p=0.0355$). Percentage of entries in open arms, travelled distances and speed presented no significant changes between the experimental groups (Figure 4C, D). For the open field test, directly following the stress condition, we found that 5-MeO-DMT treated mice spent significantly more time in the center of the arena compared to saline treated mice ($p=0.02$). Entries in the center of the arena, travelled distances and speed presented no significant changes (Figure 4C, E). Taken together, these results suggests that 5-MeO-DMT has a significant anxiolytic effect in mice, shown by lower initial levels of serum corticosterone when compared to saline, and by 5-MeO-DMT treated mice being more prone to stay in the less protected areas of the test arenas compared to the control group. This indicates that 5-MeO-DMT can act to calm animals both in non-stress situations and in stressful conditions, suggesting that 5-MeO-DMT may increase resilience to stress.

5-MeO-DMT alters mice protected and unprotected head-dipping behavior in the elevated plus maze both in normal and stressed conditions

Finally, to extract additional behavioral data from the recorded animals, we also performed ethological analysis of the 10 minutes videos of 5-MeO-DMT and saline treated male mice (in total n=35), 24 hours and 5 days after i.p. treatment, and 5 days after i.c.v. treatment under stress conditions, in the EPM. Behavioral parameters quantified were rearing, grooming, returns to the protected arms, fecal boli but we found no significant differences. Analyses of protected and unprotected head dips showed 5-MeO-DMT treatment to significantly decrease protected head dips after 24 hours (Figure 5B, $p= 0.032$) while increasing unprotected head dips 5 days after a single 5-MeO-DMT administrations, both under normal and stressed conditions (Figure 6C-D, $p=0.018$ and $p=0.016$, respectively). Also, protected head dips were decreased 5 days after 5-MeO-DMT administration under normal and stressed conditions (Figure 6C-D, $p=0.001$ and $p=0.007$, respectively). Quantifying the percentage of total head dips for the three

experimental groups (24hrs, 5 days, and 5 days + stress) showed that 5-MeO-DMT administration increase the proportion of unprotected head dips compared to protected head dips (5-MeO-DMT: uDips 84% and pDips 16%) compared to saline treated mice (saline: uDips 59% and pDips 41%; Figure 6E). Less protected head dipps indicates a diminished avoidance behavior, while an increase in unprotected head dipps indicates an anxiolytic effect of 5-MeO-DMT, interestingly seen for both normal and stressful conditions, and already at 24hrs post treatment and lasting up to 5 days.

In summary, this study reveals that 5-MeO-DMT modulates the mRNA expression of certain plasticity-related genes and promotes anxiolysis. From a translational perspective, these molecular and behavioral findings suggest that 5-MeO-DMT produces effects beyond subjective changes reported in humans, although further studies are necessary to validate clinical efficiency and unravel signaling pathways underlying the effects of 5-MeO-DMT.

References

1. Palhano-Fontes F, Barreto D, Onias H, Andrade KC, Novaes MM, Pessoa JA, et al. Rapid antidepressant effects of the psychedelic ayahuasca in treatment-resistant depression: a randomized placebo-controlled trial. Psychol Med. 2019;49:655–663.
2. Osório F de L, Sanches RF, Macedo LR, dos Santos RG, Maia-de-Oliveira JP, Wichert-Ana L, et al. Antidepressant effects of a single dose of ayahuasca in patients with recurrent depression: a preliminary report. Rev Bras Psiquiatr. 2015;37:13–20.
3. Davis AK, So S, Lancelotta R, Barsuglia JP, Griffiths RR. 5-methoxy- *N*,*N* -dimethyltryptamine (5-MeO-DMT) used in a naturalistic group setting is associated with unintended improvements in depression and anxiety. Am J Drug Alcohol Abuse. 2019;45:161–169.
4. Barsuglia J, Davis AK, Palmer R, Lancelotta R, Windham-Herman A-M, Peterson K, et al. Intensity of Mystical Experiences Occasioned by 5-MeO-DMT and Comparison With a Prior Psilocybin Study. Front Psychol. 2018;9:2459.
5. Ross S, Bossis A, Guss J, Agin-Liebes G, Malone T, Cohen B, et al. Rapid and sustained symptom reduction following psilocybin treatment for anxiety and depression in patients with life-threatening cancer: a randomized controlled trial. J Psychopharmacol Oxf Engl. 2016;30:1165–1180.

6. Agin-Liebes GI, Malone T, Yalch MM, Mennenga SE, Ponté KL, Guss J, et al. Long-term follow-up of psilocybin-assisted psychotherapy for psychiatric and existential distress in patients with life-threatening cancer. J Psychopharmacol Oxf Engl. 2020;34:155–166.
7. Sanches RF, de Lima Osório F, Dos Santos RG, Macedo LRH, Maia-de-Oliveira JP, Wichert-Ana L, et al. Antidepressant Effects of a Single Dose of Ayahuasca in Patients With Recurrent Depression: A SPECT Study. J Clin Psychopharmacol. 2016;36:77–81.
8. Winne J, Boerner BC, Malfatti T, Brisa E, Doerl J, Nogueira I, et al. Anxiety-like behavior induced by salicylate depends on age and can be prevented by a single dose of 5-MeO-DMT. Exp Neurol. 2020;326:113175.
9. Ly C, Greb AC, Cameron LP, Wong JM, Barragan EV, Wilson PC, et al. Psychedelics Promote Structural and Functional Neural Plasticity. Cell Rep. 2018;23:3170–3182.
10. Shao L-X, Liao C, Gregg I, Davoudian PA, Savalia NK, Delagarza K, et al. Psilocybin induces rapid and persistent growth of dendritic spines in frontal cortex in vivo. Neuron. 2021;109:2535-2544.e4.
11. Lima da Cruz RV, Moulin TC, Petiz LL, Leão RN. Corrigendum: A Single Dose of 5-MeO-DMT Stimulates Cell Proliferation, Neuronal Survivability, Morphological and Functional Changes in Adult Mice Ventral Dentate Gyrus. Front Mol Neurosci. 2019;12:79.
12. Olson DE. Psychoplastogens: A Promising Class of Plasticity-Promoting Neurotherapeutics. J Exp Neurosci. 2018;12:117906951880050.
13. Morales-Garcia JA, Calleja-Conde J, Lopez-Moreno JA, Alonso-Gil S, Sanz-SanCristobal M, Riba J, et al. N,N-dimethyltryptamine compound found in the hallucinogenic tea ayahuasca, regulates adult neurogenesis in vitro and in vivo. Transl Psychiatry. 2020;10:331.
14. Savalia NK, Shao L-X, Kwan AC. A Dendrite-Focused Framework for Understanding the Actions of Ketamine and Psychedelics. Trends Neurosci. 2021;44:260–275.
15. Benko J, Vranková S. Natural Psychoplastogens As Antidepressant Agents. Molecules. 2020;25:1172.
16. de Vos CMH, Mason NL, Kuypers KPC. Psychedelics and Neuroplasticity: A Systematic Review Unraveling the Biological Underpinnings of Psychedelics. Front Psychiatry. 2021;12:724606.

17. Krystal JH, Tolin DF, Sanacora G, Castner SA, Williams GV, Aikins DE, et al. Neuroplasticity as a target for the pharmacotherapy of anxiety disorders, mood disorders, and schizophrenia. Drug Discov Today. 2009;14:690–697.
18. Jaster AM, de la Fuente Revenga M, González-Maeso J. Molecular targets of psychedelic-induced plasticity. J Neurochem;n/a.
19. Krystal JH, Tolin DF, Sanacora G, Castner SA, Williams GV, Aikins DE, et al. Neuroplasticity as a target for the pharmacotherapy of anxiety disorders, mood disorders, and schizophrenia. Drug Discov Today. 2009;14:690–697.
20. Dakic V, Minardi Nascimento J, Costa Sartore R, Maciel R de M, de Araujo DB, Ribeiro S, et al. Short term changes in the proteome of human cerebral organoids induced by 5-MeO-DMT. Sci Rep. 2017;7:12863.
21. Martin DA, Nichols CD. The Effects of Hallucinogens on Gene Expression. In: Halberstadt AL, Vollenweider FX, Nichols DE, editors. Behav. Neurobiol. Psychedelic Drugs, vol. 36, Berlin, Heidelberg: Springer Berlin Heidelberg; 2017. p. 137–158.
22. Canal CE. Serotonergic Psychedelics: Experimental Approaches for Assessing Mechanisms of Action. In: Maurer HH, Brandt SD, editors. New Psychoact. Subst., vol. 252, Cham: Springer International Publishing; 2018. p. 227–260.
23. Shen H-W, Jiang X-L, Yu A-M. Nonlinear Pharmacokinetics of 5-Methoxy- *N,N* -dimethyltryptamine in Mice. Drug Metab Dispos. 2011;39:1227–1234.
24. Rojas PS, Fiedler JL. What Do We Really Know About 5-HT1A Receptor Signaling in Neuronal Cells? Front Cell Neurosci. 2016;10.
25. Polter AM, Li X. 5-HT1A receptor-regulated signal transduction pathways in brain. Cell Signal. 2010;22:1406–1412.
26. Ryskamp DA, Korban S, Zhemkov V, Kraskovskaya N, Bezprozvanny I. Neuronal Sigma-1 Receptors: Signaling Functions and Protective Roles in Neurodegenerative Diseases. Front Neurosci. 2019;13:862.
27. Inserra A, De Gregorio D, Gobbi G. Psychedelics in Psychiatry: Neuroplastic, Immunomodulatory, and Neurotransmitter Mechanisms. Pharmacol Rev. 2021;73:202–277.
28. Xu Q, Ji X-F, Chi T-Y, Liu P, Jin G, Gu S-L, et al. Sigma 1 receptor activation regulates brain-derived neurotrophic factor through NR2A-CaMKIV-TORC1 pathway to rescue the impairment of learning and memory induced by brain ischaemia/reperfusion. Psychopharmacology (Berl). 2015;232:1779–1791.

29. Ji L-L, Peng J-B, Fu C-H, Tong L, Wang Z-Y. Sigma-1 receptor activation ameliorates anxiety-like behavior through NR2A-CREB-BDNF signaling pathway in a rat model submitted to single-prolonged stress. Mol Med Rep. 2017;16:4987–4993.
30. Duman RS, Li N. A neurotrophic hypothesis of depression: role of synaptogenesis in the actions of NMDA receptor antagonists. Philos Trans R Soc B Biol Sci. 2012;367:2475–2484.
31. Pittenger C, Duman RS. Stress, Depression, and Neuroplasticity: A Convergence of Mechanisms. Neuropsychopharmacology. 2008;33:88–109.
32. Castrén E, Antila H. Neuronal plasticity and neurotrophic factors in drug responses. Mol Psychiatry. 2017;22:1085–1095.
33. Galvão-Coelho NL, de Menezes Galvão AC, de Almeida RN, Palhano-Fontes F, Campos Braga I, Lobão Soares B, et al. Changes in inflammatory biomarkers are related to the antidepressant effects of Ayahuasca. J Psychopharmacol (Oxf). 2020;34:1125–1133.
34. Ali F, Gerhard DM, Sweasy K, Pothula S, Pittenger C, Duman RS, et al. Ketamine disinhibits dendrites and enhances calcium signals in prefrontal dendritic spines. Nat Commun. 2020;11:72.
35. Ku SM, Han M-H. HCN Channel Targets for Novel Antidepressant Treatment. Neurotherapeutics. 2017;14:698–715.
36. Dwyer JM, Duman RS. Activation of mTOR and Synaptogenesis: Role in the Actions of Rapid-Acting Antidepressants. Biol Psychiatry. 2013;73:1189–1198.
37. Surges R, Kukley M, Brewster A, Rüschenschmidt C, Schramm J, Baram TZ, et al. Hyperpolarization-activated cation current Ih of dentate gyrus granule cells is upregulated in human and rat temporal lobe epilepsy. Biochem Biophys Res Commun. 2012;420:156–160.
38. Han Y, Lyman KA, Foote KM, Chetkovich DM. The structure and function of TRIP8b, an auxiliary subunit of hyperpolarization-activated cyclic-nucleotide gated channels. Channels. 2020;14:110–122.
39. Nogueira M, Golbert DC, Leão R. Laser Capture Microdissection optimization for high-quality RNA in mouse brain tissue. 2021.
40. Almeida RN de, Galvão AC de M, da Silva FS, Silva EA dos S, Palhano-Fontes F, Maia-de-Oliveira JP, et al. Modulation of Serum Brain-Derived Neurotrophic Factor by a Single Dose of Ayahuasca: Observation From a Randomized Controlled Trial. Front Psychol. 2019;10:1234.

41. Hirst JA, Howick J, Aronson JK, Roberts N, Perera R, Koshiaris C, et al. The Need for Randomization in Animal Trials: An Overview of Systematic Reviews. PLOS ONE. 2014;9:e98856.
42. Livak KJ, Schmittgen TD. Analysis of relative gene expression data using real-time quantitative PCR and the 2(-Delta Delta C(T)) Method. Methods San Diego Calif. 2001;25:402–408.
43. Lonergan ME, Gafford GM, Jarome TJ, Helmstetter FJ. Time-Dependent Expression of Arc and Zif268 after Acquisition of Fear Conditioning. Neural Plast. 2010;2010:1–12.
44. Impey S, Mark M, Villacres EC, Poser S, Chavkin C, Storm DR. Induction of CRE-Mediated Gene Expression by Stimuli That Generate Long-Lasting LTP in Area CA1 of the Hippocampus. Neuron. 1996;16:973–982.
45. Clayton DF, Anreiter I, Aristizabal M, Frankland PW, Binder EB, Citri A. The role of the genome in experience-dependent plasticity: Extending the analogy of the genomic action potential. Proc Natl Acad Sci. 2020;117:23252–23260.
46. Gallo FT, Katche C, Morici JF, Medina JH, Weisstaub NV. Immediate Early Genes, Memory and Psychiatric Disorders: Focus on c-Fos, Egr1 and Arc. Front Behav Neurosci. 2018;12:79.
47. McHugh SB, Deacon RMJ, Rawlins JNP, Bannerman DM. Amygdala and ventral hippocampus contribute differentially to mechanisms of fear and anxiety. Behav Neurosci. 2004;118:63–78.
48. Fanselow MS, Dong H-W. Are The Dorsal and Ventral Hippocampus functionally distinct structures? Neuron. 2010;65:7.
49. Jimenez JC, Su K, Goldberg AR, Luna VM, Biane JS, Ordek G, et al. Anxiety Cells in a Hippocampal-Hypothalamic Circuit. Neuron. 2018;97:670-683.e6.
50. Bertagna NB, Dos Santos PGC, Queiroz RM, Fernandes GJD, Cruz FC, Miguel TT. Involvement of the ventral, but not dorsal, hippocampus in anxiety-like behaviors in mice exposed to the elevated plus maze: participation of CRF1 receptor and PKA pathway. Pharmacol Rep PR. 2021;73:57–72.
51. Parfitt GM, Nguyen R, Bang JY, Aqrabawi AJ, Tran MM, Seo DK, et al. Bidirectional Control of Anxiety-Related Behaviors in Mice: Role of Inputs Arising from the Ventral Hippocampus to the Lateral Septum and Medial Prefrontal Cortex. Neuropsychopharmacology. 2017;42:1715–1728.

52. Dougherty KA, Nicholson DA, Diaz L, Buss EW, Neuman KM, Chetkovich DM, et al. Differential expression of HCN subunits alters voltage-dependent gating of h-channels in CA1 pyramidal neurons from dorsal and ventral hippocampus. J Neurophysiol. 2013;109:1940–1953.
53. Mikulovic S, Restrepo CE, Siwani S, Bauer P, Pupe S, Tort ABL, et al. Ventral hippocampal OLM cells control type 2 theta oscillations and response to predator odor. Nat Commun. 2018;9:3638.
54. Hilscher MM, Nogueira I, Mikulovic S, Kullander K, Leão RN, Leão KE. Chrna2-OLM interneurons display different membrane properties and h-current magnitude depending on dorsoventral location. Hippocampus. 2019;29:1224–1237.
55. Siwani S, França ASC, Mikulovic S, Reis A, Hilscher MM, Edwards SJ, et al. OLMα2 Cells Bidirectionally Modulate Learning. Neuron. 2018;99:404-412.e3.
56. Li S, Tian X, Hartley DM, Feig LA. Distinct Roles for Ras-Guanine Nucleotide-Releasing Factor 1 (Ras-GRF1) and Ras-GRF2 in the Induction of Long-Term Potentiation and Long-Term Depression. J Neurosci. 2006;26:1721–1729.
57. Autry AE, Adachi M, Nosyreva E, Na ES, Los MF, Cheng P, et al. NMDA receptor blockade at rest triggers rapid behavioural antidepressant responses. Nature. 2011;475:91–95.
58. Xu Q, Ji X-F, Chi T-Y, Liu P, Jin G, Chen L, et al. Sigma-1 receptor in brain ischemia/reperfusion: Possible role in the NR2A-induced pathway to regulate brain-derived neurotrophic factor. J Neurol Sci. 2017;376:166–175.
59. Boyce-Rustay JM, Holmes A. Genetic Inactivation of the NMDA Receptor NR2A Subunit has Anxiolytic- and Antidepressant-Like Effects in Mice. Neuropsychopharmacology. 2006;31:2405–2414.
60. Kim CS, Chang PY, Johnston D. Enhancement of dorsal hippocampal activity by knockdown of HCN1 channels leads to anxiolytic- and antidepressant-like behaviors. Neuron. 2012;75:503–516.
61. Williams SR, Stuart GJ. Site independence of EPSP time course is mediated by dendritic I(h) in neocortical pyramidal neurons. J Neurophysiol. 2000;83:3177–3182.
62. Magee JC. Dendritic Ih normalizes temporal summation in hippocampal CA1 neurons. Nat Neurosci. 1999;2:508–514.

Figure Legends

FIGURE 1. 5-MeO-DMT modulates gene expression in anxiety-related brain structures. A. Experimental design for quantifying immediate early genes (after 1 hr) or late response genes (after 5 hrs) using laser capture microdissection. B. Left, vCA1 showed mRNA downregulation of the NR2A gene 5 hrs after 5-MeO-DMT treatment (-6.8 fold, p=0.01), while no significant changes in expression of other immediate early or late response genes. Middle, 5-MeO-DMT treatment altered BLA mRNA expression by upregulation of the immediate early genes ARC (2.1 fold upregulation, p=0.008) and ZIF268 (1.8 fold upregulation, p=0.02) while BDNF, mTORC1, NFkB, CREB, TRIP8b, and NR2A genes showed no statistically significant changes. Right, anterior cingulate cortex (ACC) presented mRNA upregulation of immediate early ARC gene (1.2 fold, p=0.03) following 5-MeO-DMT treatment. ZIF268, BDNF, mTORC1, NFkB, CREB, TRIP8b and NR2A genes showed no statistically significant changes. C. Representative images (top) showing dentate gyrus before (left) and after (right) laser capture microdissection (LCM). Scale bar: 80µm. Representative images showing respectively vCA1, BLA, and ACC cresyl violet stained slices (bottom). Note that in the vCA1 slice, the hole appears larger than the ROI due to folding of the tissue next to the extracted region. Scale bar: 1mm. D. Left, vCA1 TRIP8B presented upregulation in the vCA1 region after 5 days of 5-MeO-DMT treatment (0.49 fold, p = 0.0004) while TRIP8B, BDNF, NR2A and CREB genes presented no significant changes in the DG after 5 days of 5-MeO-DMT treatment (right). Two-tailed unpaired Student's t-test. *$p\leq0.05$, **$p\leq0.01$, ***$p\leq0.001$

FIGURE 2. Mouse anxiety behavior in the elevated plus maze test under 5-MeO-DMT / saline treatment. A. Experimental design. B. EPM trajectory (top) and heatmap (bottom) of 5-MeO-DMT and saline 24 hours (left) and 5 days (right) after treatment. Yellow shows the open arms trajectory and blue shows closed arms trajectory. C. EPM analyzed variables 24 hours (left) and 5 days (right). Percentage of time spent in the open arms (top, left; p=0.02), percentage of entries in the open arms (top, right; p=0.001 and p=0.009, respectively), travelled distances (middle, right), and speed (right). Two-tailed unpaired Student's t-test. *$p\leq0.05$, **$p\leq0.01$, ***$p\leq0.001$.

FIGURE 3. Locomotor performance in the open field test under 5-MeO-DMT / saline treatment. A. Experimental design. B. OF trajectory (top) and heatmap (bottom) of 5-

MeO-DMT and saline 24 hours (left) and 5 days (right) after treatment. Blue color shows center of arena trajectory and gray shows peripheral trajectory. C. OF analyzed variables 24 hours (left) and 5 days (right). Percentage of time spent in the center of arena (top, letf), entries in the center of arena (top, right; p=0.02 and p=0.003, respectively), travelled distances (middle, right), and speed (right). Two-tailed unpaired Student's t-test. *$p \leq 0.05$, **$p \leq 0.01$.

FIGURE 4. Stressed 5-MeO-DMT treated mice presented less anxious behavior and lower corticosterone serum levels 5 days after treatment. A. Experimental design. B. Corticosterone serum levels in basal and stressed conditions, 5 days after intracerebroventricular administered 5-MeO-DMT (left; p<0.0001) and saline (middle; p<0.0001); 5-MeO-DMT treated mice presented less corticosterone levels compared to control (right, p=0.03). C. EPM and OF trajectory (top) and heatmap (bottom) of 5-MeO-DMT (left) and saline (right) treatments. Yellow shows open arms trajectory, blue shows closed arms trajectory. Blue shows center of arena trajectory and gray shows peripheral trajectory. D. EPM analysis showed more time spent in open arms (letf; p=0.03), and no difference in percentage of entries in open arms (middle, letf), travelled distances (middle, right), or speed (right) in 5-MeO-DMT treated mice. E. OF analysis showed higher percentage of time spent in the center of the arena (letf; p=0.02), but no differences in entries in the center of the arena (middle, letf), travelled distances (middle, right), and speed (right) in 5-MeO-DMT treated mice. Two-tailed unpaired Student's t-test. *$p \leq 0.05$, ***$p \leq 0.001$.

FIGURE 5. A. Unprotected (uDip) and protected (pDip) head dip ethological analysis of 5-MeO-DMT treated mice in the elevated plus maze test. B. EPM unprotected (left) and protected head dip (right) behavior in 5-MeO-DMT and control saline treated mice after 24 hours (p=0.03). C. EPM unprotected (left) and protected head dip (right) behavior in 5-MeO-DMT and control saline treated mice after 5 days (p=0.02 and p=0.001, respectively). D. EPM unprotected (left) and protected head dip (right) behavior in 5-MeO-DMT and control saline treated mice after 5 days under previous acute restraint induced stress (p=0.02 and p=0.007, respectively). E. Pie chart showing the percentages of unprotected and protected head dip in 5-MeO-DMT treated mice (left) and control saline (right). 5-MeO-DMT in yellow and saline in gray. Two-tailed unpaired Student's t-test. *$p \leq 0.05$, **$p \leq 0.01$, ***$p \leq 0.001$.

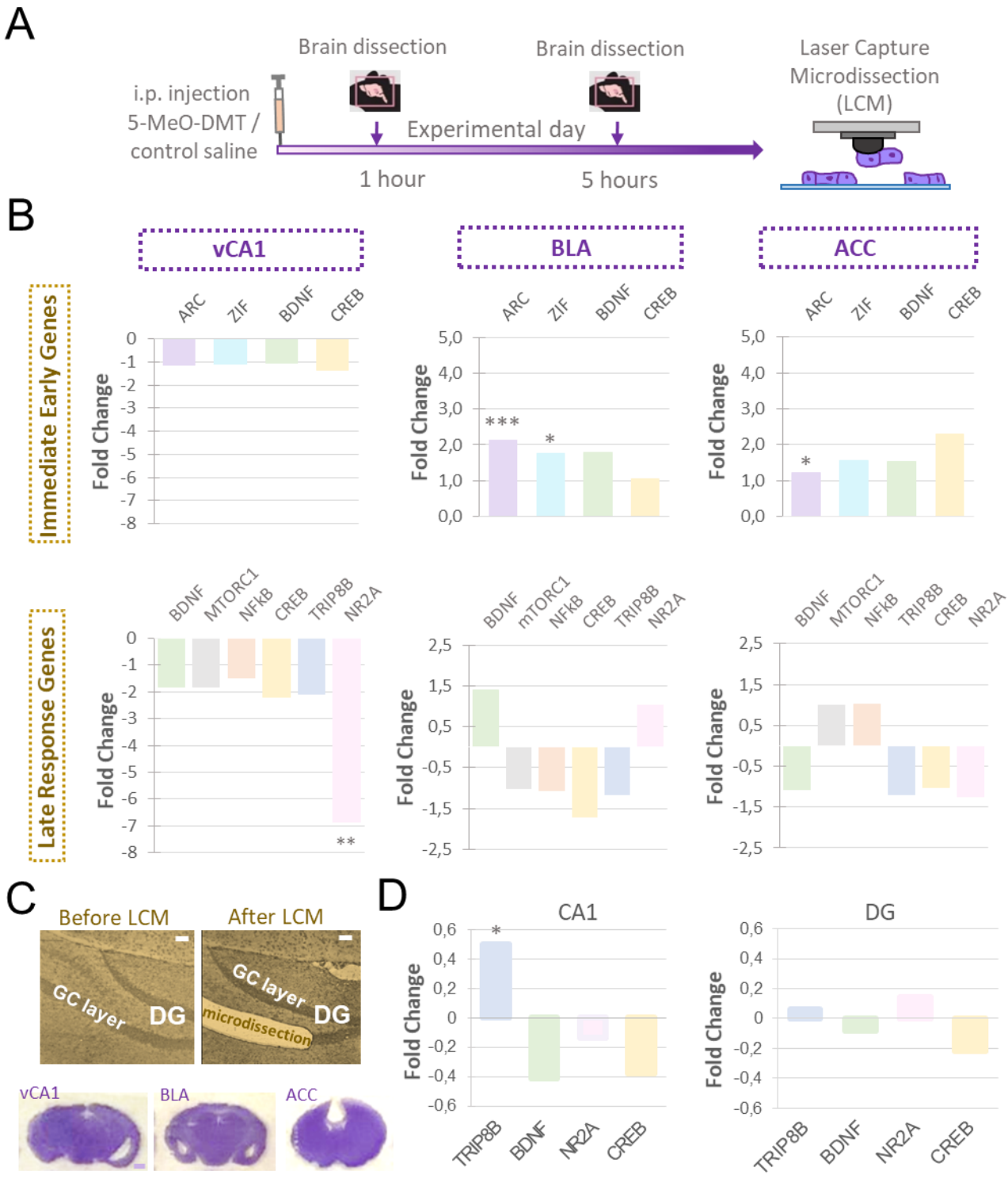
A
Brain dissection
Brain dissection
Laser Capture Microdissection (LCM)
i.p. injection 5-MeO-DMT / control saline
Experimental day
1 hour
5 hours
B
vCA1
BLA
ACC
Immediate Early Genes
ARC
ZIF
BDNF
CREB
Fold Change
Late Response Genes
BDNF
MTORC1
mTORC1
NFkB
CREB
TRIP8B
NR2A
C
Before LCM
After LCM
GC layer
DG
microdissection
vCA1
BLA
ACC
D
CA1
DG
TRIP8B
BDNF
NR2A
CREB

Figure 1

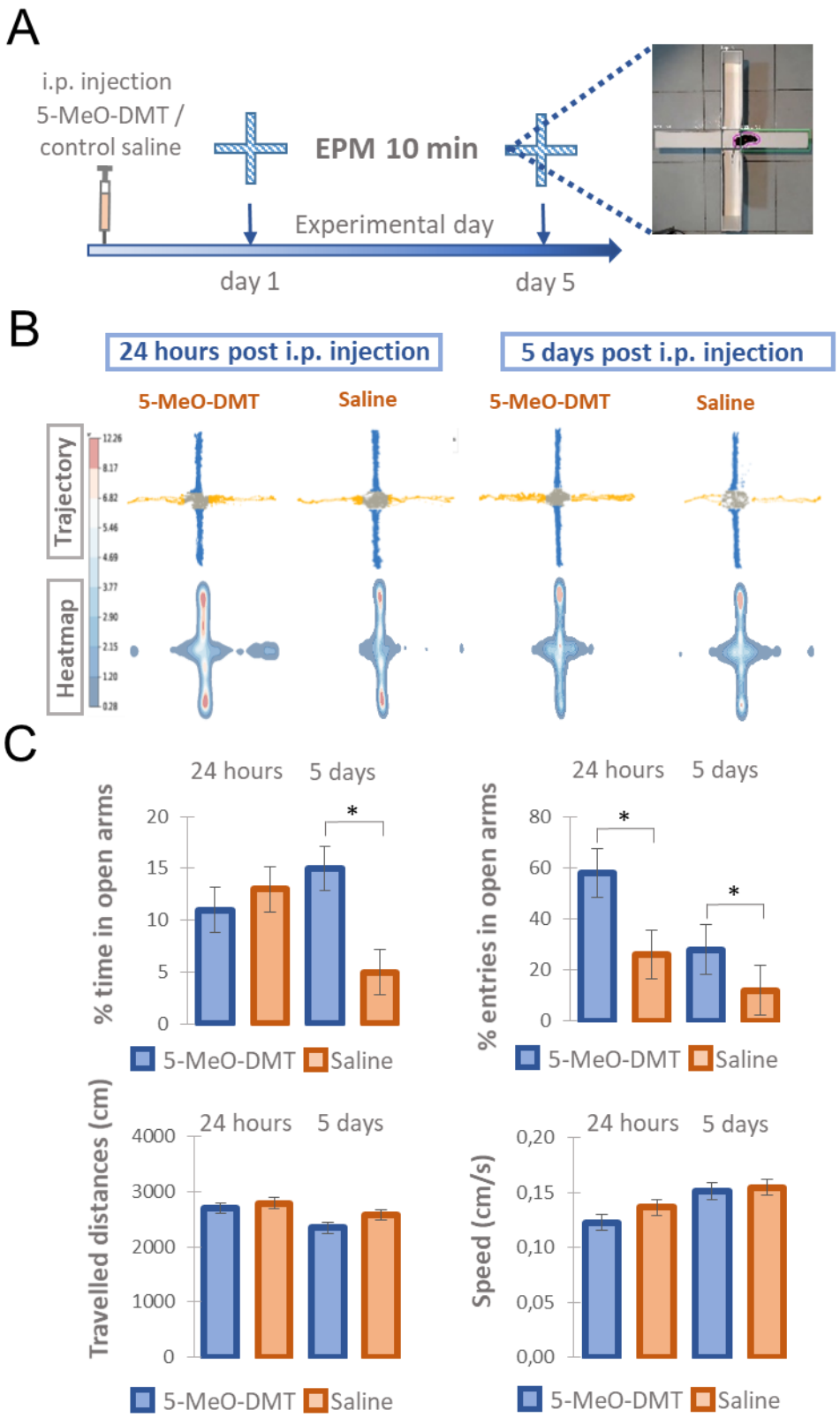
A
i.p. injection
5-MeO-DMT /
control saline
EPM 10 min
Experimental day
day 1
day 5
B
24 hours post i.p. injection
5 days post i.p. injection
5-MeO-DMT
Saline
5-MeO-DMT
Saline
Trajectory
Heatmap
C
24 hours
5 days
% time in open arms
% entries in open arms
Travelled distances (cm)
Speed (cm/s)
5-MeO-DMT
Saline

Figure 2

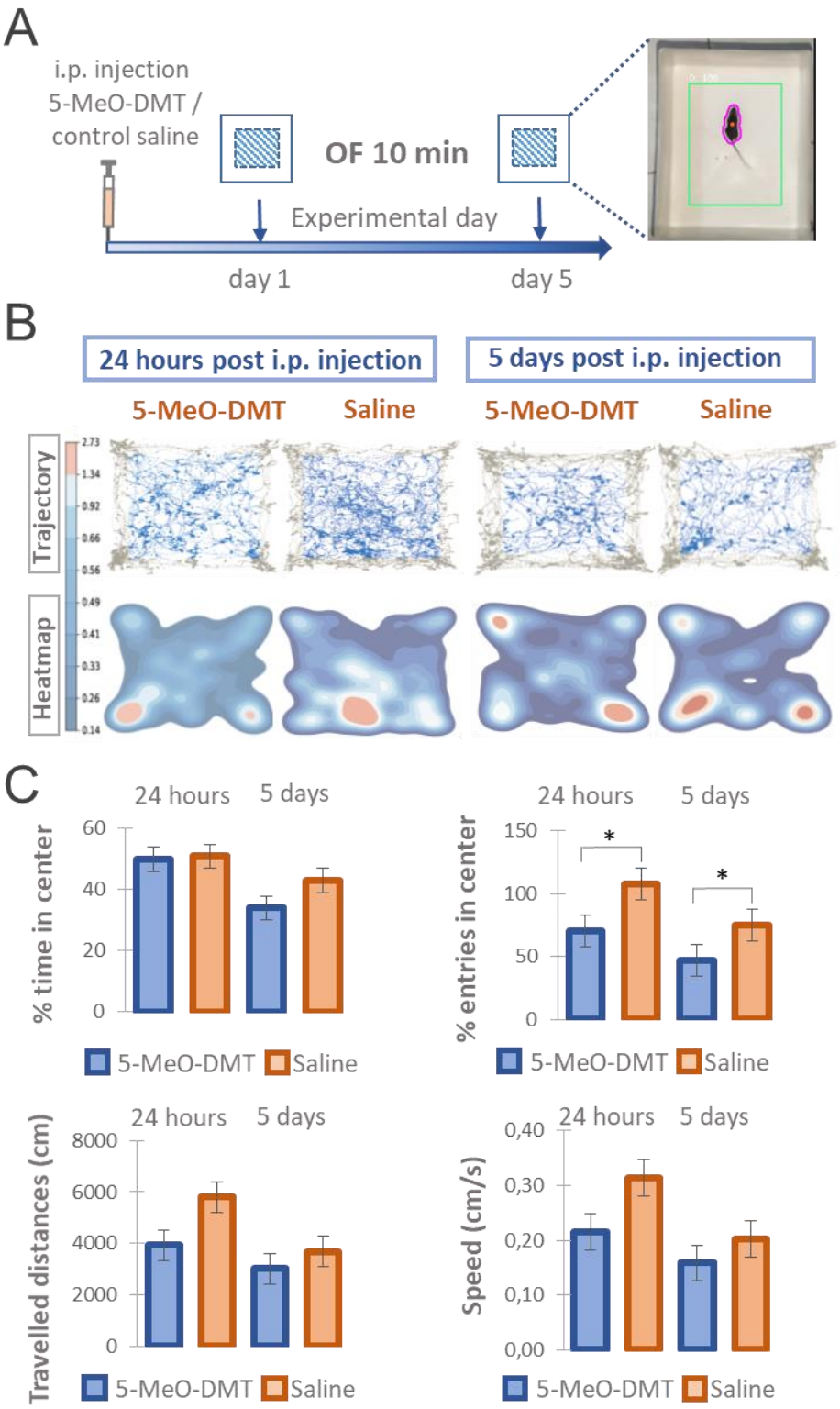
A
i.p. injection
5-MeO-DMT /
control saline
OF 10 min
Experimental day
day 1
day 5
B
24 hours post i.p. injection
5 days post i.p. injection
5-MeO-DMT
Saline
5-MeO-DMT
Saline
Trajectory
Heatmap
C
24 hours
5 days
% time in center
% entries in center
Travelled distances (cm)
Speed (cm/s)
5-MeO-DMT
Saline

Figure 3

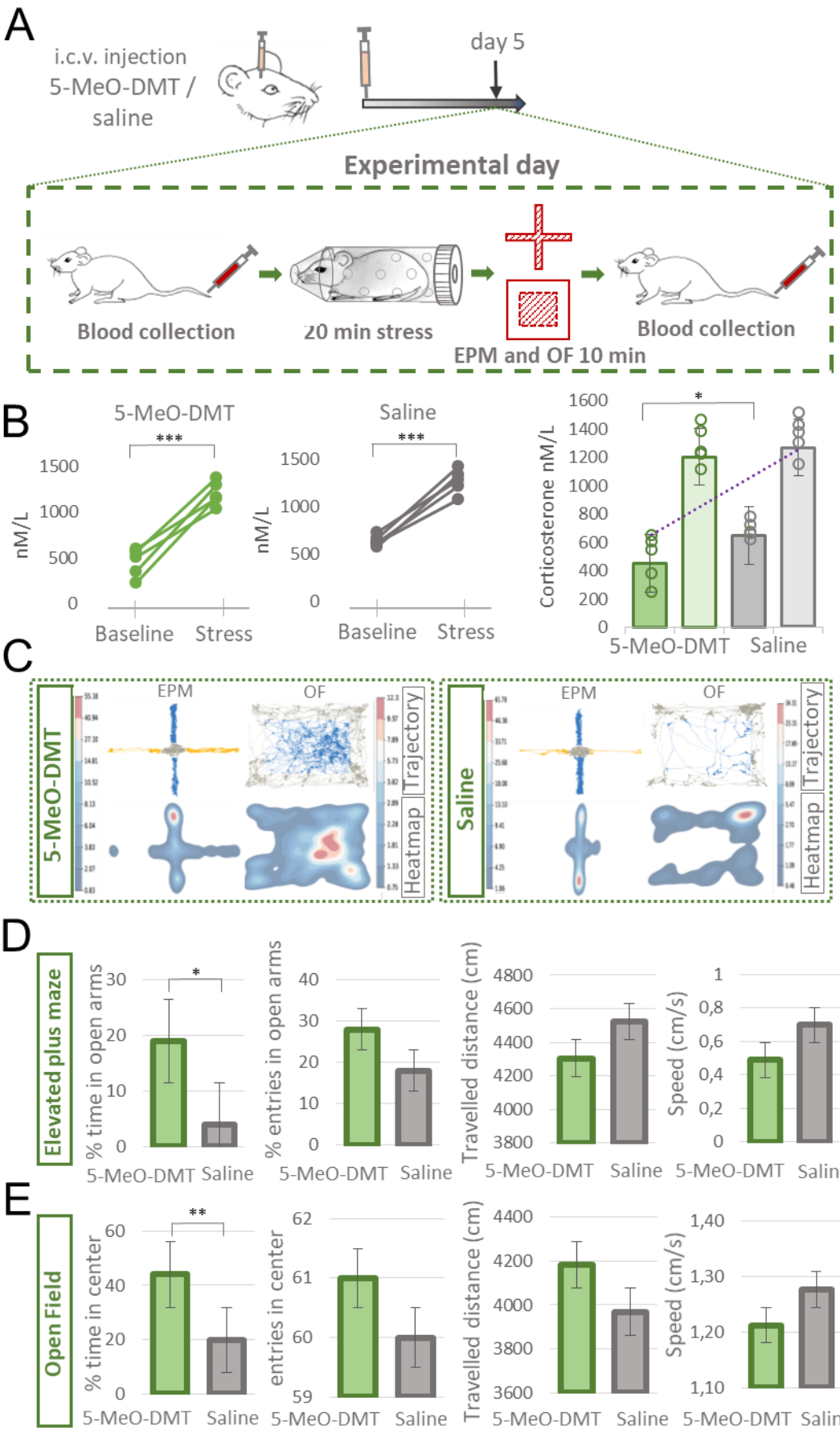
A
i.c.v. injection
5-MeO-DMT /
saline
day 5
Experimental day
Blood collection
20 min stress
EPM and OF 10 min
Blood collection
B
5-MeO-DMT
Saline
***
nM/L
Baseline
Stress
Corticosterone nM/L
5-MeO-DMT
Saline
C
5-MeO-DMT
Saline
EPM
OF
Trajectory
Heatmap
D
Elevated plus maze
% time in open arms
% entries in open arms
Travelled distance (cm)
Speed (cm/s)
E
Open Field
% time in center
entries in center
Travelled distance (cm)
Speed (cm/s)

Figure 4

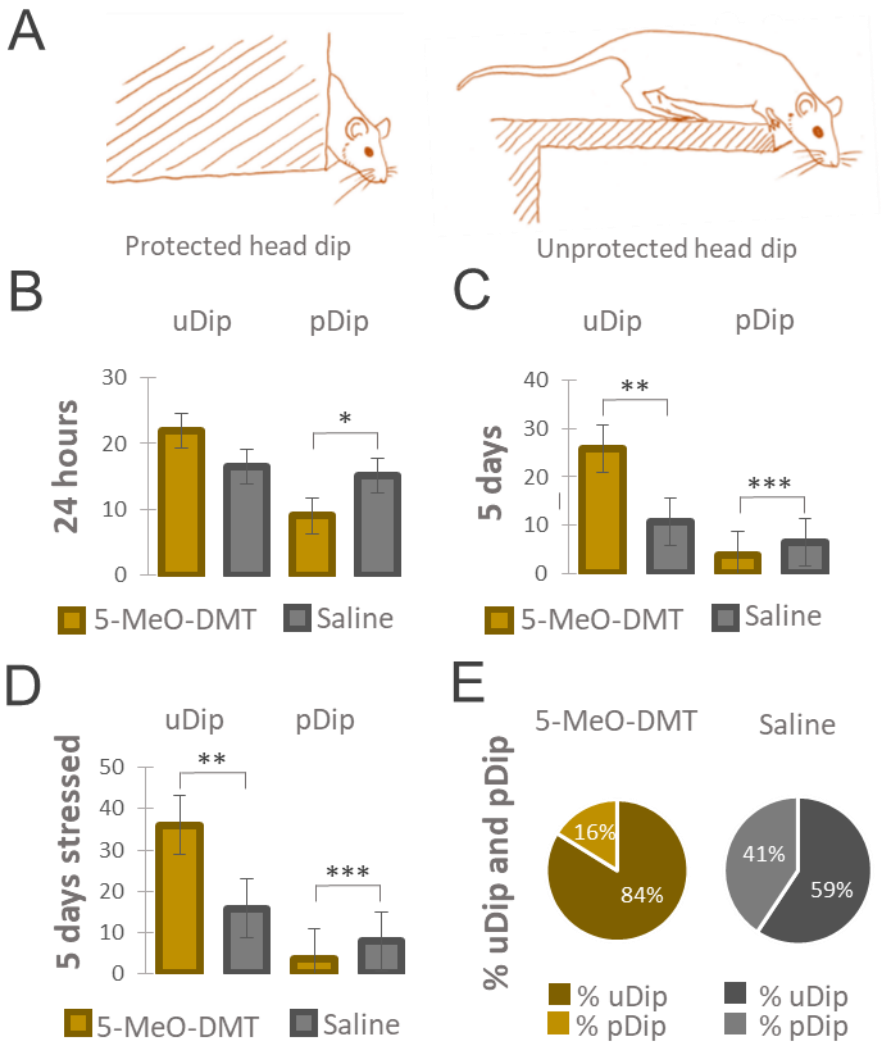
A
Protected head dip
Unprotected head dip
B
uDip
pDip
24 hours
30
20
10
0
*
5-MeO-DMT
Saline
C
uDip
pDip
5 days
40
30
20
10
0
**
***
5-MeO-DMT
Saline
D
uDip
pDip
5 days stressed
50
40
30
20
10
0
**
***
5-MeO-DMT
Saline
E
5-MeO-DMT
Saline
% uDip and pDip
16%
84%
41%
59%
% uDip
% pDip
% uDip
% pDip

Figure 5

Manuscript 3

This manuscript is under preparation and presents data from single cell electrophysiology from Ventral Dentate Gyrus of mouse brain after 5 days of 5-MeO-DMT treatment. The data presented here is going to be complemented by collaborators' work in the Ventral CA1 region for future publication.

5-methoxy-N,N-dimethyltryptamine (5-MeO-DMT) long-lasting effects on dentate gyrus electrophysiological profile

Margareth Nogueira[1], Richardson Leão[1*]

[1]Neurodynamics Lab, Brain Institute, Federal University of Rio Grande do Norte, Natal, Brazil

***Correspondence:**
Richardson Leão
richardson.leao@neuro.ufrn.br

Abstract

Serotonergic psychedelics are getting attention due to growing evidence pointing to their therapeutic capabilities against anxiety and mood disorders, often with a single dose. This long-lasting effect is possibly due to neuroprotective properties and structural plasticity. Here, we sought to verify the effect of 5-methoxy-N,N-dimethyltryptamine (5-MeO-DMT) on firing patterns and membrane properties in the hippocampus dentate gyrus granule cells (GC) 5 days after treatment. We found that 5-MeO-DMT leads to higher input resistance, hyperpolarized resting membrane potential, besides a higher voltage peak amplitude and afterhyperpolarization. On the other hand, we identified a lower firing rate in 5-MeO-DMT treated mice compared to control.

Keywords: 5-MeO-DMT, lasting effects, synaptic plasticity, neuronal activity, gene expression, calcium transients, dentate gyrus, CA1, hippocampus.

Materials and Methods

Ethics Statement

This study was approved by the local ethics committee on animal care of the Federal University of Rio Grande do Norte (Protocol 110.035/2018). The approved protocol is in accordance with the recommendations of the National Council for the Control of Animal Experimentation (CONCEA) in Brazil.

Animals

Adult C57BL6J mice from both sexes aged between 30–60 days were housed under a 12h light /12h dark cycle, with food and water *ad libitum* and controlled temperature at 23^{o}C.

5-MeO-DMT treatment

Mice from both sexes were anesthetized with isoflurane (4% L/min for induction and 1.5% L/min for maintenance; Lima da Cruz et al., 2018) and received a single ICV injection of 1μL 5-MeO-DMT solution prepared fresh (100μg 5-MeO-DMT in 10% DMSO/90% saline). The control group received 1μL of 10% DMSO in saline at 0.9% (stereotaxic coordinates: 0.2 mm AP, 1.0 mm ML and 2.25 mm DV; Lima da Cruz et al., 2018).

Electrophysiology

4 – 8 weeks C57BL6J mice from both sexes were anesthetized with ketamine (90 mg/kg) and then intracardially perfused standard artificial cerebrospinal fluid (aCSF; in mM: NaCl 124; KCl, 2.5; NaH_2PO_4,1.2; $NaHCO_3$, 24; glucose, 12.5; $CaCl_2$, 2; $MgCl_2$, 2) at room temperature. Brains were dissected and then transferred to a Vibratome (VT1200, Leica Microsystems) chamber containing ice-cold aCSF. Horizontal slices with 400μm thickness were collected and transferred to a holding chamber containing recover N-methyl-D-glucamine (NMDG) solution (in mM NMDG, 92; KCl, 2.5; NaH_2PO_4,1.25; $NaHCO_3$, 30; HEPES, 20; glucose, 25; thiourea, 2; sodium-ascorbate, 5; sodium-pyruvate, 3; $CaCl_2 \cdot 4H_2O$, 0.5; $10MgSO_4 \cdot 7H_2O$, 10; pH controlled to 7.3–7.4 with 2N HCl solution) at 34◦C for 15 min, and then returned to aCSF for at least 1 hour at room temperature before recordings. The slices were kept in standard aCSF, constantly bubbled

with carbogen 95% O2 and 5% CO2. (White-Martins; Ting et al., 2014). Then, the tissue was transferred to a submerged chamber filled with standard oxygenated aCSF under a ZEISS microscope. Borosilicate glass capillaries (GC150F-10, Harvard Apparatus, MA, USA) were pulled on a vertical puller (PC-10, Narishige, Japan). Micropipettes (8-12 MΩ resistance) were filled with K-gluconate internal solution (in mM, K-Gluconate, 145; HEPES, 10; EGTA, 1; Mg-ATP, 2; Na_2-GTP, 0.3; $MgCl_2$, 2; 290–300 mOsm; pH 7.3, adjusted using KOH). Granule cells were identified by DIC light transmission (Olympus, Japan) in the dentate gyrus granule layer of hippocampus. Current-clamp recordings (to analyze trigger properties of action potentials in DG granular cells) were obtained using an Axopatch amplifier 200B (Molecular Devices) in whole-cell configuration using the winWCP Strathclyde Electrophysiology Software (J. Dempster, University of Strathclyde).

Data analysis

Current clamp data were analyzed using winWCP software. Passive and active membrane properties were examined in response to a 500ms long 100pA current step and a 1500ms long ramp to 200pA current clamp protocol. All active properties were assessed by the first action potential of a 100pA current stimulus. The AP threshold was defined as the voltage in which the rate of rise reaches a value superior to 20 mv/ms. The peak amplitude was measured from the resting membrane potential. The latency was considered as the time between the depolarizing stimulus and the peak of the action potential. The afterhyperpolarization amplitude (AHP) was taken from the threshold to the lower limit of the voltage. Finally, the rheobase was considered as the minimum current necessary to trigger an action potential and was measured through the ramp protocol.

Statistical Analysis

Changes in membrane and synaptic properties were evaluated by comparing the 5-MeO-DMT group and saline control, unpaired two-tailed *t*-test (GraphPad Prism, available online, https://www.graphpad.com/quickcalcs/ttest1.cfm). All statistical data are presented as the mean ± standard error of the mean (SEM).

Results

5-MeO-DMT affects passive and active membrane properties of granular cells.

In order to verify any effects on electrophysiological properties of dentate gyrus granule cells, we performed whole-cell patch-clamp recordings in slices from mice that had received intracerebroventricular (ICV) injection of 5-MeO-DMT 5 days prior to the experiment. Granule cells were identified by imaging the dentate gyrus granule layer (figure 1A). Current clamp recordings showed similar patterns of action potentials and hyperpolarizing traces in response to positive (+100pA) and negative (-100pA) current steps, respectively (Figure 1B) from 5-MeO-DMT treatment and control saline injected mice. However, cells from 5-MeO-DMT treated mice presented a higher input resistance and a more hyperpolarized resting membrane potential in comparison to control saline treated animals 5 days after a 5-MeO-DMT ICV injections (saline: 330.45 ±26.51MΩ, n = 11; 5-MeO-DMT: 418.79 ±30.41 MΩ, n = 12, p = 0.04 and saline: -75.54 mV ±0.38, n = 13; 5-MeO-DMT: -77.88 mV ±0.25, n = 16, p <0.0001, unpaired t-test, Figures 1C-D, respectively).

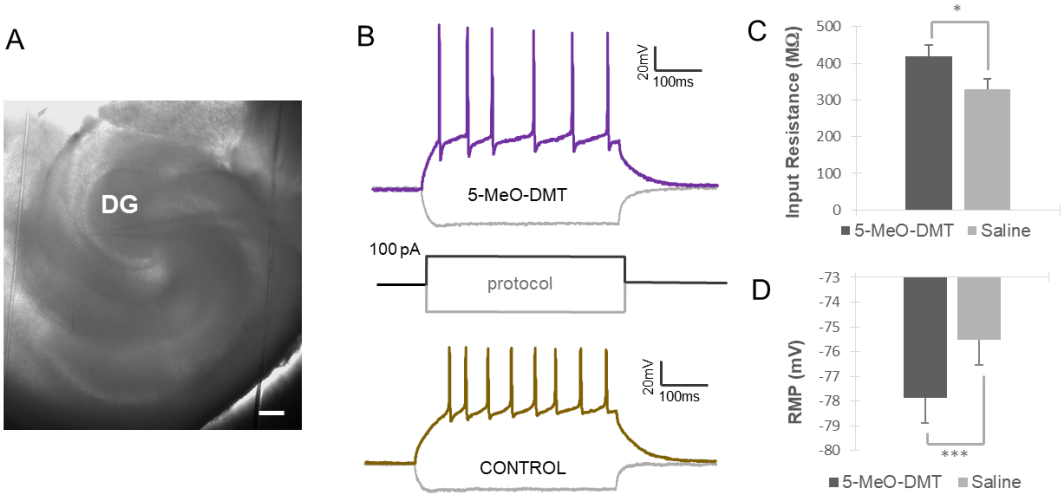

Figure 1 5-MeO-DMT alters input resistance and resting membrane potential in the ventral Dentate Gyrus cells after 5 days. (A) Horizontal section showing region of interest. Scale bar: 200µm. **(B)** Representative traces in response to current steps from 5-MeO-DMT (top) and saline control (bottom). **(C)** Mean input resistance. **(D)** Mean resting membrane potential. *p = 0.04 and ***p <0.0001

Next action potential features were analyzed in detail, by quantifying the first action potential in response to +100pA current step (Figure 2A). First, the action potential peak amplitude was higher in 5-MeO-DMT treated cells (saline: 92.37 ±3.66mV, n=13; 5-MeO-DMT: 106.52 ±3.95 mV, n=16, *p*=0.01, Figure 2B). These cells also showed wider half-width (saline: 1.20±0.06 ms, n=12; 5-MeO-DMT: 1.48±0.08 ms, n=15, *p*=0.01, Figure 2C), although the rate of rise and the action potential threshold presented no significant differences. The afterhyperpolarization amplitude was higher in 5-MeO-DMT treated cells but not the afterhyperpolarization duration (saline: -7.43±0.89mV, n=12; 5-MeO-DMT: -12.31 ±0.71mV, n=15, *p*=0.0002, Figure 2D; and saline: 135.41 ±5.61 ms, n=12; 5-MeO-DMT: -166.69 ±024.11 ms, n=15, *p*=0.26, Figure 2E).

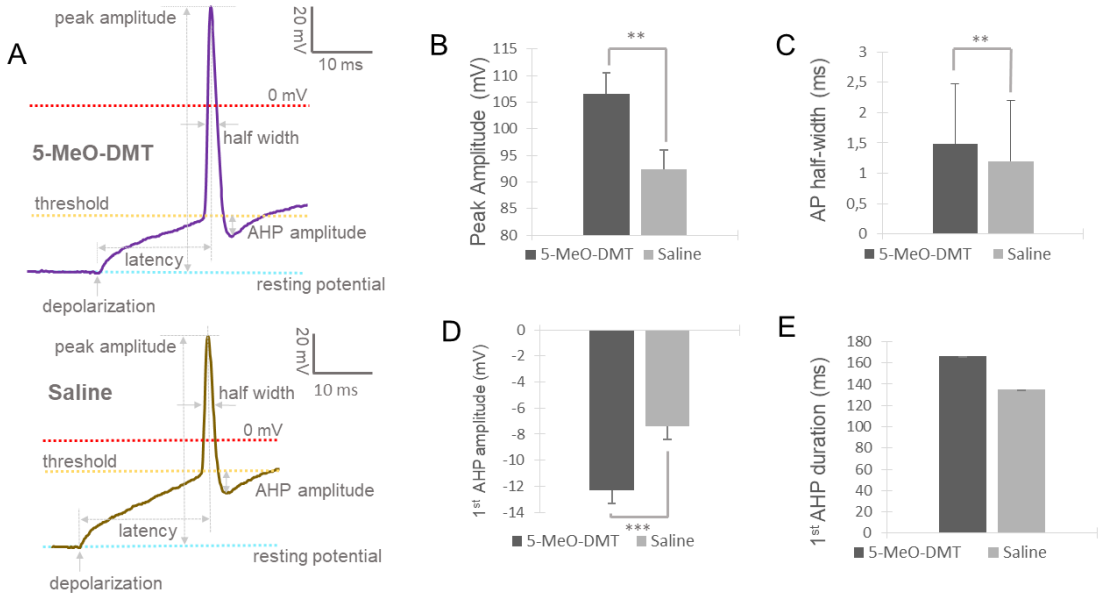

Figure 2 Action Potential properties of Dentate Gyrus Granule Cells reveals higher peak amplitude, wider half-width and a higher first AP AHP amplitude. (A) Representative traces of the first action potential elicited by a 100pA current step, 5-MeO-DMT (top) and control saline (bottom). **(B)** Peak amplitude comparison. **(C)** Action potential half-width. **(D)** First AP AHP amplitude **(E)** First AP AHP duration. ***p* = 0.01, ***p* = 0.01 and ****p* =0.0002, respectively

As 5-MeO-DMT could potentially interfere with the excitability of granule cells, we wanted to examine the minimum current needed to generate spikes (rheobase). Using a ramp protocol (1500ms duration, 0-200pA) we found no difference in rheobase or the number of spikes generated by the ramp protocol between the 5-MeO-DMT treated or saline treated mice (Figure 3A-C).

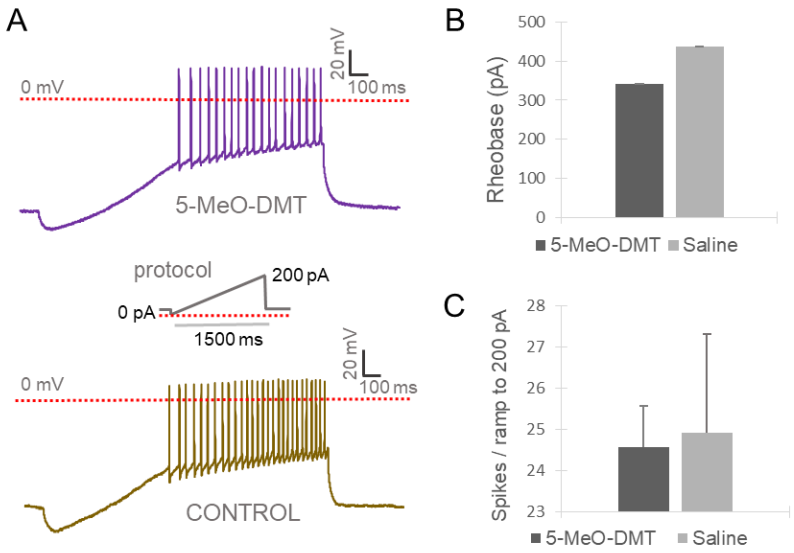

Figure 3 Ramp protocol analysis. (A) Representative traces of ramp 5-MeO-DMT (top) and control saline (bottom). Rheobase **(B)** and number of spikes **(C)**.

When analyzing the firing rate in response to depolarizing current steps (100 – 250pA, 500ms duration) from horizontal slices from animals sacrificed 5 days after 5-MeO-DMT or saline treatment we found the mean firing frequency was significantly lower for 5-MeO-DMT treated mice at a 100pA current step (saline: 26.30 ±1.92Hz, n=11; 5-MeO-DMT: 21.09 ±1.69Hz, n=14, p=0.05, Figure 5A-C). Comparing firing frequency in response to higher current steps also showed steady state frequency to, at higher current steps (250pA) be lower in 5-MeO-DMT treated mice compared to saline treated mice (p=0.03, Figure 5D). Examining initial firing frequency (from the ISI of the first two action potentials), no significant differences were found. , Finally, the mean firing frequency was also significant lower at 200pA and 250pA steps, but increased linearly in response to higher currents in both experimental conditions (150pA, 200pA and 250pA,

p=0.17, *p*=0.024 and *p*=0.03, respectively, Figure 5E). All membrane properties are summarized in Table 1.

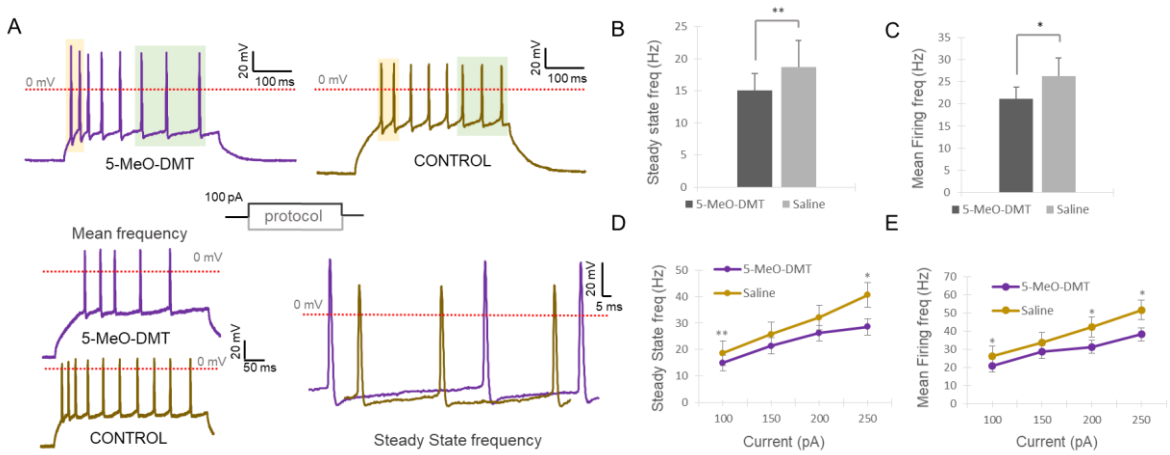

Figure 4 5-MeO-DMT alters firing frequency in the ventral Dentate Gyrus Granule Cells after 5 days. (A) Representative traces showing firing frequency in response to a 500ms current injection of 100 pA. Yellow shadows highlight the first two APs used for calculating initial frequency and green shadows highlight the last 3 APs used for calculating steady-state frequency (top). Representative traces of mean firing frequency from each group are shown in bottom left (5-MeO-DMT on top and control saline on bottom). Higher magnification of traces highlighting the difference in steady state frequency of 5-MeO-DMT and saline treated mice after 5 days (bottom right). Magenta traces refers to 5-MeO-DMT treatment and yellow traces refers to saline control. **(B)** Steady state frequency comparison between 5-MeO-DMT and saline groups. **(C)** Firing frequency comparison between 5-MeO-DMT and saline injected animals. ***p*=0.01 and **p* = 0.05, respectively. **(D)** Steady state frequency over current plots. ***p*=0.01 and **p*=0.03 **(E)** Mean firing frequency over current plots. **p*=0.05, **p*=0.02, and **p*=0.03.

Table 1 Passive and active membrane properties extracted from dentate gyrus Granule cells (GC) after 5 days of 5-MeO-DMT and saline treatments.

	SALINE	SEM	n	5-MeO-DMT	SEM	n	*p* value
RMP (mV)	-75.54	±0.38	13	-77.88	±0.25	16	**0.0001**
$R_{inp\ (M\Omega)}$	330.45	±26.51	11	418.79	±30.41	16	**0.04**
Latency (ms)	130.89	±22.76	13	124.20	±21.00	16	0.83
Threshold (mV)	-37.25	±4.11	13	-39.75	±2.68	16	0.60
Rate of Rise (mV/ms)	68.33	±7.72	13	83.42	±10.30	16	0.27
Peak Amplitude (mV)	92.37	±3.66	13	106.52	±3.95	16	**0.01**
Half width (ms)	1.20	±0.06	12	1.48	±0.08	15	**0.01**
AHP amplitude (mV)	-7.43	±0.89	12	-12.31	±0.71	15	**0.0002**
AHP duration (ms)	135.41	±5.61	12	166.69	±24.11	15	0.26
Rheobase (pA)	426.75	±23.49	13	362.35	±34.88	18	0.17
ISI (ms)	40.24	±3.22	12	49.48	±3.43	13	0.06
ISI initial (ms)	27.41	±4.52	11	31.87	±6.17	14	0.64
ISI steady state (ms)	55.33	±3.22	11	69.20	±3.33	14	**0.01**
$Frequency_{mean}$ (Hz)	26.30	±1.92	11	21.09	±1.69	14	**0.05**
$Frequency_{initial}$ (Hz)	50.43	±8.80	11	46.00	±7.71	14	0.70
$Frequency_{steady\ state}$ (Hz)	18.70	±1.10	11	15.01	±0.92	14	**0.01**

RMP – resting membrane potential. R_{inp} – input resistance. ISI – interspike interval. AHP – afterhyperpolarization. Rheobase, was assessed from the current ramp protocol.Student's t-Test, two-tailed, equal variance. Data show Standard Error of the Mean (SEM). * $p \leq 0.05$ *.

Conflict of Interest

The authors declare that the research was conducted in the absence of any commercial or financial relationships that could be construed as a potential conflict of interest.

Funding

This study was supported by CAPES, an agency of the Brazilian government's Ministry of Science and Technology dedicated to the coordination and improvement of higher education personnel.

General Discussion

This thesis investigates molecular, cellular and behavioral effects of 5-MeO-DMT in mice. Specifically, this study sought to verify whether 5-MeO-DMT plays a role in the modulation of plasticity-related genes and on neuronal activity, in anxiety-related brain structures. The main techniques applied were mRNA extracted from microdissected samples (Manuscript 1), RT-qPCR, hormone measurements and anxiety tests (Manuscript 2), and single-cell electrophysiology (Manuscript 3).

The first study is a methodological manuscript describing high-quality RNA acquisition from neuronal subregions. By this, we first calibrated the microdissection equipment (PALM, Zeiss) and tested adequate sample preparation for RNA extraction. In this process we identified that an adjustment in the standard laser capture microdissection (LCM) protocol, decreasing sample handling and temperature variation, provided high-quality RNA, which we now describe in detail in a pre-printed article (Nogueira et al., 2021). Thereby the first study was a necessary methodological effort to allow for the second study of this thesis where we aimed to investigate whether a single dose of 5-MeO-DMT modulates plasticity-related genes and affects anxiety-related behavior in mice. Without the refinement of the protocol for the RNA collected samples and a tight quality control, the accuracy of results could be affected, as degradation affects transcripts differently, generating a bias in gene quantification (Reiman et al., 2017). Hence, extraction of high-quality RNA is critical in gene quantification studies.

In general, the consequences of gene expression modulation by a treatment can be varied. Outcome depends on the functions of the gene, the cell type expressing the gene, the circuit, brain structure or the signaling pathway in which it is involved. However, a gene can be activated by a compound through a signaling cascade, without necessarily changing expression level. Here, our second manuscript is a first step in examining the role of a given gene in synaptic plasticity under 5-MeO-DMT treatment. To note, it is important to also focus on genes that remain at normal levels, showing no change in expression hours or days after 5-MeO-DMT administration. Here BDNF, CREB, and mTORC1 are key-genes involved in structural plasticity and included in other psychedelics studies (Ly et al., 2018; Galvão-Coelho et al., 2020; de Vos et al., 2021; de Almeida et al., 2019). No change in expression of these genes suggests that the

mechanisms of action of 5-MeO-DMT may not go through their signaling pathways. This is surprising, since BDNF and CREB are important plasticity-related genes, and here we found no relative expression alteration at either of the three time points examined.

One hypothesis suggests that the long-term effects of psychedelics are due to neuroplasticity. A recent systematic review identified only 16 preclinical studies involving psychedelics and plasticity (de Vos et al., 2021). Added to this small number, the study also identified a large variability of methodological approaches, such as studies in rodents and humans, with different psychedelic substances, doses, targets, types of plasticity, as well as different times of post-treatment detection. Among the 16 studies, all except one showed positive results towards a modulation through plasticity, however, the lack of reproducibility added to the different types of approaches indicates that there is still no clear evidence on the mechanisms of action underlying plasticity induced by the classic psychedelics (Ali et al., 2020). BDNF is the main factor of neurogenesis, neuritogenesis, and synaptic plasticity regulation and highly expressed in many brain regions (Pittenger and Duman, 2008) and anxious and depressed individuals present decreased levels of BDNF (Duman and Li, 2012). BDNF, CREB and mTOR are together all part of signaling pathways involved in plasticity (de Vos et al., 2021), which makes it important that studies confirm their modulation under 5-MeO-DMT treatment. Here we examined 8 different plasticity related genes and also quantified effects of a single dose of 5-MeO-DMT on anxiety behavior. Anxiety is tightly linked to memory formation and one consequence of neuronal activity, as for memory formation, is the synaptic plasticity induced by the transcription of genes that ultimately trigger *de novo* protein synthesis (dendritic or axonal protein synthesis). Still, it is also important to investigate immediate early genes, as effects of psychedelics such as 5-MeO-DMT can be rapid (Nutt, 2020).

Here, to evaluate the response of immediate early genes, which express rapidly without the need of *de novo* protein synthesis, we collected samples one hour after 5-MeO-DMT administration, because as soon as these transient expression genes reach a peak they return to their basal state (Lonergan et al., 2010; Clayton et al., 2020). Two immediate early genes are ARC and ZIF268 that have peak of RNA expression levels between 30 and 60 minutes and are involved in synaptic plasticity (such as long-term potentiation; LTP) and in the induction of late-response gene transcription (Lonergan et al., 2010; Impey et al., 1996; Clayton et al., 2020; Gallo et al., 2018). ZIF268 is a transcription factor that participates in intracellular signal transduction pathways and initial genomic

response together with epigenetic actors, such as microRNAs (miRNAs) and long noncoding RNAs (lncRNAs) (Lonergan et al., 2010**)**. The expression of ZIF268 depends on synaptic activity and NMDA activation, which takes part of LTP the induction (Lonergan et al., 2010). ARC is an effector immediate early gene related to memory consolidation and is strongly linked to LTP and rapidly expressed in response to synaptic activity and mostly expressed in excitatory neurons, thereby underlying glutamatergic transmission (Lonergan et al., 2010). Both genes were upregulated in regions such as ACC and BLA, suggesting that 5-MeO-DMT may play a modulating role on synaptic plasticity.

To note, immediate early genes, which characterize cellular activity, were unchanged in the ventral CA1. Instead, 5-MeO-DMT decreased 6.8 fold the expression of NR2A mRNA in the vCA1 compared to control animals 5 hours after 5-MeO-DMT intake. NR2A subunits contribute to the electrophysiological properties of the NMDA receptor (Canal, 2018b; Autry et al., 2011; Xu et al., 2017; Xu et al., 2015). It has been previously shown that genetic inactivation of NR2A has anxiolytic effects in mice tested in EPM, OF and dark/light exploration test (Boyce-Rustay and Holmes, 2006), which corroborates our results where we found NR2A downregulation in combination with anxiolytic effects in mice treated with 5-MeO-DMT. In addition, 5 days after a single 5-MeO-DMT dose, TRIP8b mRNA expression was upregulated in the vCA1 compared to control animals. One possible mechanism of psychedelic action is the modulation of hippocampal activity due to an increase in HCNs activity and the hyperpolarization-activated current (I_h) (Santoro and Shah, 2020; Braun, 2009; Ku and Han, 2017; Lewis et al., 2011; Piskorowski et al., 2011; Shah, 2014). The TRIP8b regulates the activation of HCN channels, thereby contributing to modulating neuronal excitability if HCN channels are active at rest (Magee, 1999). An upregulation of 0.5 fold in the expression of the TRIP8b gene, 5 days after treatment, in the ventral CA1 may indicate a lowered neuronal activity in this region. Further studies using voltage and current clamp can show if the stronger expression of TRIP8b leads to increased I_h, and the I_h blocker ZD7288 could confirm whether the increased TRIP8b expression is modulating vCA1 activity. Nevertheless, a limitation of our study is that we evaluate all genes of interest in the same preparation thereby it was not possible to collect individual gene samples (ie. sacrifice the animal) at the respective time of peak expression (Lonergan et al., 2010). To circumvent this, we performed independent experiments at three moments. We verified the peak expression

timing for each gene, and adopted an approximate average of the peak expression of each gene analyzed.

Synaptic plasticity involves many genes (Gallo et al., 2018; Xu et al., 2017; Santoro and Shah, 202; Benko and Vranková, 2020), but here we chose the following ARC, ZIF268, BDNF, CREB, NR2A, mTORC1, TRIP8b, and NF-kB, as they have been implicated for having a psychedelic action (Inserra et al., 2021; Dakic et al., 2017; Ly et al., 2018; Olson, 2018). Here, laser capture microdissection has enormous advantages regarding the accuracy of the tissue collected because it precisely defines the region studied, avoiding signals from adjacent tissue. However, the amount of RNA extracted is small and does not allow the evaluation of many genes per sample. Genes related to the HPA axis, anxiety markers like NPTX, genes involved in the sigma-1 receptor pathway, and other genes involved with plasticity such as the VGF and Hif-1 were not studied due to the limitation in the number of genes analyzed. Instead, the RNA-Sequencing method could fully cover the genes that vary in expression and are a more precise alternative to microarrays (which just cover predefined genes and is a hybridization-based technique). Also, RNA-seq allows a full sequence of the whole transcriptome, besides splice variants (isoforms generated by alterations in the process of joining exons), and non-coding transcripts involved in epigenetic regulation, such as microRNA (miRNA) and long non-coding RNA (lncRNA) (Rao et al., 2019). The RNA-sequencing method could provide a more detailed understanding of neural circuits, and specific single-cell RNA-sequencing (scRNA-seq) can provide insights to the pathways that underlie pharmacological plasticity-induction in anxiety-related circuits (Ressler et al., 2020; Ressler and Maren, 2019). However, RNA-sequencing is an expensive method and still suffers expression-timing issues.

Another way to study effects of pharmacological substances such as 5-MeO-DMT is to examine any long-lasting electrophysiological effects it may have on certain neurons. Here we examined granule cells of the hippocampal dentate gyrus granule layer, using whole-cell patch-clamp 5 days after a single injection of 5-MeO-DMT. Although no correlation can be made between the cellular and molecular results, especially because we found transcriptional alterations in the vCA1, but not in the DG, neuronal activity in the DG after 5 hours of treatment was significantly decreased. Specifically, we found that mean and steady-state firing frequency was significantly lower for 5-MeO-DMT treated mice compared to saline control. Also, 5-MeO-DMT affects passive and active membrane

properties. RMP is hyperpolarized and Rinp is increased compared to control saline treated animals. 5-MeO-DMT leads to higher peak amplitude, wider half-width, and a more hyperpolarized afterhyperpolarization (AHP).

Another factor that is important to discuss is that dose-dependence has an influence on gene expression. A study has reported an increase in neurogenesis at a single low dose of psilocybin (0.1 mg/kg, i.p.) and a decrease in neurogenesis at a single high dose (1.0mg/kg) (de Vos et al., 2021; Catlow et al., 2013). Another study applying chronic Ayahuasca administration to rats has shown no hippocampal alteration of BDNF protein levels (Galvão-Coelho et al., 2020). However, after 3 hours, rats treated with high doses of Ayahuasca presented increased hippocampal BDNF, which suggests dose-dependence and chronic vs. acute administration differences (de Vos et al., 2021; Colaço et al., 2020). In addition, a single dose of psilocybin (0.20, 0.24, 0.5, 1.0mg/kg i.p.) differentially induced expression of immediate early genes depending on dose and time point (de Vos et al., 2021). Between the normally used 5-MeO-DMT i.p. doses (low 2 mg/kg, the middle 10mg/kg, and the higher 20mg/kg) in mice (Halberstadt, 2016) (Halberstadt, 2016; Shen, 2011; Jiang et al., 2016; Halberstadt, 2017), we choose the higher dose as it presented a clear response (Shen, 2011; Jiang et al., 2016). Regarding agonist action of 5-MeO-DMT, when studying serotonergic psychedelics binding to the 5HT-2A, 5HT-1A, and sigma-1 receptor, it is important to consider that 5-MeO-DMT may cause synergistic effects since the 5HT1A and sigma1 receptors share the IP3 pathway in the endoplasmic reticulum. Still, such synergistic effects remain to be further investigated.

This thesis has also demonstrated that 5-MeO-DMT promotes anxiolysis 24 hours and 5 days after treatment, and lowers basal serum corticosterone levels. The results indicate that 5-MeO-DMT promotes long-lasting alterations in the brain as well as modulates behavior, observed until 5 days after drug exposure. However, it is still premature to support the hypothesis that the action of 5-MeO-DMT in affective disorders is based on neuroplasticity through the candidate genes analyzed. Many questions remain to be elucidated regarding psychedelics and plasticity, such as a clear definition of the pathways involved, optimal doses to reach plasticity effects, circuits involved as well as integration of firing and interneuron participation, among several others. Therefore, further studies are needed to reproduce and complement the findings. However, the present thesis provides starting points to elucidate the 5-MeO-DMT mechanisms of action and to what extent these molecular changes can influence behavior.

Conclusion

This thesis reveals that 5-MeO-DMT modulates the mRNA expression of four out of eight plasticity-related candidate genes and promotes anxiolysis, in addition to leading to changes in the electrophysiological profile of hippocampal neurons. Besides, this thesis contributed to an optimized protocol for LCM acquision, resulting in high-quality RNA, which is important to minimize bias related do RNA degradation. Altogether, these results point towards a long-lasting role of 5-MeO-DMT in mouse physiology and behavior. From a translational perspective, extrapolating animal results to humans is difficult in psychedelic research, due to natural behavioral and pharmacokinetic differences. However, the molecular, cellular, and behavioral findings suggest that 5-MeO-DMT produces effects beyond subjective changes observed in humans. For possible therapeutic effects, further studies are necessary to validate the clinical efficiency and unravel which signaling pathways underlie the 5-MeO-DMT role on synaptic plasticity.

References

Aday JS, Mitzkovitz CM, Bloesch EK, Davoli CC, Davis AK (2020) Long-term effects of psychedelic drugs: A systematic review. Neuroscience & Biobehavioral Reviews 113:179–189.

Adhikari A (2014) Distributed circuits underlying anxiety. Front Behav Neurosci 8 Available at: http://journal.frontiersin.org/article/10.3389/fnbeh.2014.00112/abstract [Accessed September 29, 2021].

Adhikari A, Topiwala MA, Gordon JA (2011) Single Units in the Medial Prefrontal Cortex with Anxiety-Related Firing Patterns Are Preferentially Influenced by Ventral Hippocampal Activity. Neuron 71:898–910.

Alamia A, Timmermann C, Nutt DJ, VanRullen R, Carhart-Harris RL (2020) DMT alters cortical travelling waves van Wassenhove V, Behrens TE, Alexander DM, eds. eLife 9:e59784.

Ali F, Gerhard DM, Sweasy K, Pothula S, Pittenger C, Duman RS, Kwan AC (2020) Ketamine disinhibits dendrites and enhances calcium signals in prefrontal dendritic spines. Nat Commun 11:72.

Autry AE, Adachi M, Nosyreva E, Na ES, Los MF, Cheng P, Kavalali ET, Monteggia LM (2011) NMDA Receptor Blockade at Rest Triggers Rapid Behavioural Antidepressant Responses. Nature 475:91–95.

Barsuglia J, Davis AK, Palmer R, Lancelotta R, Windham-Herman A-M, Peterson K, Polanco M, Grant R, Griffiths RR (2018a) Intensity of Mystical Experiences Occasioned by 5-MeO-DMT and Comparison With a Prior Psilocybin Study. Front Psychol 9:2459.

Barsuglia JP, Polanco M, Palmer R, Malcolm BJ, Kelmendi B, Calvey T (2018b) A case report SPECT study and theoretical rationale for the sequential administration of ibogaine and 5-MeO-DMT in the treatment of alcohol use disorder. In: Progress in Brain Research, pp 121–158. Elsevier. Available at: https://linkinghub.elsevier.com/retrieve/pii/S0079612318300931 [Accessed September 29, 2021].

Benko J, Vranková S (2020) Natural Psychoplastogens As Antidepressant Agents. Molecules 25:1172.

Boyce-Rustay JM, Holmes A (2006) Genetic Inactivation of the NMDA Receptor NR2A Subunit has Anxiolytic- and Antidepressant-Like Effects in Mice. Neuropsychopharmacology 31:2405–2414.

Braun AP (2009) Alternative splicing of TRIP8b diversifies its actions as an accessory subunit of neuronal HCN channels. Channels 3:217–218.

Calhoon GG, Tye KM (2015a) Resolving the neural circuits of anxiety. Nat Neurosci 18:1394–1404.

Calhoon GG, Tye KM (2015b) Resolving the neural circuits of anxiety. Nat Neurosci 18:1394–1404.

Cameron LP, Nazarian A, Olson DE (2020) Psychedelic Microdosing: Prevalence and Subjective Effects. Journal of Psychoactive Drugs 52:113–122.

Canal CE (2018b) Serotonergic Psychedelics: Experimental Approaches for Assessing Mechanisms of Action. Handb Exp Pharmacol 252:227–260.

Carhart-Harris RL, Bolstridge M, Rucker J, Day CMJ, Erritzoe D, Kaelen M, Bloomfield M, Rickard JA, Forbes B, Feilding A, Taylor D, Pilling S, Curran VH, Nutt DJ (2016) Psilocybin with psychological support for treatment-resistant depression: an open-label feasibility study. Lancet Psychiatry 3:619–627.

Catlow BJ, Song S, Paredes DA, Kirstein CL, Sanchez-Ramos J (2013) Effects of psilocybin on hippocampal neurogenesis and extinction of trace fear conditioning. Exp Brain Res 228:481–491.

Chaudun F (2016) Involvement of dorsomedial prefrontal projections pathways to the basolateral amygdala and ventrolateral periaqueductal grey matter in conditioned fear expression. :160.

Chrousos GP (2009) Stress and disorders of the stress system. Nat Rev Endocrinol 5:374–381.

Clayton DF, Anreiter I, Aristizabal M, Frankland PW, Binder EB, Citri A (2020) The role of the genome in experience-dependent plasticity: Extending the analogy of the genomic action potential. Proc Natl Acad Sci USA 117:23252–23260.

Colaço CS, Alves SS, Nolli LM, Pinheiro WO, de Oliveira DGR, Santos BWL, Pic-Taylor A, Mortari MR, Caldas ED (2020) Toxicity of ayahuasca after 28 days daily exposure and effects on monoamines and brain-derived neurotrophic factor (BDNF) in brain of Wistar rats. Metab Brain Dis 35:739–751.

Dakic V, Minardi Nascimento J, Costa Sartore R, Maciel R de M, de Araujo DB, Ribeiro S, Martins-de-Souza D, Rehen SK (2017) Short term changes in the proteome of human cerebral organoids induced by 5-MeO-DMT. Sci Rep 7:12863.

Davis AK, Barsuglia JP, Lancelotta R, Grant RM, Renn E (2018) The epidemiology of 5-methoxy- *N*, *N* -dimethyltryptamine (5-MeO-DMT) use: Benefits, consequences, patterns of use, subjective effects, and reasons for consumption. J Psychopharmacol (Oxf) 32:779–792.

de Almeida RN, Galvão AC de M, da Silva FS, Silva EADS, Palhano-Fontes F, Maia-de-Oliveira JP, de Araújo L-SB, Lobão-Soares B, Galvão-Coelho NL (2019) Modulation of Serum Brain-Derived Neurotrophic Factor by a Single Dose of Ayahuasca: Observation From a Randomized Controlled Trial. Front Psychol 10:1234.

De Gregorio D, Aguilar-Valles A, Preller KH, Heifets BD, Hibicke M, Mitchell J, Gobbi G (2021) Hallucinogens in Mental Health: Preclinical and Clinical Studies on LSD, Psilocybin, MDMA, and Ketamine. J Neurosci Off J Soc Neurosci 41:891–900.

De Gregorio D, Enns JP, Nuñez NA, Posa L, Gobbi G (2018) d-Lysergic acid diethylamide, psilocybin, and other classic hallucinogens: Mechanism of action

and potential therapeutic applications in mood disorders. In: Progress in Brain Research, pp 69–96. Elsevier. Available at: https://linkinghub.elsevier.com/retrieve/pii/S0079612318300694 [Accessed February 12, 2022].

de Vos CMH, Mason NL, Kuypers KPC (2021) Psychedelics and Neuroplasticity: A Systematic Review Unraveling the Biological Underpinnings of Psychedelics. Front Psychiatry 12:724606.

dos Santos RG, Bouso JC, Alcázar-Córcoles MÁ, Hallak JEC (2018) Efficacy, tolerability, and safety of serotonergic psychedelics for the management of mood, anxiety, and substance-use disorders: a systematic review of systematic reviews. Expert Rev Clin Pharmacol 11:889–902.

dos Santos RG, Hallak JE, Baker G, Dursun S (2021) Hallucinogenic/psychedelic 5HT2A receptor agonists as rapid antidepressant therapeutics: Evidence and mechanisms of action. J Psychopharmacol (Oxf) 35:453–458.

Dougherty KA, Islam T, Johnston D (2012) Intrinsic excitability of CA1 pyramidal neurones from the rat dorsal and ventral hippocampus. J Physiol 590:5707–5722.

Duman RS, Li N (2012) A neurotrophic hypothesis of depression: role of synaptogenesis in the actions of NMDA receptor antagonists. Philos Trans R Soc B Biol Sci 367:2475–2484.

Fanselow MS, Dong H-W (2010) Are the Dorsal and Ventral Hippocampus Functionally Distinct Structures? Neuron 65:7–19.

Felix-Ortiz AC, Beyeler A, Seo C, Leppla CA, Wildes CP, Tye KM (2013) BLA to vHPC Inputs Modulate Anxiety-Related Behaviors. Neuron 79:658–664

Fontanilla D, Johannessen M, Hajipour AR, Cozzi NV, Jackson MB, Ruoho AE (2009) The Hallucinogen *N,N* -Dimethyltryptamine (DMT) Is an Endogenous Sigma-1 Receptor Regulator. Science 323:934–937.

Gallo FT, Katche C, Morici JF, Medina JH, Weisstaub NV (2018) Immediate Early Genes, Memory and Psychiatric Disorders: Focus on c-Fos, Egr1 and Arc. Front

Behav Neurosci 12 Available at: https://www.frontiersin.org/article/10.3389/fnbeh.2018.00079 [Accessed February 12, 2022].

Galvão-Coelho NL, de Menezes Galvão AC, de Almeida RN, Palhano-Fontes F, Campos Braga I, Lobão Soares B, Maia-de-Oliveira JP, Perkins D, Sarris J, de Araujo DB (2020) Changes in inflammatory biomarkers are related to the antidepressant effects of Ayahuasca. J Psychopharmacol (Oxf) 34:1125–1133.

Halberstadt AL (2016) Behavioral and pharmacokinetic interactions between monoamine oxidase inhibitors and the hallucinogen 5-methoxy-N,N-dimethyltryptamine. Pharmacol Biochem Behav 143:1–10.

Herman JP, McKlveen JM, Ghosal S, Kopp B, Wulsin A, Makinson R, Scheimann J, Myers B (2016) Regulation of the hypothalamic-pituitary-adrenocortical stress response. Compr Physiol 6:603–621.

Hunsaker MR, Kesner RP (2008) Dissociations across the dorsal-ventral axis of CA3 and CA1 for encoding and retrieval of contextual and auditory-cued fear. Neurobiol Learn Mem 89:61–69.

Impey S, Mark M, Villacres EC, Poser S, Chavkin C, Storm DR (1996) Induction of CRE-Mediated Gene Expression by Stimuli That Generate Long-Lasting LTP in Area CA1 of the Hippocampus. Neuron 16:973–982.

Inserra A (2018) Hypothesis: The Psychedelic Ayahuasca Heals Traumatic Memories via a Sigma 1 Receptor-Mediated Epigenetic-Mnemonic Process. Front Pharmacol 9:330.

Inserra A, De Gregorio D, Gobbi G (2021) Psychedelics in Psychiatry: Neuroplastic, Immunomodulatory, and Neurotransmitter Mechanisms Nader M, ed. Pharmacol Rev 73:202–277.

Janak PH, Tye KM (2015) From circuits to behaviour in the amygdala. Nature 517:284–292.

Jiang X-L, Shen H-W, Yu A-M (2016) Modification of 5-methoxy-N,N-dimethyltryptamine-induced hyperactivity by monoamine oxidase A inhibitor

harmaline in mice and the underlying serotonergic mechanisms. Pharmacol Rep PR 68:608–615.

JiaWen W, Hong S, ShengXiang X, Jing L (2018) Depression- and anxiety-like behaviour is related to BDNF/TrkB signalling in a mouse model of psoriasis. Clin Exp Dermatol 43:254–261.

Knapska E, Radwanska K, Werka T, Kaczmarek L (2007) Functional Internal Complexity of Amygdala: Focus on Gene Activity Mapping After Behavioral Training and Drugs of Abuse. Physiological Reviews 87:1113–1173.

Kelmendi B, Kaye AP, Pittenger C, Kwan AC (2022) Psychedelics. Curr Biol CB 32:R63–R67.

Kourrich S, Su T-P, Fujimoto M, Bonci A (2012) The sigma-1 receptor: roles in neuronal plasticity and disease. Trends Neurosci 35:762–771.

Ku SM, Han M-H (2017) HCN Channel Targets for Novel Antidepressant Treatment. Neurotherapeutics 14:698–715.

Laubach M, Amarante LM, Swanson K, White SR (2018) What, If Anything, Is Rodent Prefrontal Cortex? eNeuro 5:ENEURO.0315-18.2018.

LeDoux JE (2000) EMOTION CIRCUITS IN THE BRAIN. :30.

Lewis AS, Vaidya SP, Blaiss CA, Liu Z, Stoub TR, Brager DH, Chen X, Bender RA, Estep CM, Popov AB, Kang CE, Van Veldhoven PP, Bayliss DA, Nicholson DA, Powell CM, Johnston D, Chetkovich DM (2011) Deletion of the Hyperpolarization-Activated Cyclic Nucleotide-Gated Channel Auxiliary Subunit TRIP8b Impairs Hippocampal Ih Localization and Function and Promotes Antidepressant Behavior in Mice. Journal of Neuroscience 31:7424–7440.

Liberzon I, Duval E, Javanbakht A (2015a) Neural circuits in anxiety and stress disorders: a focused review. TCRM:115.

Lima da Cruz RV, Moulin TC, Petiz LL, Leão RN (2019) Corrigendum: A Single Dose of 5-MeO-DMT Stimulates Cell Proliferation, Neuronal Survivability, Morphological and Functional Changes in Adult Mice Ventral Dentate Gyrus. Front Mol Neurosci 12:79.

Lonergan ME, Gafford GM, Jarome TJ, Helmstetter FJ (2010) Time-Dependent Expression of Arc and Zif268 after Acquisition of Fear Conditioning. Neural Plasticity 2010:1–12.

Lukasiewicz K, Baker JJ, Zuo Y, Lu J (2021) Serotonergic Psychedelics in Neural Plasticity. Front Mol Neurosci 14:748359.

Ly C, Greb AC, Cameron LP, Wong JM, Barragan EV, Wilson PC, Burbach KF, Soltanzadeh Zarandi S, Sood A, Paddy MR, Duim WC, Dennis MY, McAllister AK, Ori-McKenney KM, Gray JA, Olson DE (2018) Psychedelics Promote Structural and Functional Neural Plasticity. Cell Rep 23:3170–3182.

Magee JC (1999) Dendritic Ih normalizes temporal summation in hippocampal CA1 neurons. Nat Neurosci 2:508–514.

McKlveen JM, Myers B, Herman JP (2015) The Medial Prefrontal Cortex: Coordinator of Autonomic, Neuroendocrine and Behavioural Responses to Stress. J Neuroendocrinol 27:446–456.

McNaughton N, Gray JA (2000) Anxiolytic action on the behavioural inhibition system implies multiple types of arousal contribute to anxiety. J Affect Disord 61:161–176.

Mikulovic S, Restrepo CE, Siwani S, Bauer P, Pupe S, Tort ABL, Kullander K, Leão RN (2018) Ventral hippocampal OLM cells control type 2 theta oscillations and response to predator odor. Nat Commun 9:3638.

Murnane KS (2018) The renaissance in psychedelic research: What do preclinical models have to offer. In: Progress in Brain Research, pp 25–67. Elsevier. Available at: https://linkinghub.elsevier.com/retrieve/pii/S0079612318300955 [Accessed September 29, 2021].

Nichols DE, Johnson MW, Nichols CD (2017) Psychedelics as Medicines: An Emerging New Paradigm. Clin Pharmacol Ther 101:209–219.

Nogueira M, Golbert DC, Leão R (2021) Laser Capture Microdissection optimization for high-quality RNA in mouse brain tissue. :2021.08.30.458265 Available at:

https://www.biorxiv.org/content/10.1101/2021.08.30.458265v1 [Accessed February 12, 2022].

Nutt D, Erritzoe D, Carhart-Harris R (2020) Psychedelic Psychiatry's Brave New World. Cell 181:24–28.

Olson DE (2018) Psychoplastogens: A Promising Class of Plasticity-Promoting Neurotherapeutics. J Exp Neurosci 12:117906951880050.

Ortiz S, Latsko MS, Fouty JL, Dutta S, Adkins JM, Jasnow AM (2019) Anterior Cingulate Cortex and Ventral Hippocampal Inputs to the Basolateral Amygdala Selectively Control Generalized Fear. J Neurosci 39:6526–6539.

Padilla-Coreano N, Bolkan SS, Pierce GM, Blackman DR, Hardin WD, Garcia-Garcia AL, Spellman TJ, Gordon JA (2016) Direct Ventral Hippocampal-Prefrontal Input Is Required for Anxiety-Related Neural Activity and Behavior. Neuron 89:857–866.

Palhano-Fontes F et al. (2019) Rapid antidepressant effects of the psychedelic ayahuasca in treatment-resistant depression: a randomized placebo-controlled trial. Psychol Med 49:655–663.

Palhano-Fontes F, Andrade KC, Tofoli LF, Santos AC, Crippa JAS, Hallak JEC, Ribeiro S, de Araujo DB (2015) The psychedelic state induced by ayahuasca modulates the activity and connectivity of the default mode network. PloS One 10:e0118143.

Piskorowski R, Santoro B, Siegelbaum SA (2011) TRIP8b Splice Forms Act in Concert to Regulate the Localization and Expression of HCN1 Channels in CA1 Pyramidal Neurons. Neuron 70:495–509.

Pittenger C, Duman RS (2008) Stress, Depression, and Neuroplasticity: A Convergence of Mechanisms. Neuropsychopharmacol 33:88–109.

Polter AM, Li X (2010) 5-HT1A receptor-regulated signal transduction pathways in brain. Cell Signal 22:1406–1412.

Rao MS, Van Vleet TR, Ciurlionis R, Buck WR, Mittelstadt SW, Blomme EAG, Liguori MJ (2019) Comparison of RNA-Seq and Microarray Gene Expression Platforms for the Toxicogenomic Evaluation of Liver From Short-Term Rat Toxicity

Studies. Front Genet 9 Available at: https://www.frontiersin.org/article/10.3389/fgene.2018.00636 [Accessed February 12, 2022].

Reiman M, Laan M, Rull K, Sõber S (2017) Effects of RNA integrity on transcript quantification by total RNA sequencing of clinically collected human placental samples. FASEB J 31:3298–3308.

Ressler KJ (2020) Translating Across Circuits and Genetics Toward Progress in Fear- and Anxiety-Related Disorders. Am J Psychiatry 177:214–222.

Ressler RL, Goode TD, Evemy C, Maren S (2020) NMDA receptors in the CeA and BNST differentially regulate fear conditioning to predictable and unpredictable threats. Neurobiol Learn Mem 174:107281.

Ressler RL, Maren S (2019) Synaptic Encoding of Fear Memories in the Amygdala. Curr Opin Neurobiol 54:54–59.

Riga MS, Lladó-Pelfort L, Artigas F, Celada P (2018) The serotonin hallucinogen 5-MeO-DMT alters cortico-thalamic activity in freely moving mice: Regionally-selective involvement of 5-HT1A and 5-HT2A receptors. Neuropharmacology 142:219–230.

Ryskamp DA, Korban S, Zhemkov V, Kraskovskaya N, Bezprozvanny I (2019) Neuronal Sigma-1 Receptors: Signaling Functions and Protective Roles in Neurodegenerative Diseases. Front Neurosci 13:862.

Santoro B, Shah MM (2020) Hyperpolarization-Activated Cyclic Nucleotide-Gated Channels as Drug Targets for Neurological Disorders. Annu Rev Pharmacol Toxicol 60:109–131.

Savalia NK, Shao L-X, Kwan AC (2021) A Dendrite-Focused Framework for Understanding the Actions of Ketamine and Psychedelics. Trends Neurosci 44:260–275.

Schmidt A, Müller F, Dolder PC, Schmid Y, Zanchi D, Egloff L, Liechti ME, Borgwardt S (2018) Acute Effects of Methylphenidate, Modafinil, and MDMA on Negative Emotion Processing. Int J Neuropsychopharmacol 21:345–354.

Shah MM (2014) Cortical HCN channels: function, trafficking and plasticity: Cortical HCN channels. J Physiol 592:2711–2719.

Shao L-X, Liao C, Gregg I, Davoudian PA, Savalia NK, Delagarza K, Kwan AC (2021) Psilocybin induces rapid and persistent growth of dendritic spines in frontal cortex in vivo. Neuron 109:2535-2544.e4.

Sharma D, Golla N, Singh D, Onteru SK (2018) A highly efficient method for extracting next-generation sequencing quality RNA from adipose tissue of recalcitrant animal species. J Cell Physiol 233:1971–1974.

Shen H-W, Jiang X-L, C. Winter J, Yu A-M (2010) Psychedelic 5-Methoxy-N,N-Dimethyltryptamine: Metabolism, Pharmacokinetics, Drug Interactions, and Pharmacological Actions. Curr Drug Metab 11:659–666.

Sousa MBC de, Silva HPA, Galvão-Coelho NL (2015) Resposta ao estresse: I. Homeostase e teoria da alostase. Estud Psicol 20:1–10.

Strange BA, Witter MP, Lein ES, Moser EI (2014) Functional organization of the hippocampal longitudinal axis. Nat Rev Neurosci 15:655–669.

Sylvers P, Lilienfeld SO, LaPrairie JL (2011) Differences between trait fear and trait anxiety: Implications for psychopathology. Clin Psychol Rev 31:122–137.

Szabo A, Kovacs A, Riba J, Djurovic S, Rajnavolgyi E, Frecska E (2016) The Endogenous Hallucinogen and Trace Amine N,N-Dimethyltryptamine (DMT) Displays Potent Protective Effects against Hypoxia via Sigma-1 Receptor Activation in Human Primary iPSC-Derived Cortical Neurons and Microglia-Like Immune Cells. Front Neurosci 10 Available at: http://journal.frontiersin.org/Article/10.3389/fnins.2016.00423/abstract [Accessed February 12, 2022].

Terluin B, Oosterbaan DB, Brouwers EP, van Straten A, van de Ven PM, Langerak W, van Marwijk HW (2014) To what extent does the anxiety scale of the Four-Dimensional Symptom Questionnaire (4DSQ) detect specific types of anxiety disorder in primary care? A psychometric study. BMC Psychiatry 14:121.

Tye KM, Prakash R, Kim S-Y, Fenno LE, Grosenick L, Zarabi H, Thompson KR, Gradinaru V, Ramakrishnan C, Deisseroth K (2011) Amygdala circuitry mediating reversible and bidirectional control of anxiety. Nature 471:358–362.

Uthaug MV, Lancelotta R, van Oorsouw K, Kuypers KPC, Mason N, Rak J, Šuláková A, Jurok R, Maryška M, Kuchař M, Páleníček T, Riba J, Ramaekers JG (2019) A single inhalation of vapor from dried toad secretion containing 5-methoxy-N,N-dimethyltryptamine (5-MeO-DMT) in a naturalistic setting is related to sustained enhancement of satisfaction with life, mindfulness-related capacities, and a decrement of psychopathological symptoms. Psychopharmacology 236:2653–2666.

WHO-MSD-MER-2017.2-eng.pdf.

Winne J, Boerner BC, Malfatti T, Brisa E, Doerl J, Nogueira I, Leão KE, Leão RN (2020) Anxiety-like behavior induced by salicylate depends on age and can be prevented by a single dose of 5-MeO-DMT. Experimental Neurology 326:113175.

Vollenweider FX, Kometer M (2010) The neurobiology of psychedelic drugs: implications for the treatment of mood disorders. Nat Rev Neurosci 11:642–651.

Xu Q, Ji X-F, Chi T-Y, Liu P, Jin G, Chen L, Zou L-B (2017) Sigma-1 receptor in brain ischemia/reperfusion: Possible role in the NR2A-induced pathway to regulate brain-derived neurotrophic factor. J Neurol Sci 376:166–175.

Xu Q, Ji X-F, Chi T-Y, Liu P, Jin G, Gu S-L, Zou L-B (2015) Sigma 1 receptor activation regulates brain-derived neurotrophic factor through NR2A-CaMKIV-TORC1 pathway to rescue the impairment of learning and memory induced by brain ischaemia/reperfusion. Psychopharmacology (Berl) 232:1779–1791.

.

Appendices

The studies presented in these appendices are related to previous work or ongoing collaborations. The abstracts contextualize the whole project, methods and results refer only to experiments performed by the author of this thesis.

Appendix 1

5-MeO-DMT increases insulin sensitivity in brain organoids and diabetic mice

Livia Goto-Silva[1], Juliana M. Nascimento[2], Isis Ornelas[1], Margareth Nogueira[3], Emanuelle V. de Lima, Claudia P. Figueiredo, Magno Junqueira, Richardson N. Leão[3], Daniel Martins-de-Souza, Stevens K. Rehen[1]
1. D'Or Institute for Research and Education, Rio de Janeiro, Brazil;
2.Federal University of the Rio de Janeiro, Rio de Janeiro, Brazil.
3.Neurodynamics Lab, Brain Institute, Federal University of the Rio Grande do Norte, Natal, Brazil

Highlights:
· 5-MeO-DMT regulates protein targets related to glucose homeostasis which overlap targets of Peroxisome Proliferator-activated Receptor Gamma (PPARγ);
· PI3K/Akt pathway is up-regulated upon 5-MeO-DMT treatment;
· 5-MeO-DMT decreases blood glucose levels.

Keywords: psychedelics, 5-MeO-DMT, 5-HT receptors, serotonin agonist, brain, insulin, diabetes.

Abstract

The use of psychedelic compounds has been proposed for treatment-resistant depression and other mental disorders. Still, the therapeutic potential of psychedelics just started to be unraveled. 5-MeO-DMT is a natural psychedelic agonist of serotonin receptors, which has been shown to decrease depression and anxiety symptoms in naturalistic settings. First, we took a data mining approach to investigate prospective unaddressed effects of 5-MeO-DMT. We analyzed a published proteomics dataset of human brain organoids treated with 5-MeO-DMT using a databank of drug regulated genes. Our search significantly matched hits regulated by Peroxisome Proliferator-activated Receptor Gamma (PPARγ) agonists, insulin sensitizer drugs, which use has been proposed in cognitive decline and Alzheimer's disease (AD) treatment. We show that 5-MeO-DMT regulates PI3K/Akt pathway in the brain and glucose peripheral metabolism, suggesting that 5-MeO-DMT could have a beneficial action in the treatment of AD and associated peripheral metabolic disorders.

Method

Glucose blood levels from twelve C57BL/6 male mice, between 9 and 12 weeks old were assessed using an Accu-chek active whole-blood glucometer (Roche). Mice were previously housed with food and water “ad libitum”, 12 hours light /dark cycle and temperature controlled at 24ºC. The cages were located in a ventilated rack. Before the experiment, mice were fasted for 6 hours with water supply. Animals were divided into two groups. Six mice received intra peritoneal (IP) injection of 5-MeO-DMT (20mg/kg) and six mice received saline (0,9%) injection. Randomly, fasted mice were injected and blood glucose levels were monitored at time zero (T0) one (T1), two (T2), three (T3) and four (T4) hours later. This experiment was carried out in accordance with the recommendations of the National Council for the Control of Animal Experimentation (CONCEA) in Brazil under the protocol 110.035/2018 from the Ethics Committee on Animals Use (CEUA) from Federal University of Rio Grande do Norte.

Result

5-MeO-DMT reduces fasting glucose levels in mice

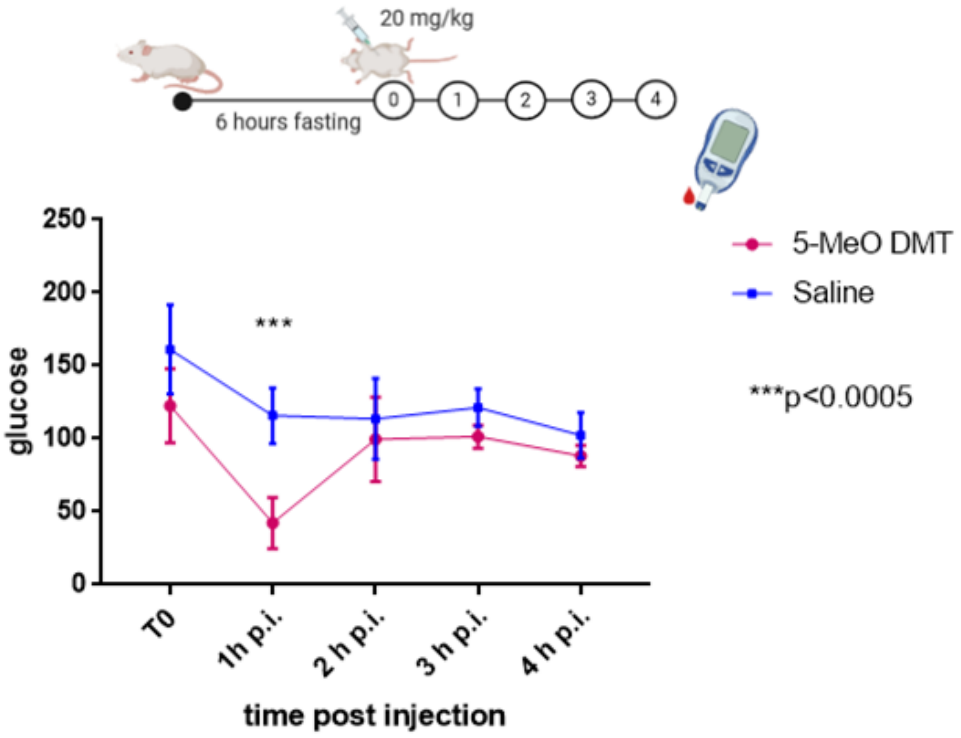

Figure 1.1 5-MeO-DMT reduces fasting glucose levels in mice. Glucose levels post treatment injection.

Appendix 2

A noncanonical auditory pathway modulates theta oscillations and place cells activity in the hippocampus

Jessica Winne[1], George Nascimento[2], Margareth Nogueira[1], Katarina Leão[1] and Richardson Leão[1,3,*] .

1. Neurodynamics Lab, Brain Institute, Federal University of the Rio Grande do Norte
2. Department of Biomedical Engineering,Federal University of the Rio Grande do Norte
3. Developmental Genetics, Department of Neuroscience, Uppsala University, Husarg 3, Uppsala, 75234, Sweden.

Abstract

The hippocampus provides spatial maps essential to navigation across different environments. During exploratory behavior, the hippocampus integrates multimodal sensory information from the environmental context, essential for survival. Hippocampal neural activity correlates with variables for physical space representations like head direction, location, edges and speed. However, sensory aspects of the environment also contribute to hippocampal coding of cognitive maps . A recently discovered ascendant auditory pathway that reaches the hippocampus via the medial septum/entorhinal cortex could provide auditory information for hippocampal polysensorial integration. We studied the role of the dynamic modulation of speed and place cell coding in the hippocampus by sound arising from a noncanonical reticular-limbic auditory pathway. By using sound and optogenetic stimulation/inhibition of the dorsal cochlear nucleus, medial septum, entorhinal cortex and pontine nuclei, we found that theta oscillations loose dependence on speed when this noncanonical pathway is activated. Calcium imaging reveals that firing of CA1 stratum pyramidale interneurons do not respond to increased running speed when loud broadband sounds (known to activate the noncanonical pathway) are presented. Moreover, loud broadband sounds mask place cell activity when mice are running in a linear track. The reticular-limbic auditory pathway carries information on aversive sounds and the modulation of spatial memory networks by this pathway may switch off spatial memory coding in favor of fleeing.

Keywords: Noncanonical auditory pathway, theta oscillations, place cells, hippocampus

Mice training method

6 adult C57BL6J mice were trained 10 days before the sound stimulation protocol, which consists of 5 minutes walking in the 8 maze, recording baseline and 5 minutes with sound stimulation, twice. The training for each animal consists of two 10-minute blocks, where each animal explores the 8 maze in order to get used to the setup. We control the setup and the hatches, and note the amount of turns completed by each animal.

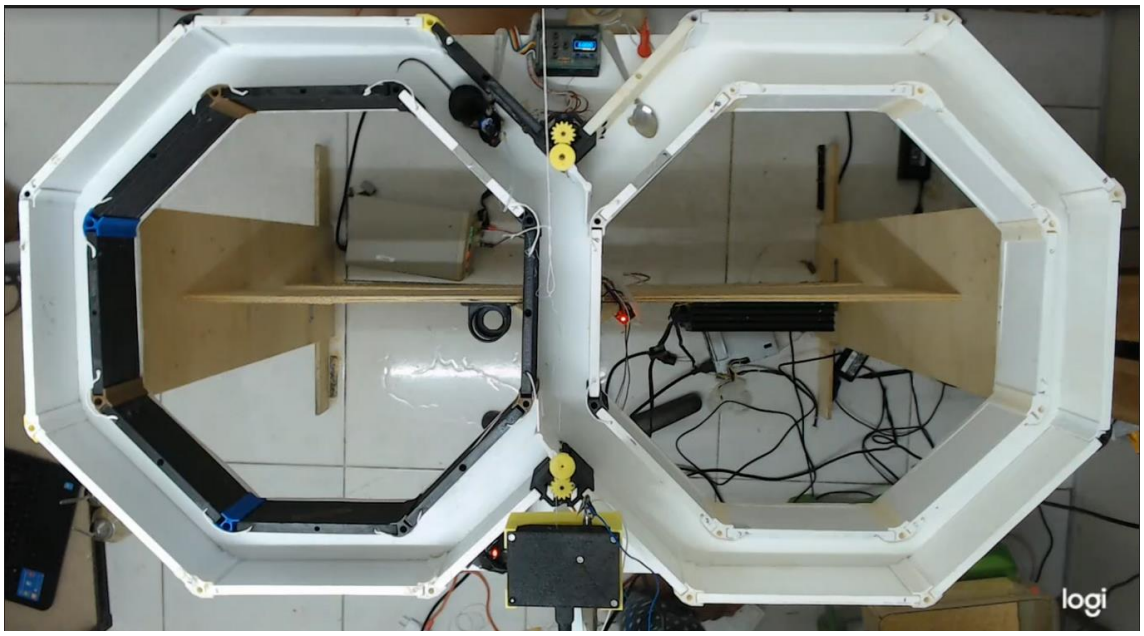

Figure 2.1 Mouse walking through the Maze in 8. Animal in training.

Appendix 3

Characterization of Chrna2 amygdala cells

Margareth Nogueira[1,2], Sanja Mikulovic[2], Klas Kullander[2] and Richardson Leão[1,2*]

1. Neurodynamics Lab, Brain Institute, Federal University of the Rio Grande do Norte
2. Developmental Genetics, Department of Neuroscience, Uppsala University, Husarg 3, Uppsala, 75234, Sweden.

Abstract

Chrna2 is a gene that encodes the alpha-2 subunit of nACHr (nicotinic acetylcholine receptor). Chrna2 amygdala cells are a subpopulation of neurons that can be targeted using a Chrna 2/tomato transgenic mouse. Here, we characterized the Chrna2 cells in Amygdala, more specifically those connecting to the ventral hippocampus, featuring the circuitry through the morphological, electrophysiological, and connective profile. Several types of Chrna2 neurons all over the body have been characterized before, such as Martinotti cells in the cortex, OLM cells in the hippocampus, and Renshaw cells in the spinal cord. However, Chrna2 Amygdala cells still have not been well characterized in the literature. Here, we performed a whole-cell patch-clamp to identify the electrophysiological profile of Chrna2 amygdala cells. We also performed imaging to determine anatomical distribution, virus tracing, and dye imaging for morphological identification, recognizing axonal projections and connections.

Keywords: Chrna2, amygdala, interneurons.

Introduction

Bringing phenomenological experience onto the brain stage is one of the major challenges of systems neuroscience. Neurons form networks that encode perception, cognition, and emotion. Understanding the communication in neural circuits requires finding optimal markers for characterization and manipulation purposes. For example, the hippocampus alone has more than twenty different types of interneurons[1]. It is essential to access interneurons; however, some of the most commonly used markers nowadays are nonspecific.

A Swedish group discovered a marker that is very specific for some interneurons located in the mouse nervous system - the Chrna2 gene promoter - which encodes the alpha 2 unit of the nicotinic acetylcholine receptor[3]. This discovery allowed investigating with greater accuracy the OLM cells in the hippocampus[3,5,6,7,8], the Martinotti in layer 5 of the cortex[2] and the Renshaw cells in the medulla[4]. Other cell subpopulations are also marked in the amygdaloid body, the olfactory bulb, and the striatum. Currently, transgenic animals are generated using the CRISPR-cas9 gene-editing technique, but until recently, these animals were developed from BAC (Bacterial Artificial Chromosome) technology, which is a DNA construct based on plasmids, double circular DNA molecules capable of replicating independently of chromosomal DNA. Although they are more stable than other types of cloning vectors, the technique makes possible a variability in the expression of Cre. The plasmids are composed of a gene promoter, in this case, Chrna2, and the gene of interest, which encodes the Cre recombinase enzyme. Depending on the insertion site of the promoter, there may be more or less restriction in gene expression. Animals generated in Sweden, which are the same animals used in Brazil have a more restricted expression than the Chrna2-cre_OE25 and Chrna2-cre_OE26, found in the mouse brain atlas site, from the Allen Brain Institute[9]. In situ hybridization experiments have indicated that Chrna2 is expressed in both the dorsal and ventral hippocampus and areas such as CA3, for example (mouse.brain-map.org/experiment/show/75551460)[9,5]. In the case of the animal generated at Uppsala University, Sweden, the expression sites are slightly different, presenting low expression in the dorsal hippocampus and none in CA3. In situ hybridization can prove the high degree of specificity of the Swedish samples, of

92.0%[3,5]. This discovery contributed to the understanding of the behavior and functionality of these cells.

In other words, the higher the specificity of a marker, the more efficient the access to a cell population. Most of the classical markers of interneurons are not specific, that is, they mark different populations of cells. The discovery of Chrna2 cells turned out to be a finding of great importance as it allows one to draw a general panel of the profiles of various interneurons and their functions.

Emotional disorders such as anxiety, post-traumatic stress, and obsessive-compulsive disorder are commonly associated with alterations in the synaptic transmission process. The amygdala is a structure related to emotional responses, survival, and motivations. It is also closely related to learning and memory. Knowing the neural substrate related to circuits involved in emotional processes is a first step toward understanding how information flow underlies behavior. In this sense, the role of synaptic transmission is fundamental. Synaptic inhibition is responsible for modulating the activity of principal neurons and also of other interneurons, exerting selective filtering of synaptic excitation, which determines the control of information flow. Understanding the role of inhibition through interneurons is crucial for understanding the functional basis of emotion-related circuits (Pelkey KA., 2017). Chrna2 an excellent marker of some types of interneurons located in the cortex, hippocampus, and amygdala. Chrna2 cells in the amygdala are a subpopulation of neurons that can be marked using a transgenic mouse carrying the Chrna2 promoter gene and the red fluorescent protein tdTomato (Mikulovic S. et al, 2015). Therefore, characterizing Chrna2 cells in the amygdala and their role in emotion-related circuits, specifically in relation to the ventral hippocampus, can disclose the role of inhibition in this process.

Method

4 – 8 weeks C57BL6J mice from both sexes were anesthetized with ketamine (90 mg/kg) and then intracardially perfused standard artificial cerebrospinal fluid (aCSF; in mM: NaCl 124; KCl, 2.5; NaH_2PO_4,1.2; $NaHCO_3$, 24; glucose, 12.5; $CaCl_2$, 2; $MgCl_2$, 2) at room temperature. Brains were dissected and then transferred to a Vibratome (VT1200, Leica Microsystems) chamber containing ice-cold aCSF. Horizontal slices with 400μm thickness were collected and transferred to a holding chamber containing recover N-methyl-D-glucamine (NMDG) solution (in mM NMDG, 92; KCl, 2.5; NaH_2PO_4,1.25; $NaHCO_3$, 30; HEPES, 20; glucose, 25; thiourea, 2; sodium-ascorbate, 5; sodium-pyruvate, 3; $CaCl_2 \cdot 4H_2O$, 0.5; $10MgSO_4 \cdot 7H_2O$, 10; pH controlled to 7.3–7.4 with 2N HCl solution) at 34◦C for 15 min, and then returned to aCSF for at least 1 hour at room temperature before recordings. The slices were kept in standard aCSF, constantly bubbled with carbogen 95% O2 and 5% CO2. (White-Martins; Ting et al., 2014). Then, the tissue was transferred to a submerged chamber filled with standard oxygenated aCSF under a ZEISS microscope. Borosilicate glass capillaries (GC150F-10, Harvard Apparatus, MA, USA) were pulled on a vertical puller (PC-10, Narishige, Japan). Micropipettes (8-12 MΩ resistance) were filled with K-gluconate internal solution (in mM, K-Gluconate, 145; HEPES, 10; EGTA, 1; Mg-ATP, 2; Na_2-GTP, 0.3; $MgCl_2$, 2; 290–300 mOsm; pH 7.3, adjusted using KOH). Chrna2-tomato amygdala cells were identified by fluorescence. Current-clamp recordings were obtained using an Axopatch amplifier 200B (Molecular Devices) in whole-cell configuration using the winWCP Strathclyde Electrophysiology Software (J. Dempster, University of Strathclyde). Two protocols were used in current clamp: 100 ms-long current steps with 50 pA increment ranging from −100 pA to 400 pA and a ramp ranging from −50 pA to 200 pA in 1500 ms.

Results

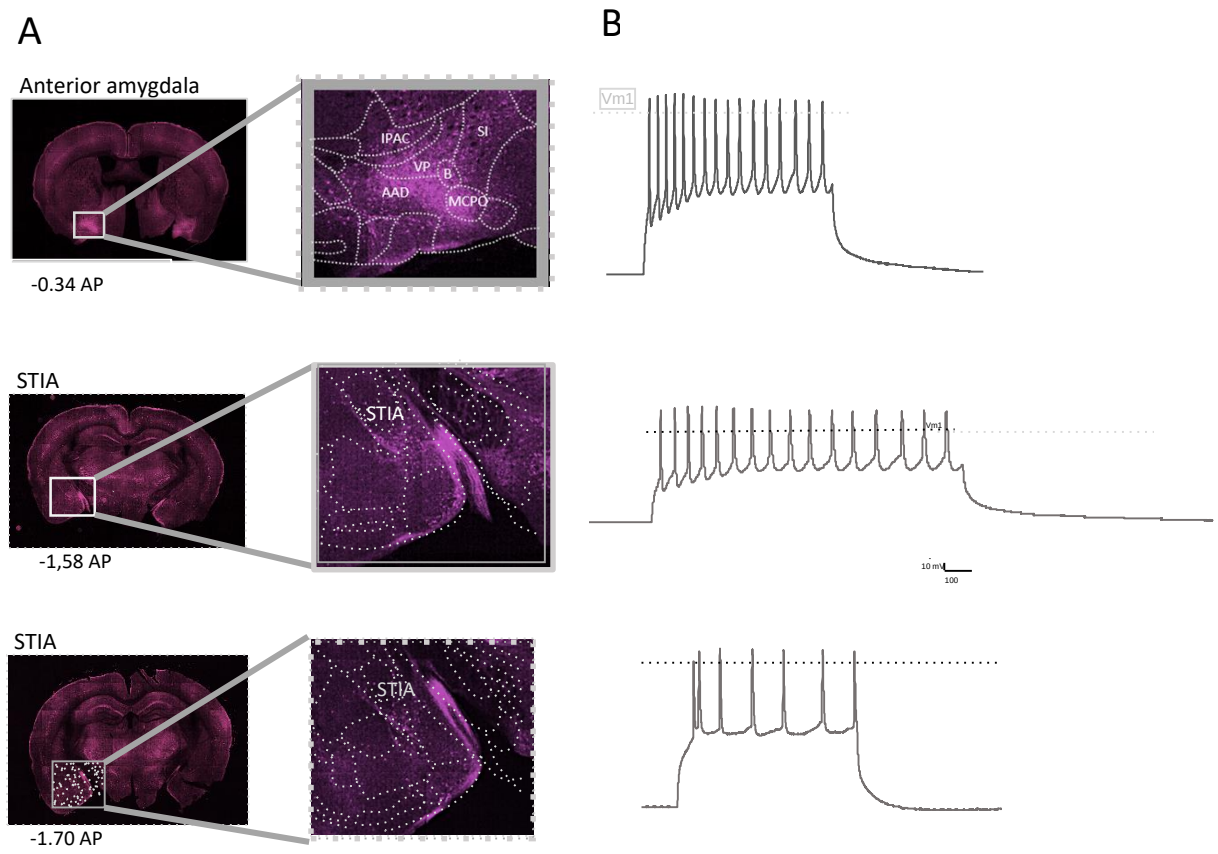
A
Anterior amygdala
IPAC
SI
VP
B
AAD
MCPO
-0.34 AP
STIA
STIA
-1,58 AP
STIA
STIA
-1.70 AP
B
Vm1
C

Figure 3.1 Characterization of Chrna2 amygdala cells. (A) Anatomic distribution of Chrna2 amygdala cells **(B)** Confocal images of Chrna2 cells morphology **(C)** Representative trace responses to step current stimulus of the Chrna2 amygdala cells **(D)** confocal imaging of Chrna2^{+} cells in amygdala medial nucleus.

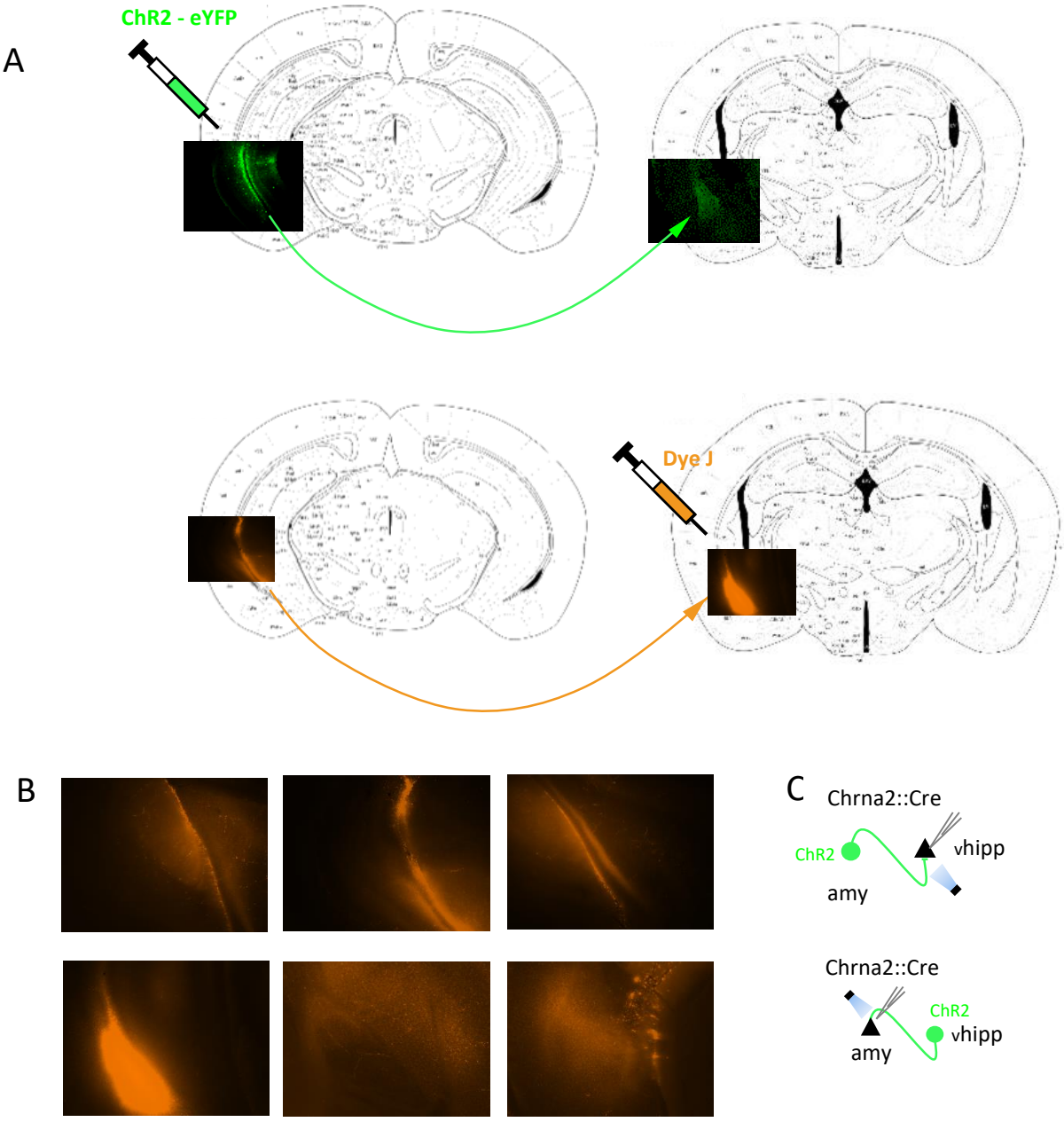

Figure 3.2 Characterization of Chrna2 amygdala/hippocampal circuitry. (A) injection of anterograde AAV-DIO-ChR2 on ventral hippocampus projecting to amygdala and DyeJ retrograde tracing from vhipp to amy **(B)** DyeJ retrograde tracing from amy to vhippocampus **(C)** experimental design

References

1. Pelkey KA et al. **Hippocampal GABAergic Inhibitory Interneurons.** Physiol Rev. 2017
2. Hilsher et al. **Chrna2-Martinotti Cells Synchronize Layer 5 Type A Pyramidal Cells via Rebound Excitation.** PLoS Biol. 2017
3. Leão et al. **OLM interneurons differentially modulate CA3 and entorhinal inputs to hippocampal CA1 neurons.** Nat Neurosci. 2012
4. Perry, S. et al. **Firing properties of Renshaw cells defined by Chrna2 are modulated by hyperpolarizing and small conductance ion currents Ih and ISK.** Eur J Neurosci. 2015
5. Mikulovic et al. **Novel markers for OLM interneurons in the hippocampus**. Front Cell Neurosci. 2015
6. Mikulovic et al. **Ventral hippocampal OLM cells control type 2 theta oscillations and response to predator odor.** Nature Communications. 2018
7. Siwani et al. **OLMa2 Cells Bidirectionally Modulate Learning.** Neuron. 2018
8. Winne et al. **Salicylate induces anxiety-like behaviour and slow theta oscillation and abolishes the relationship between running speed and fast theta oscillation frequency.** Hippocampus. 2018
9. **Mouse Allen brain atlas. http://mouse.brain-map.org/static/atlas.** Access on 22/09/2018
10. Luo et al. **Genetic Dissection of Neural Circuits:A Decade of Progress.** Neuron. 2018
11. Zeisel et al. **Cell types in the mouse cortex and hippocampus revealed by single-cell RNA-seq.** Science. 2018

Appendix 4

MINISTÉRIO DA EDUCAÇÃO
UNIVERSIDADE FEDERAL DO RIO GRANDE DO NORTE
COMISSÃO DE ÉTICA NO USO DE ANIMAIS – CEUA
Av. Salgado Filho, S/N – CEP: 59072-970 – Natal / RN
Fone: (84) 9229-6491 / e-mail: ceua@reitoria.ufrn.br

Natal, 08 de maio de 2020.

PARECER nº 04

(Referente ao ADENDO Nº 01 submetido em 02/03/2020)

1)PROTOCOLO Nº : 035/2018

2) TÍTULO DO PROJETO:
"Função das células Chrna2 no circuito amigdalo-hipocampal relacionado a emoção""

3) PESQUISADOR RESPONSÁVEL:
Richardson Naves Leão

4) MOTIVO DO ADENDO:

Mudança/Inclusão de metodologia? [X] Sim [ ] Não

"Ao longo da pesquisa surgiu a necessidade de verificar outros aspectos relacionados ao circuito amigdalohipocampal relacionado a emoção. Outros estudos no laboratório identificaram que a 5-MeO-DMT induz a neurogênese e que pode prevenir o comportamento ansioso induzido pelo salicilato. Fez-se então necessária a verificação da função ansiolítica da 5-MeO-DMT nos circuitos relacionados à emoção."

Extensão de cronograma? [x] Sim [ ] Não

VIGÊNCIA DO PROJETO	**JUNHO 2021**
Relatório	Julho 2021

Inclusão de colaborador? [x] Sim [ ] Não

Elis Brisa dos Santos (aluna de doutorado do prof. Richardson Leão)
Cibele Leônidas de Sousa (aluna de iniciação científica do prof. Richardson Leão)

5) PARECER:

APÓS AJUSTE DO CRONOGRAMA, ESTE **ADENDO FOI APROVADO** POR ESTA COMISSÃO.

Informamos ainda que, segundo o Cap. 2, Art. 13, do Regimento Interno desta CEUA, é função do professor/pesquisador responsável pelo projeto a **elaboração de relatório** de acompanhamento que deverá ser entregue tão logo a pesquisa seja concluída. **O descumprimento desta norma poderá inviabilizar a submissão de projetos futuros.**

Alianda Maira Cornélio da Silva
Vice-Coordenadora da CEUA-UFRN
Gestão 2019-2020

www.ceua.propesq.ufrn.br